Microbubbling and microencapsulation by Co-axial electrohydrodynamic atomization

A thesis submitted in partial fulfilment of the requirements for the degree of

Doctor of Philosophy

By

Uthumankandu Farook, BASc (Eng)

Department of Mechanical Engineering

University College London

Torrington Place, London WC1E 7JE

U.K

August, 2009

Declaration

I, Uthumankandu Farook, confirm that the work presented in this thesis is my own. Where information has been derived from other sources, I confirm that this has been indicated in the thesis.

……..

Uthumankandu Farook

Abstract

Microbubbles coated with polymers or surfactants have been used in medical imaging for several years as ultrasound contrast agent particles and are now being investigated by researchers as drug and gene delivery vehicles and blood substitutes. Current methods available for the preparation of microbubbles are insufficient as they result in microbubbles with a wide size distribution and as such filtration is necessary before their use. With a view to fill the above demand, a detailed investigation has been carried out in this research to learn the viability of co-axial electrohydrodynamic atomization (CEHDA) technique to prepare microbubbles. The research also focuses on the effects of the process parameters such as flow rates, applied voltage and material parameters such as electrical conductivity, surface tension and viscosity with the objective of preparing polymer or surfactant coated stabilized microbubbles with diameters < 8 μm and with a narrow size distribution. A model glycerol-air system was used so that the CEHDA technique was modified to generate suspensions of microbubbles to a diameter < 8 μm with a narrow size distribution and then to characterise the CEHDA microbubbling process in terms of size and stability with varying process parameters and material parameters. Construction of a parametric plot between the air flow rate and the liquid flow rate was extremely useful in identifying the flow rate regime of air and liquid or suspension or solution for the continuous microbubbling of the system used. With further investigations into the CEHDA microbubbling technique, it was possible to develop strategies, first, to prepare suspensions of stabilized phospholipids-coated microbubbles with a mean diameter of ~ 5 μm and a polydispersivity index of 9%, and second, polymeric microspheres with a mean diameter of 400 nm and a polydispersivity index of 8% using a biocompatible polymer.

Publications, Conference Presentations and Patents

Publications

1**. Farook** U**,** Zhang HB, Edirisinghe M, Stride E, Saffari N (2007) Preparation of microbubble suspensions by co-axial electrohydrodynamic atomization. Med Eng Phys 29: 749- 754.

2**. Farook** U, Stride E, Edirisinghe M, Moaleji R (2007) Microbubbling by co-axial electrohydrodynamic atomization. Med Bio Eng Comput 45: 781- 789.

3. Pancholi KP, **Farook** U, Moaleji R, Stride E, Edirisinghe M (2007) Novel methods for preparing phospholipid coated microbubbles. Eur Biophys J 37: 515-520.

4**. Farook** U, Edirisinghe M, Stride E, Colombo P (2008) Novel co-axial electrohydrodynamic *in-situ* preparation of liquid-filled polymer-shell microspheres for biomedical applications. J Microencapsul 25(4): 241-247.

5. **Farook** U, Stride E, Edirisinghe M (2009) Preparation of suspensions of phospholipid-coated microbubbles by coaxial electrohydrodynamic atomization. J R Soc Interface 6(32): 271-277.

6. **Farook** U, Stride E, Edirisinghe M (2009) Stability of microbubbles prepared by co-axial electrohydrodynamic atomization. Eur Biophys J 38(5): 713-718.

7. **Farook** U, Stride E, Edirisinghe M (2009) Controlling the size and size distribution of electrohydrodynamically prepared microbubbles. Bubble Science, Engineering & Technology 1(1-2): 53-57.

8. **Farook** U, Stride E, Edirisinghe M, Luklinska Z (2009) Preparing submicrometre size polymeric spheres using co-axial electrohydrodynamic microbubbling. Submitted to Soft Matter.

9. Ahmad Z, Zhang HB, **Farook** U, Edirisinghe M, Stride E, Colombo P (2008) Generation of multilayered structures for biomedical applications using a novel tri-needle co-axial device and electrohydrodynamic flow. J R Soc Interface 5(27); 1255-1261.

10. Nangrejo M, Bernardo E, Colombo P, **Farook** U, Ahmad Z, Stride E, Edirisinghe M (2009) Electrohydrodynamic forming of porous ceramic capsules from a preceramic polymer. Materials letters 63(3-4): 483-485.

Conference Presentations

1. **Farook** U, Moaleji R, Stride E, Edirisinghe M. Development of a novel technique for the preparation of microbubble suspensions for ultrasound imaging and drug delivery. Annual Scientific meeting of the Institute of Physics and Engineering in medicine South East Group, March 29, 2007, St Mary's Hospital, Portsmouth, UK.

2. **Farook** U, Stride E & Edirisinghe M. Stabilized phospholipid-coated microbubbles with low polydispersity index via co-axial electrohydrodynamic microbubbling, 6th International workshop on Drug Delivery systems for Nonomedicine, nanostructures and their Biomedical Applications. October 3-6, 2008, Liblice Castle, Czech Republic.

3. **Farook** U, Stride E & Edirisinghe M. Preparation of stabilized phospholipid-coated microbubbles with low polydispersivity, Symposium on Encapsulation for Drug delivery & Microbubbling. November 14, 2008, University College London, UK.

Patents

1. Edirisinghe M, Stride E, Moaleji R, Pancholi K & **Farook** U., International Patent Application: "Systems and Methods for Microbubble Production", PCT/GB2008/001050, March 2008.

Acknowledgements

At the very outset my wholehearted thanks go to my supervisor Professor Mohan Edirisinghe for first of all accepting me under his wings as a research student at UCL and then for his continuous guidance, constructive criticism, confidence building and valuable support during the period of this research study. Professor Edirisinghe is one of my role models, a world renowned materials scientist and a source of inspiration. I am extremely delighted to have realized my greatest ambition of doing this research study under his mentorship.

My thanks are equally due to my joint-supervisor Dr. Eleanor Stride for her co-operation, constructive guidance and support. Her expertise on the subject of microbubbles was of immense use in shaping up my research career. I feel extremely privileged to be jointly supervised by Prof. Edirisinghe and Dr.Stride.

I also like to thank UCL and EPSRC (UK) for their funding assistance in carrying out this research study.

Continuous and invaluable support provided by my colleagues, Dr. Anushini Muthutantri, Dr. Dong Yong Sun , Dr. Ketan Pancholi, Dr. Rafique Nangrejo, Miss. Raheleh Bakshi, Dr. Reza Moaleji, Dr. Sundaravathanan Mahalingam, Dr. Suren Samarasinghe, Dr. Xiang Li, Dr.Zeeshan Ahmad, and Dr.H.B.Zhang is unforgettable and many thanks to them. The lovely memories I have with these guys will always be cherished.

Thanks to Kevin Reeves of the Department of Archaeology of UCL, for his invaluable assistance in obtaining SEM images.

My dream of doing this research study wouldn't have been possible if not for the unparalleled understanding, love and support extended to me and my family by my beloved brother-in-law, Imtiaz Ahamed, a man with a magnificent heart. I thank my brother-in-law very much. I like to also thank our family friend Richard Tomlinson, who worked hand in hand with my brother-in-law in facilitating my research student career and is a good friend in deed.

Continuous love and support provided by my nephew Rasalie and my niece Marzi are unforgettable. They are my friends in no uncertain terms as well. I thank Rasalie and Marzi very much. I thank my mother-in-law, Azeez and Mahira, Farook and Fowmy, Ahamedlebbe and Mehrun, Nafeel and Sherin for their love and support in numerous ways. I thank my mother and father-in-law for their encouraging words during telephone conversations. I also thank my sister and brothers for looking after my mother during the time I was away from her for many years. My thanks are also due to John, Nilani, Soori, Faamy, Bushra, Rehman, Christopher, Saalim, Fowzy, Sahabdeen, Patricia, Paulet, Rizwana, Haleem, Abey, Saffina, Siddeek, Nisa, Sapna, Koffi, Nowfer and Akin for being my good friends.

Last but not least, I thank my beloved wife Razi for her unwavering support, unblemished love and total commitment in making this value addition a reality. I also thank my beloved children Shadheela and Farooz for everything they did in making my research student career a great success.

DEDICATION

To

My children

Farooz and Shadheela,

my brother-in-law

Imtiaz Ahamed,

my wife

Razi,

and

my mother Zeenath

for their extreme sacrifices

during the time of this research

TABLE OF CONTENTS

List of Tables

List of Figures

Glossary of abbreviations

BSA	Bovine serum albumin
CAP	Contrast agent particles
CEHDA	Co-axial electrohydrodynamic atomization
CEUS	Contrast enhanced ultrasound
DDS	Drug delivery systems
EHDA	Electrohydrodynamic atomization
FDA	Food and drug administration, USA
MPC	2-methacryloyloxyethyl phosphorylcholine
PC	Personal computer
PDMS	Polydimethylsioxane
PEG	Poly ethylene glycol
PFC	Per fluorocarbon
PGA	Polyglycolides
PLA	Polylactides
PLGA	Poly lactide-co-glycolic acid
PVA	Poly vinyl alcohol
SEM	Scanning electron microscope
TEM	Transmission electron microscope
UCA	Ultrasound contrast agents

CHAPTER 1

INTRODUCTION

1.1. Background

Co-axial electrohydrodynamic atomization (CEHDA) has proved its ability to produce encapsulated particles with liquid or solid incipient in the nanometric and micrometric ranges. The method allows for good control over the size of the coated particles, with narrow size distribution, and good control over the thickness of the coating (Lopez-Herrera *et al*. 2003). In CEHDA, two different liquids or suspensions are pumped through two concentrically placed needles, which are subjected to an applied voltage and the co-flowing liquids are capable of experiencing various modes of atomization. Eventual jet break-up can result in near monodisperse compound aerosols with the outer material surrounding or encapsulating the inner one. This phenomenon has particular importance for encapsulation of food additives, targeted drug delivery, and material processing (Loscertales *et al.* 2002). Composite ceramics and bio microstructures have also been prepared through CEHDA by encapsulating suspensions of zirconia by suspensions of alumina (Balasubramanian *et al.* 2006) and protein in starch (Pareta and Edirisinghe 2006), respectively.

Preparation of microspheres dates back to the early 1950s and microencapsulated products are available as liquid crystals, adhesives, perfumes and fragrances, cosmetics, insecticides, algaecides, fertilizers, washing powders, insulation materials, animal feedstocks, artificial kidneys, medicinal products, ultrasound contrast agents etc. (Arshady 1990, Schmidt and Roessling 2006). The microspheres normally consist of particles with diameters between 50 nm and 1000 μm with solid, liquid, or gaseous

core. The wall material can be made from polymers, surfactants, glass, oxide ceramics, mixed oxides or even metals (Bertling *et al.* 2004, Gaponik *et al.* 2004). The main motivations for microencapsulation are separation of incompatible components, protection of immediate environment, conversion of liquids, reduction of material weight, encapsulation and immobilization of bioactive substances, modification of impact strength of compounds, and better thermal and acoustical insulation (Arshady 1989).

In medical and pharmaceutical applications, there is rapidly growing interest in the use of microbubbles and microspheres as ultrasound contrast agent particles, drug delivery systems and in the synthesis of artificial cell structures (Bertling *et al*. 2004**,** Botchwey *et al*. 2004). A prerequisite for using microbubbles and microspheres as contrast agent particles in ultrasound radiography is that they degrade *in-vivo* within hours and that the largest particle does not exceed 8 μm diameter, in order to avoid capillary blockage (Raisinghani and DeMaria 2002). Most contrast agent particles are coated either with a surfactant or polymer shell to counter the effects of surface tension and hence improve the stability. Besides their diagnostic use, microspheres may also be used therapeutically. A microsphere partially filled with an entrapped therapeutic agent can transport the substance through blood vessels and release its load at a targeted site when excited by an ultrasound field (Schmidt and Roessling 2006, Stride and Saffari 2003). Polymeric materials can be used in encapsulating drugs in developing drug delivery systems (DDS) for sustained and controlled release of drugs. These DDS are used to provide a predetermined amount of drug at an appropriate time and at a targeted site over duration from several minutes to several years (Kawaguchi 2000, Pareta and Edirisinghe 2006, Yadav *et al.* 1997, Zhang *et al.* 2005). However, incorporating a

therapeutic agent into microspheres requires chemical compatibility and a filling space in the shell, which is relatively small in conventional microspheres. Thicker polymeric shells or solid multilayered microspheres can overcome this drawback, in addition to providing greater stability to the microspheres (Bekeredjian *et al.* 2005, Cavalieri *et al.* 2005, Liu *et al.* 2005, Pekarek *et al.* 1994, Unger *et al.* 2002).

Many techniques such as layer-by-layer-deposition, *in-situ* polymerization on template particles, sol gel methods, and liquid phase deposition, pH-induced micellization of grafted copolymer and core-free-template strategy have been developed to prepare polymeric microspheres whose size ranges from tens of nanometres to a few micrometres (Cheng *et al.* 2006). Emerging techniques for creating monodisperse microbubbles and microspheres utilize controlled flow fields and electrohydrodynamic forces to induce regular microbubble/microsphere break-up (Sgraja *et al.* 2006).

Precision particle fabrication technology and microfluidic technology have proved to be capable of producing suspensions of monodisperse microspheres, but carry limitations either with regard to the size or the stability of the microspheres or the high cost of the preparation technique (Berkland *et al.* 2007, Sgraja *et al.* 2006, , Zoldesi *et al.* 2006). Monodisperse microspheres means, the microspheres are of the same size and, if the microspheres are of not the same size, it is a situation of polydispersivity. For a narrower size distribution, polydispersivity index would have a lower value and vice versa. [Polydispersivity index = (standard deviation/mean size)100].

1.2. Objectives of the research

The features available in CEHDA as a technique to prepare encapsulated particles of nanometric and micrometric size range with near-monodispersivity is the primary attraction for the germination of the idea to use CEHDA as an alternative method to prepare microbubbles for biomedical applications. However, to the best of author's knowledge, CEHDA had not been developed into a technique to prepare microbubbles until the investigations described in **Chapter 4** of this thesis were performed. This is the unique reason why enabling CEHDA to generate microbubbles becomes the primary objective of this research.

Since the microbubbles are highly echogenic due to the difference in compressibility and density between the microbubble and the surrounding medium, they resonate when excited in an ultrasound field permitting the detection techniques to differentiate microbubbles from the surrounding medium. Due to the resonance frequency of bubble is directly related to its diameter and the ultrasound systems have limited frequency bandwidth, it is necessary to have an entire population of microbubbles of the same diameter matched to the bandwidth (Dayton *et al.*2002). This is the main reason why the second objective of this research becomes enabling the CEHDA technique to prepare microbubbles with diameters < 8 µm with a very low polydispersivity. Interestingly, CEHDA is already a technique with basic features to control the size and size distribution of the encapsulated particles by way of manipulating the process parameters and material parameters. However, selections of materials, compositions and preparation methods of encapsulating fluid do play a major role in deciding the characteristics of the final product.

The third objective of the research was relatively simple and straight forward. As CEHDA microbubbling was found to be a promising technique to prepare microbubbles with required size and size distribution, third objective of the research became preparing suspension of microbubbles using CEHDA microbubbling with materials that were already used in compositions to prepare microbubbles using other techniques. In order to fulfil this objective, L-α-phosphatidylcholine, a phospholipid, was used to prepare phospholipid-coated microbubbles. Lipid-coated microbubbles are well received in biomedical applications for their great potential as ultrasound contrast agent particles and drug and gene delivery vehicles (Unger *et al.* 2004). The use of a polymer in CEHDA microbubbling and subsequent preparation of polymeric spheres of submicrometre size has added a new dimension to CEHDA microbubbling technique and complimented the third objective of this research. The organisation of this thesis is given in the following section.

1.3. The structure of the thesis

This **Chapter 1** gives an overview about the basics of co-axial electrohydrodynamic atomization and other related techniques that are used for microbubbling and microencapsulation. The objectives of the research are clearly discussed. The organisation of this thesis and scope of the research are also discussed within this chapter.

Chapter 2 covers a detailed literature survey that has provided necessary tools to carry out the investigations described in **Chapters 4**, **5** and **6**. Since the research is to prepare microbubbles and microspheres through CEHDA to be used as ultrasound contrast agents and drug and gene delivery vehicles, an extensive collection of literature has been surveyed to understand the ultrasound procedure and its use, the materials and the methods used for the preparation of polymeric microspheres, and the principles behind

electrohydrodynamic atomization and co-axial electrohydrodynamic atomization. The literature on microfluidic flow focusing technique has also been reviewed in order to have a comprehensive understanding on the microbubbling and microencapsulation process, with a view to explore the viability of CEHDA as a technique that can generate microbubbles and microspheres suitable for biomedical applications.

Chapter 3 discusses the experimental details and procedures under taken in the research described in **Chapters 4**, **5** and **6**. It describes the materials and preparation methods followed in preparing suspensions and solutions used in the investigations. The characterisation techniques and procedures used are explained in detail. The apparatus and equipment used for the characterisation and co-axial electrohydrodynamic microbubbling are described. The characterisation techniques used for the suspensions of microbubbles and microcapsules also explained while briefly discussing the basic principles behind the characterisation techniques.

Chapter 4 discusses the conversion of conventional co-axial electrohydrodynamic atomization (CEHDA) technique into a technique that can also generate microbubbles and microspheres for various purposes, particularly for medical applications. A model glycerol-air system was used to generate microbubbles through the modified CEHDA experimental set-up and to characterise the CEHDA microbubbling process. Defining the modes of microbubbling and introducing the construction of a parametric plot between the flow rate of gas and the flow rate of liquid, as described in this chapter, were stepping stones for the research described in proceeding chapters. The uses of optical microscopy and Sympatec Laser diffractometry for characterising the suspension of microbubbles also have been discussed in this chapter. In addition, a detailed stability

study conducted on the microbubbles prepared by CEHDA microbubbling also discussed.

Chapter 5 describes an important step forward in taking this research to a different level. This chapter discusses how co-axial electrohydrodynamic atomization was used in preparing stabilized phospholipid-coated microbubbles with a mean size and size distribution that is suitable for ultrasound medical imaging, drug & gene delivery. Stability studies conducted on phospholipid-coated microbubbles prepared at ambient temperature (22^0C) and human body temperature (37^0C) are also discussed in detail. A section of this chapter has also been devoted to describe how a surfactant could be used to stabilize and to reduce the polydispersivity index of a microbubble population. Details are also given about the characterisation studies conducted on the phospholipid-coated microbubbles using ultrasound attenuation measurement and ultrasound imaging.

Chapter 6 discusses a novel route for the preparation of polymeric microspheres using CEHDA microbubbling technique. This chapter explains how a biocompatible polymer was dissolved in ethanol and the solution was microbubbled into a container of distilled water and the suspension of microspheres thus prepared were subsequently characterised. A detailed description is also given in this chapter about the use of parametric plot between the flow rate of air and the flow rate of polymer solution in reducing the microsphere size to a submicrometre size with a low polydispersivity index. The Transmission Electron Microscopic examination results also discussed in conjunction with other characterisation results, which led to the conclusion that the microspheres prepared were of matrix nature and that the liquid absorbed by the microspheres could be distributed throughout the polymer sphere.

Chapter 7 has been divided into two sections. Section 1 summarizes the experimental results and presents the conclusions of the work described in different chapters of this thesis. Section 2 discusses some recommendations for future work, employing CEHDA microbubbling and beyond, to continue the research presented in this thesis in new directions. Finally, the literature referred to throughout the thesis is listed in the **References** section.

1.4. The benefits of the research

The fundamental benefit that this research has yielded, for the use of scientific community and perhaps the industry at large, is the conversion of CEHDA as a microbubbling technique for the first time. With this pioneering conversion, the main objectives of this research of preparing microbubbles with diameters < 8 µm and a narrow size distribution has also been achieved, for the possible use of microbubbles in biomedical applications. CEHDA has now become a complete technique that can not only be used for encapsulating liquids and solids but also gases.

A systematic approach has thereafter been introduced in meeting the size and size distribution requirements of microbubbles and microspheres for a given application, by making use of the fundamental principles of electrohydrodynamic atomization (EHDA) that also govern CEHDA to a large extent. This has been demonstrated by preparing microbubbles and microspheres with size and size distribution that suits biomedical applications such as ultrasound imaging and drug and gene delivery. However, this approach can be further refined by making changes to other parameters such as needle geometry, collection distance of microspheres, ground electrode configuration etc.

Suspensions of phospholipid-coated microbubble prepared by CEHDA microbubbling have been subjected to a preliminary ultrasound imaging study with the use of a gelatine phantom. However, studying the physical and behavioural properties of ultrasound contrast agents that are already in use, comparing these properties with microbubbles prepared by CEHDA, adding new features to correct deficiencies, and subjecting the microbubbles to *in-vitro* and *in-vivo* studies are areas for further research.

This research has also led to preparing polymeric microspheres starting from a micrometric range to submicrometric range using CEHDA microbubbling, paving the way for the preparation of spheres of nanometric range. These microspheres have shown to absorb the liquid in which they are collected in. The potential this finding has is enormous as these spheres could be used for absorbing drugs in this way and releasing them at targeted sites by controlled delivery.

In addition to the influence that liquids or suspensions or solutions can have on the electrohydrodynamic process itself, by way of their physical properties such as surface tension, electrical conductivity and viscosity, the structural changes that these materials can make in microbubbles resulting in lower polydispersivity and better stability are also investigated in this research. These investigations provide an insight to the complexities that are involved in using CEHDA microbubbling technique from the stage of designing compositions of materials to the stage of preparing microbubbles and microspheres with required structural, dimensional, and qualitative features.

CHAPTER 2

LITERATURE REVIEW

2.1. Introduction

The summary of objectives of this research is to carry out investigations in the direction of enabling co-axial electrohydrodynamic atomization as a viable processing technique to prepare microbubbles and microspheres with size and size distribution that is suitable for biomedical applications, particularly as ultrasound contrast agent particles (CAPs) and drug and gene delivery vehicles.

In order to fulfil this, the literature related to ultrasound imaging, contrast-enhanced ultrasound (CEUS) and drug delivery systems (DDS), current preparation methods of microbubbles and microspheres and behavioural properties of microbubbles and microspheres have been surveyed in the first instance. Secondly, the current and previous literature available on processing techniques such as microfluidic flow focusing technique, electrohydrodynamic atomization (EHDA), and co-axial electrohydrodynamic atomization (CEHDA) have been reviewed in order, first, to understand these techniques and, second, to extract ideas from these techniques and conduct further investigations to fulfil the objectives of this research.

2.2. Ultrasound imaging

High frequency sound beyond the range of human hearing (approximately 20 kHz) is called ultrasound. Medical ultrasound images, such as those of a fetus in the womb, are made by directing ultrasonic waves into the body, where they bounce off internal organs and other objects and are reflected back to a detector.

The potential of ultrasound imaging as an imaging modality was realized as early as the late 1940s when, utilizing sonar and radar technology developed during World War II, several groups of investigators around the world started exploring diagnostic capabilities of ultrasound. In the early 1950s, John Wild and John Reid in Minnesota developed a prototype B-mode ultrasonic imaging instrument and were able to demonstrate the capability of ultrasound for imaging and characterisation of cancerous tissues at frequencies as high as 15 MHz (Shung 2006).

2.2.1. General ultrasound imaging

Ultrasound imaging, also called ultrasound scanning or sonography, involves exposing part of the body to high-frequency sound waves to produce images of the inside of the body (**Figure 2.1**). Because ultrasound images are captured in real-time, they can show the structure and movement of the body's internal organs, as well as blood flowing through blood vessels. Ultrasound imaging is a non-invasive medical test that helps physicians diagnose and treat medical conditions. Conventional (B-mode) ultrasound displays the images in thin, flat sections of the body. Advancements in ultrasound technology include three-dimensional (3-D) ultrasound that formats the sound wave data into 3-D images. Four-dimensional (4-D) ultrasound is 3-D ultrasound in motion (Goldberg *et al.* 1997 a, Harvey *et al*. 2002, Sidhu 2004, Bamber 2005).

A Doppler ultrasound study may be part of an ultrasound examination. Doppler ultrasound is a special ultrasound technique that evaluates blood as it flows through a blood vessel, including the body's major arteries and veins in the abdomen, arms, legs and neck. There are three types of Doppler ultrasound: (1) Colour Doppler uses a computer to convert Doppler measurements into an array of colours to visualize the

(a)

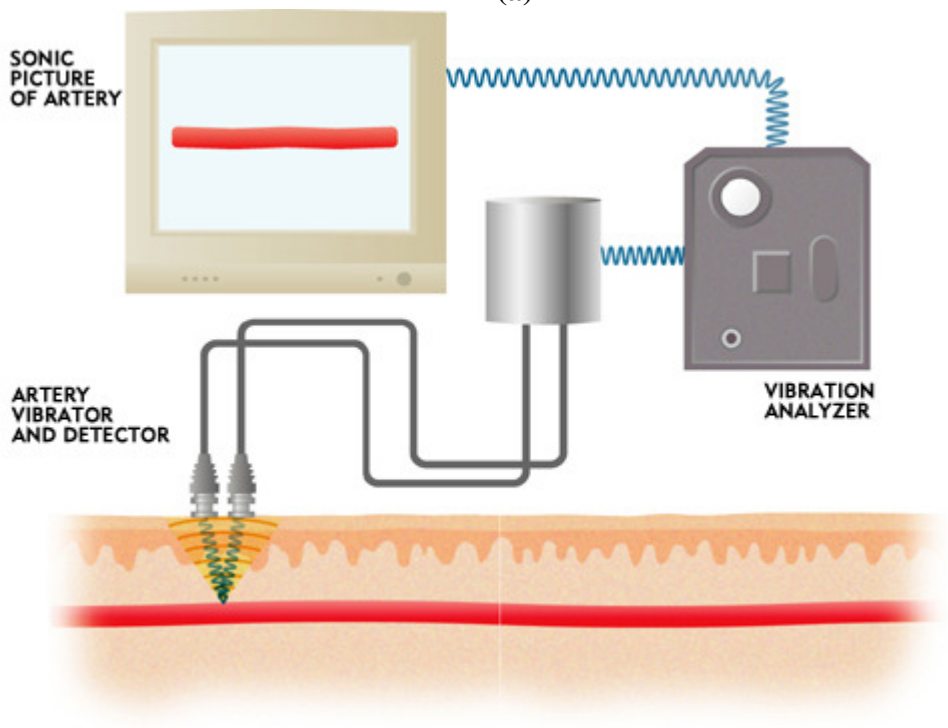

(b)

The ultrasound machine transmits high-frequency (1 to 5 MHz) sound pulses into the body using a probe

↓

The sound waves travel into the body and hit a boundary between tissues (e.g. an artery)

↓

Some of the sound waves get reflected back to the probe, while some travel on further until they reach another boundary and get reflected

↓

The reflected waves are picked up by the probe and relayed to the machine

↓

The machine calculates the distance from the probe to the tissue or organ (boundaries) using the speed of sound in tissue and the time of the each echo's return

↓

The machine displays the distances and intensities of the echoes on the screen, forming an image

Figure 2.1. **(a)** Schematic of the ultrasound imaging set up **(b)** Flow chart of the ultrasound imaging process (Freudenrich).

speed and direction of blood flow through a blood vessel, (2) Power Doppler is a newer technique that is more sensitive than colour Doppler and capable of providing greater detail of blood flow, especially when blood flow is little or minimal. Power Doppler, however, does not help the radiologist determine the direction of blood flow, which may be important in some situations, and (3) Spectral Doppler displays blood flow measurements graphically, in terms of the distance travelled per unit of time. (Goldberg *et al.* 1997, Harvey *et al*. 2002, Sidhu 2004, Bamber 2005).

2.2.2. Untargeted contrast enhanced ultrasound imaging

The use of suspensions of coated microbubbles is rapidly expanding in the field of medical engineering, particularly in the area of ultrasound applications. Microbubbles are small gas-filled microspheres whose high compressibility makes them useful as contrast agents in ultrasound imaging (Dijkmans *et al*. 2004). One in four imaging procedures in the world today is an ultrasound procedure, and this proportion is steadily increasing (Wells 2001). When used within the safety levels established by FDA, ultrasound represents the safest, fastest and least expensive method of scanning for many types of medical diagnosis. Compared with techniques such as magnetic resonance imaging, however, the quality of the images obtained is relatively poor and methods for improving this are therefore of great importance (Stride and Saffari 2003).

Since their discovery in the late 1960's (Gramiak and Shah 1968), gas microbubbles stabilized by a surfactant or polymer shell have become established as the most effective means of contrast enhancement in ultrasound imaging and a number of commercial agents are currently available (Dijkmans *et al.* 2004). Surfactants are organic compounds with hydrophobic tail groups and hydrophilic head groups and polymers are large molecules composed of repeating structural units typically connected

by covalent bonds. The high compressibility of microbubbles makes them much more efficient scatterers of ultrasound than red blood cells and injecting a suspension of microbubbles intravenously into the systemic circulation enables the contrast between blood vessels and the surrounding tissue in an ultrasound image to be improved by several orders of magnitude (Stride and Safari 2003, Wells 2001).

Gas microbubbles were employed initially with conventional (B-mode) imaging methods to provide enhancement of the backscattered signal and hence in the definition of features such as the endocardium in echocardiography (Gramiak *et al.* 1969). Subsequently, they were used to improve the sensitivity of Doppler measurements by increasing the amplitude of the signal from blood vessels (Bleeker *et al.* 1990). It was found, however, that greater benefits could be derived by exploiting the non-linear behaviour of contrast agent particles (CAPs) and this led to the development of harmonic imaging (Schrope *et al.* 1992) and subsequently "Pulse Inversion" imaging (Simpson *et al.*1999), which enables superior image resolution to be attained, and "loss-of-correlation" imaging which enables the sensitivity to small features such as metastases to be greatly increased (Harvey *et al.* 2002).

First generation contrast agents were however made of air filled bubbles and a very weak shell so that they were easily destroyed by the acoustic pressure and therefore could only enhance the vasculature for a very short time. Second generation contrast agents, for example, SonoVue® contains Sulphur Hexafluoride as gas for the microbubbles and for the shell a phospholipidic monolayer. This composition makes the agent stable and resistant to acoustic pressure and allows for real-time imaging. Depending on the frequency and amplitude of the ultrasound wave, SonoVue®

microbubbles may show a continuous image or a transient response. Although the surrounding tissue also responds with a harmonic answer, the remarkable property of SonoVue® microbubbles is that at harmonic frequencies, the echoes of SonoVue® microbubbles are considerably larger than that of tissue. Contrast specific imaging modes can accurately discriminate between the harmonic response from microbubbles and the soft tissue (Holsbeke and Timmerman 2005). A harmonic frequency is a multiple of a fundamental frequency. A fundamental frequency of 500 Hz has a first harmonic frequency of 1000 Hz, double the fundamental frequency. Its second harmonic is 1500 Hz, the third harmonic is 2000 Hz and so on.

2.2.3. Targeted contrast enhanced ultrasound imaging

The idea of targeted contrast-enhanced ultrasound centers around the use of gas-filled microbubbles with ligands attached to them. A targeting ligand (or a mixture of targeting ligands) may be attached to the shell of the ultrasound contrast agent either before or after the contrast microbubble has been assembled, depending on the chemical composition of the agent. For example, protein-coated microbubbles possess primary amino groups on the albumin shell. These amino groups can be used for covalent coupling of the ligand to preformed bubbles. Alternatively, a ligand can be first covalently attached to an anchor residue that will incorporate in the shell when the latter is formed around the bubble. Otherwise, the anchor might be incorporated in the microbubble first, and attached to the ligand after the bubble/shell assembly has been completed. The anchor can be either lipid or polymer/protein that is compatible with the microbubble shell. To incorporate it in the shell, it is simply added to the aqueous phase containing other shell components prior to microbubble preparation. One can use covalent (**Figure 2.2**a) or noncovalent (e.g. via an avidin-biotin pair, **Figure 2.2**b)

means of attachment of the ligand to the preformed microbubble shell. It is also possible to insert a long flexible polymer spacer arm (**Figure 2.2**c), for instance, poly (ethylene glycol) between the anchor molecule and the ligand (Klibanov 1999, Hughes *et al*. 2003).

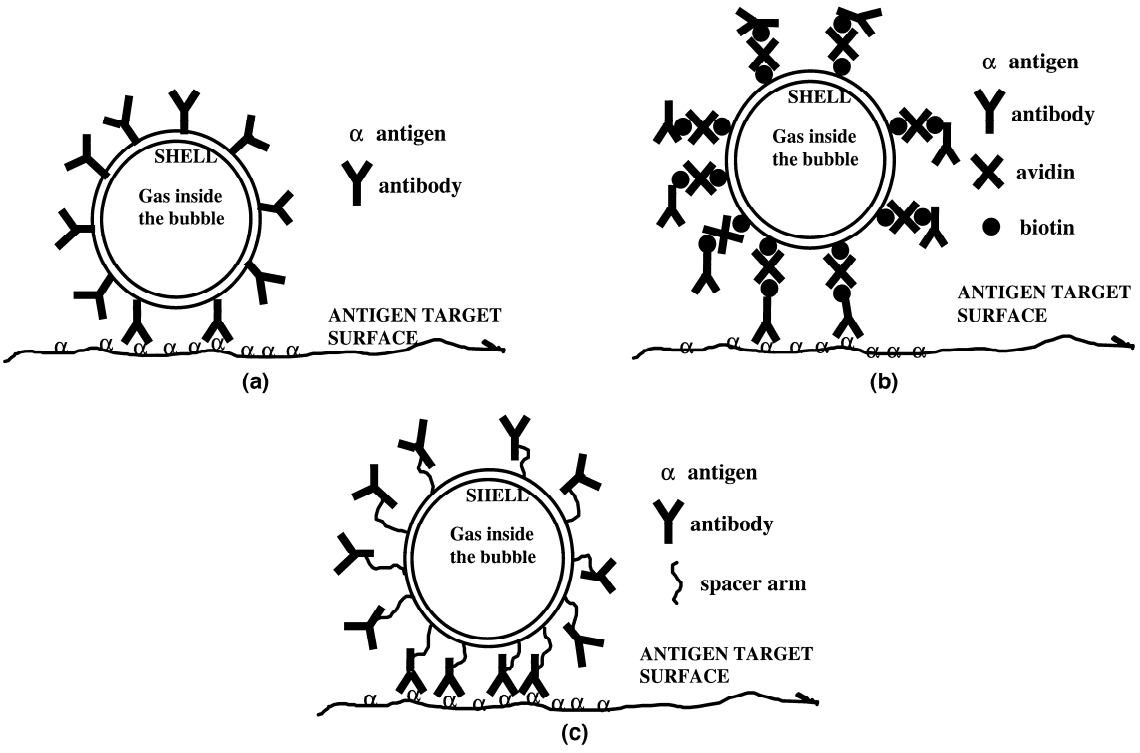

Figure 2.2. Schematic showing the attachment of ligands to microbubble surface: (a) direct, (b) via avidin-biotin bridge, (c) via a flexible spacer arm (Klibanov 1999, Ferrara *et al.* 2007).

Microbubbles theoretically travel through the circulatory system, eventually finding their respective targets and binding specifically. Ultrasound waves can then be directed on the area of interest. The targeted microbubbles reflect a unique echo that stands in stark contrast to the surrounding tissue due to the orders of magnitude mismatch between microbubble and tissue echogenicity. The ultrasound system converts the strong echogenicity into a contrast-enhanced image of the area of interest, revealing the location of the bound microbubbles (Klibanov 1999, Dayton and Ferrara 2002). Detection of bound microbubbles may then show that the area of interest is expressing that particular molecule, which can be indicative of a certain disease state, or identify particular cells in the area of interest (Linder 2004).

2.2.4. Ultrasound assisted drug delivery

In addition to their use in diagnostic imaging, microbubbles with shells have also shown great promise in therapeutic applications such as targeted drug delivery, thrombolysis, and gene therapy and focused ultrasound surgery (Mizushige *et al.* 1999, Poliachik *et al.* 1999, Schmidt and Roessling 2006, Unger *et al.* 2001). Drugs or DNA can be incorporated into the microbubble coating, traced through the body using low intensity ultrasound and then released by destroying the microbubbles with high intensity ultrasound at a target site such as a tumour. By localizing the treatment in this way, the use of microbubbles and ultrasound has become an effective method of tumour therapy and the harmful side-effects from chemotherapy can be reduced (Bao *et al.* 1997, van Wamel *et al.*2004).

The destruction of the microbubbles may also enhance the uptake of the drugs by temporarily increasing the membrane permeability of the nearby cells known as

sonoporation or cellular sonication. The shell membrane can be permeabilised when subjected to short ultrasound pulses. This effect is enhanced when a contrast microbubble is vibrating nearby the cell. This membrane alternation can be reversible leaving the shell viability unaffected. Radionuclides have shown to be effective in tumour therapy. The use of sonoporation in the treatment of tumours has increased the anti-tumour efficacy of radionuclide treatment (van Wamel *et al.* 2004). Recently it has further been suggested that contrast agent particles may also be used to monitor anti-angiogenic therapy induced changes in tumour volume and to inhibit the development of blood vessel networks supplying cancerous tumours (angiogenesis) (Forsberg *et al.* 2004) and this is a growing area of research.

2.2.5. Acoustic behaviour of ultrasound contrast agents

2.2.5.1. Development of ultrasound contrast agents

The discovery of microbubbles as acoustic contrast agents came from a chance observation by a cardiologist, Dr. Claude Joyner, in the late 1960s. Dr. Joyner, while performing M-mode echocardiogram to identify and observe the wall of the aortic root, observed transient increase in the ultrasound (US) signal after each supravalvular aortic injection of saline solution (Gramiak and Shah 1968). The first publication on contrast agent echocardiography can be traced back to an article in 1968 by Gramiak and Shah, who investigated the echo enhancement achieved by injecting indocyanine green dye (Gramiak and Shah 1968). Subsequent research by both Gramiak and an electrical engineering graduate student Fred Kremkau, showed that the enhancement in US was a result of small bubbles forming at the tip of the catheter and not from the dye itself (Goldberg *et al.* 1997b).

Coating layers (shells) not only protect microbubbles during storage and handling, but also influence their acoustic properties. Microbubbles with no shells can respond to ultrasound with large amplitude non-linear oscillations, but amplitudes, scattering cross section, and non-linearity can be much reduced by thick or more rigid shells. Resonance frequency increases with thickness and stiffness of shells. However, short ultrasound pulses of diagnostic amplitudes can also disrupt bubble shells. After shell rupture, air microbubbles have short lifetimes, comparable to dissolution times of free bubbles of the same size, typically 1-30 ms. The acoustic behaviour of CAPs is complex because many, often non-linear, effects are associated with the interaction of ultrasound waves, bubbles, and other objects like red cells or vessel walls (Uhlendorf *et al.* 2000).

2.2.5.2. Linear acoustic properties of contrast agents

All CAPs behave linearly at sufficiently low driving amplitude, but some diagnostic scanners do not allow to reduce transmit amplitudes in all imaging modes to such a lower level without external acoustic attenuation. Other scanners do allow amplitude variation over a very wide range without a dramatic loss of image quality in fundamental B-mode. While transmit levels need not necessarily affect pre-contrast images, absolute acoustic pressure amplitudes *in-situ* become extremely important in ultrasound contrast imaging with microbubbles of CAPs. The upper end of the linear range depends on elastic shell properties. In the range of linear CAP response, tissues also scatter linearly and can produce a significant background. Enhancement of 25-30 dB can only be obtained with a background as low as for blood in large vessels or heart chambers, or when in very small objects no shadowing is seen. However, enhancement at low amplitude in linear imaging mode is severely affected when the tissue background is high. In tissues like heart muscle or liver this occurs in regions

where blood vessels are acoustically not resolved. In addition, blood flow in these regions is too slow for conventional Doppler detection (Uhlendorf *et al.* 2000).

2.2.5.3. Non-linear acoustic properties of contrast agents

The main examples of non-linear behaviour of an aqueous medium without bubbles are: (1) propagation of high amplitude waves and (2) acoustic streaming by radiation force. Radiation forces increase when bubbles are added, but also new acoustic non-linearities arise: (1) non-linear behaviour of bubble shells leading to air bubble dissolution after shell rupture and (2) non-linear pulsation of bubbles. Non-linear wave propagation, and much larger non-linear effects found for many CAPs, allows applications in diagnostic imaging. Non-linear propagation of ultrasound in tissue or water without bubble, apparently a small effect, is important because it improves image quality in tissue harmonic imaging (HI) without CAP, but it adds to the background in HI with CAP. When a stabilizing coating layer is sufficiently elastic, microbubble pulsation can be very strong and non-linear. For diagnostic contrast imaging, it is essential that higher harmonics and/or sub-harmonics of the transmit frequency can be generated much more easily by bubbles than by non-linear propagation in tissue (Uhlendorf *et al.*2000, Stride *et al.* 2008).

2.2.6. Importance of size control in microbubbles for ultrasound imaging

The current methods of producing lipid-encapsulated microbubbles consist of sonication and mechanical agitation. The use of either method results in the production of polydisperse microbubbles. Currently available ultrasound contrast agents have a fairly wide size distribution. An FDA approved ultrasound contrast agent, DEFINITY® (Bristol-Myers Squibb Medical Imaging, NY, USA), has a mean diameter of 1.1-3.3 µm

with a maximum bubble diameter as large as 20 μm. Encapsulated microbubbles are highly echogenic because of differences in compressibility and density between the microbubble and the surrounding fluid. One of the unique properties of microbubble contrast agents is that they resonate when excited in an ultrasound field, which permits detection strategies where the signal from contrast agents is differentiated from that of surrounding tissue. Because the resonance frequency of a bubble is directly related to its size and available ultrasound systems have limited-frequency bandwidth, it is optimal to have an entire population of contrast agents of the same diameter matched to the bandwidth. Therefore, the size and monodispersivity of contrast agents are important in diagnostic and therapeutic applications with ultrasound (Dayton and Ferrara 2002, Talu *et al.* 2006).

2.3. Conventional preparation methods of microbubbles

In order to prepare microbubble suspensions, a gas is usually dispersed in a liquid containing surfactant or other material that is to cover the surface of the bubble. This is normally achieved either with the assistance of a sonicator or a high-shear mixer. During the dispersion of gas in the liquid, the coating material moves onto the newly formed gas-liquid interface and deposits there. However, this method has the disadvantage of producing a broad size distribution and it is necessary to filter out microbubbles having diameters > 10 μm. Even then, the remaining size distribution is still relatively broad, resulting in a wide range of microbubble resonance frequencies (Klibanov 1999).

Use of differential centrifugation to isolate microbubbles of desired size range from a sonicated suspension of microbubbles has been investigated by several research groups.

Previously, using differential centrifugation, microbubbles of < 700 nm were isolated from a sonicated suspension of surfactants to target cells outside the capillaries (Oeffinger and Wheatley 2004). Recently, microbubbles with diameters 1-2 µm and 4-5 µm were isolated from a mutimodal suspension of lipid-coated perfluorobutane-filled microbubbles with a low polydispersivity ranging from 2%-15% (Feshitan *et al.*2009). Although other reported methods such as spray drying, solvent evaporation and freeze drying are adequately developed, they are considered to be too complicated owing to the large number of processing steps involved and usually require organic solvents (Schmidt and Roessling 2006).

2.4. Behaviour of microbubbles

Early contrast agents could not achieve left-sided cardiac opacification because these microbubbles could not traverse the pulmonary circulation and remain intact. When a microbubble with a thin shell is introduced into the blood stream, the gas within the bubble immediately begins to leak into the blood. Such transfer of gas from bubble ultimately results in the dissolution of the microbubble. The specific shell materials and gas used determine the properties of microbubbles, including stability, fragility. Stability, perhaps the most important property of a microbubble, has been achieved by new generation agents through the use of shells or surfactants and by substituting high-density, high molecular weight gas for air. Today's agents readily achieve opacification, not only of the cardiac chambers but also of the myocardium (Raisinghani and DeMaria 2002).

Injecting gas bubbles into the blood may seem potentially dangerous, however, it has been shown that the small volumes used in imaging (< 200 µl) are safe (Nanda and

Carstension 1997). There are certain requirements that a contrast agent needs to meet. The agent should not alter the blood flow, it should be less than 8 μm in diameter to pass unimpeded through the circulation, and should be stable enough to perfuse the tissue and last the duration of imaging (Jong and Cate 1996).

2.4.1. Dissolution of microbubbles

The ultrasound contrast agent in ultrasound field backscatters part of the energy and attenuates the passing ultrasound beam. The backscattering properties deteriorate with time and this may present a serious problem when using contrast agent particles for clinical purposes. The deterioration is associated with shrinkage of gas spheres, caused by outward diffusion of gas from the sphere into the surrounding liquid through the encapsulating shell (Krasovitski and Kimmel 2006).

The Laplace equation relates the difference in pressure on either side of the microsphere surface, ΔP, to the uniform surface tension (γ): $\Delta P = 2\gamma/R$; where R is the radius of microsphere. If the microbubble surface is not rigid but is compressible, the size of the microsphere will continue to decrease in order to satisfy the principle of the energy minimization. However, for continuous shrinking of the bubble, gas has to leak out of the bubble and the decrease in the microbubble size will increase ΔP and if the encapsulated gas pressure is higher than the collapse pressure of the microbubble surface, the microbubble will be destroyed (Wang *et al.* 1996).

2.4.2. Stabilization of microbubbles

First generation microbubbles are filled with ordinary air and these air microbubbles disappear in a few seconds after intravenous administration as the solubility of air in

blood is high. Therefore, they are not useful for opacifying the left cardiac chamber. Improved stability and survival was reached by stabilizing microbubbles with a thin shell of a material such as albumin or galactose palmitic acid. These microbubbles are capable of passing the pulmonary capillary bed, but cannot resist arterial pressure gradients. To increase stability of microbubbles further, second generation contrast agents are filled with a high molecular weight gas such as sulphur hexafluoride or perflouropropane, which decreases solubility, thus improving survival and stability under higher pressure. For example, SonoVue®, a second generation contrast agent, is a phospholipid-coated, sulphur hexafluoride containing microbubble used in diagnostic imaging (Dijkmans *et al.* 2004, Cui *et al.* 2005).

2.4.2.1. Effect of surface tension and gas concentrations on the stability of microbubbles

The Laplace equation for the pressure difference across the surface of a bubble can also be expressed as (Krasovitski and Kimmel, 2006):

$$p_L = p_b - p_o = \frac{2\sigma}{R} \qquad (2.1)$$

Where, p_L is the Laplace or over-pressure, p_b is the pressure of the gas inside the bubble and p_o is the ambient pressure, R is the radius of the bubble and σ is the interfacial (surface) tension at the bubble surface. From equation (1) it is clear that a bubble subject to a higher surface tension will experience a higher over-pressure and so tend to dissolve more rapidly.

Even in the absence of surface tension, the presence of a gas concentration gradient between the bubble and the surrounding liquid will provide an additional driving force for microbubble dissolution. Clearly, this will depend upon the difference between the initial dissolved gas concentration (c_i) in the aqueous medium and the dissolved gas

concentration at the bubble surface (c_s). The gas in the bubble is in equilibrium with the gas concentration at the bubble surface and is therefore equal to c_s (Duncan and Needham, 2004). When $c_s > c_i$, the gas inside the bubble will diffuse outwards into the liquid causing a reduction in the bubble diameter $D = 2R$.

The roles of surface tension (σ) and the role of c_s and c_i in determining the stability of a bubble are well represented by the differential equation, (2), developed by Epstein & Plesset (1950):

$$\dot{R} = \frac{k(c_i - c_s)BT}{M\left(p_o + \frac{4\sigma}{3R}\right)}\left(\frac{1}{R} + \frac{1}{\sqrt{\pi kt}}\right) \tag{2.2}$$

where $\dot{R}$ is the rate of change of bubble radius, k is the coefficient of diffusivity, B is the universal gas constant, T is the absolute temperature, M is the molecular weight of the gas and t is time.

It is clear from eqn (2) that the rate of bubble diffusion will be higher for larger values of ($c_i - c_s$). The third factor affecting bubble stability is the effective diffusivity of the interface, k. Both k and σ will depend upon the gas and liquid under investigation and also the presence of any coating material at the bubble surface which may reduce surface tension and significantly increase the resistance to gas diffusion (Borden and Longo 2002). These quantities will also be affected by the temperature and pressure at the bubble surface, as will the value of the dissolved gas concentration (c_s) there.

An approximate equation which accounts for the effect of surface tension upon c_s can also be derived following Epstein and Plesset as

$$\dot{R} \approx \frac{-kBTc_{sat}\left(1+\frac{2\sigma}{R_o p_o}-\frac{c_i}{c_{sat}}\right)}{Mp_o\left(1+\frac{4\sigma}{3Rp_o}\right)}\left(\frac{1}{R}+\frac{1}{\sqrt{\pi kt}}\right) \tag{2.3}$$

where c_{sat} is the saturation concentration for the gas in the surrounding liquid at a given temperature and pressure and R_o is the initial bubble radius. This equation neglects, however, any dependence of σ, k, or c_s upon the bubble radius R.

The role of shell resistance (R_{shell}) and surface tension of the shell (σ_{shell}) in stabilizing the microbubbles is shown in a modified Epstein-Plesset equation as

$$\dot{R} \approx \frac{L}{\frac{r}{D_w}+R_{\text{shell}}}\left(\frac{1+\frac{2\sigma_{\text{shell}}}{P_a r}-f}{1+\frac{3\sigma_{\text{shell}}}{4P_a r}}\right) \tag{2.4}$$

where L is the Ostwald's coefficient, Dw is the gas diffusivity in water, and $f = c_{\text{i}}/c_{\text{s}}$ (Ferrara *et al*.2007)

2.4.2.2. Stabilization by surfactants

The sonication of mixtures of two non-ionic surfactants such as Span 60 and Tween 80 or Span 40 and Tween 40 produces stable microbubbles. Although a variety of surfactants lend great flexibility to the production of stabilized microbubbles, only some surfactant combinations in certain molar ratios are successful. The surfactant stabilized microbubbles have a solid-condensed monolayer "skin" which functions to reduce the surface tension, prevent coalescence between microbubbles, and increase their aqueous compatibility. The higher surface pressure obtained for the case of a microbubble

preparation indicates that sonication enhances the structure of surfactant monolayer and makes the microbubbles extremely stable (Singhal *et al.*1993, Wang *et al.* 1996).

The stability of bubbles depends on both inter and intra bubble interactions. Span 40 or Span 60 alone cannot form stable microbubbles without an anti-coalescence agent and a component to enhance their aqueous compatibility. Similarly, Tween 40 or Tween 80 alone cannot form stable microbubbles, due to insufficient surface activity to reduce surface tension. For example, Span 40 and Tween 40 can form stable microbubbles by the following methods: (1) The skin of the microbubbles is a solid-condensed zig-zag monolayer in which the head-groups of Tween 40 are squeezed out of the head-group plane of Span 40, (2) The well-packed monolayer inhibits the encapsulated gas diffusion through the surface of the microbubbles, (3) Span 40 functions as a surface-active component to reduce the surface tension, (4) Tween 40 functions by creating an energy barrier to prevent the coalescence of microbubbles and by increasing the compatibility of the microbubbles with the aqueous environment, (5) Sonication enhances the structure of the surfactant monolayer by reducing surface tension to nearly zero (Singhal *et al.*1993, Wang *et al.* 1996).

2.4.2.3. Stabilization by polymers

Although the primary goal of the ultrasound contrast agents is to enhance the diagnostic image, there is a good use of polymeric microbubbles in targeted drug delivery. In designing a contrast agent for therapeutic use, the material of which the shell is composed is critical. Polymeric microbubbles have many advantages; they are stable, provide a good surface to adsorb or carry the drug, and have good shelf life stability. Poly lactic-*co*-glycolic acid (PLGA) is a popular Food and Drug Administration (FDA)

approved biodegradable biocompatible polymer. PLGA slowly degrades by nonenzymatic hydrolysis of the ester backbone into lactic and glycolic acids. Lactic acid is a natural body metabolite and glycolic acid is broken down by enzymes. Both degrade to carbon dioxide and water and produce no toxic effects in the body (El-Sherif and Wheatley 2003). However, it may be necessary to add polymers such as 2-methacryloyloxyethyl phosphorylcholine (MPC) to reduce the inflammatory reaction that may occur on PLGA (Iwasaki *et al.*2002).

2.4.2.4. Stabilization by amphiphilic molecules

The use of amphiphilic molecules such as phospholipid as the coating material is that they self-assemble into a monolayer shell around the gas core, allowing better control of the shell surface architecture and greater flexibility when adding functional molecules. The monolayer shell that coats a microbubble is generally composed of a main phospholipid component with long, saturated acyl chains and an emulsifier with a hydrophilic PEG head-group for optimum production yield, shelf life and *in-vivo* stability. The monolayer shell is typically represented as a homogeneous film, in which these components are fully miscible and uniformly distributed over the entire microbubble surface. In general, hydrophobic chain length will make phospholipid-coated microbubbles more robust. The increased stiffness of the shell for longer chain lengths is attributed to an increase in attractive dispersion forces between the hydrophobic tails of adjacent phospholipid molecules, resulting in a more cohesive shell. Accordingly one might expect to see a decrease in the permeability of the shell to gases as the phospholipid monolayer becomes more cohesive with increasing lipid acyl chain length, leading to a more stable bubble (Borden and Longo 2002, Borden *et al.*

2004, Unger *et al.* 2004). Phospholipid-based gas-filled microbubbles are biocompatible and biodegradable echogenic agents of low toxicity as well (Zhao *et al.*2005).

Several mechanisms for the stabilization of a gas microbubble by a monolayer shell have been proposed. Most of these mechanisms attribute the stabilization effect to mechanical properties of the shell. Yount (1979) described a theoretical "skin" of surface-active molecules that may halt the impetus for dissolution by introducing a mechanical surface pressure that counters the Laplace pressure. Similary, van Liew (1997) argued that the shell reduces surface tension and puts a mechanical limit on the amount that the bubble can shrink. Although Wang *et al.* (1996) suggested three possible mechanisms for microbubble stabilization by the shell, including reduction in surface tension, surface hardening, and resistance to gas transport, shell resistance has been the primary stabilization mechanism for microbubbles coated with lipids (Borden and Longo 2002).

2.4.2.5. Stabilization by high density gases

Gas bubbles, being highly compressible, scatter ultrasound several orders of magnitude more effectively than blood, providing powerful echo and bright contrast. However, simple air bubbles dissolve very rapidly in the blood under the combined action of Laplace pressure, arterial pressure, oxygen metabolism and ultrasound energy, hence have little utility. Perfluorochemical-containing gaseous microbubbles have recently come into the limelight as a result of approval by health authorities of several injectable microbubble suspensions for use as contrast agents for diagnostic ultrasound imaging. Perfluorochemicals, and in particular perfluorocarbons (PFCs), when used as the filling gas or part of it, delay bubble dissolution very effectively, due to very low diffusivity

and low concentration of saturation in blood, thus providing ample time for patient examination. The low diffusivity keeps the gas in the bubble, and the low concentration of saturation would result in rapid saturation of the blood with the gas (Raisinghani and DeMaria 2002, Riess 2003).

The amount of gas that needs to be administered to a patient for effective contrast enhancement is very small, typically on the order of a fraction of 1 ml, dispersed within some 10^8 bubbles a few micrometers in diameter. The PFC is subsequently exhaled by the patient unchanged within minutes. The initially marketed ultrasound contrast agent, Albunex® was a room air bubble with an albumin shell. The currently available commercial ultrasound agents in USA have replaced air with PFCs. Optison™ (GE Healthcare, Princeton, New Jersey, USA) represents the refinement of Albunex® (Molecular Biosystems Inc., San Diego, CA), and it uses perfluoroprapane with an albumin shell (Raisinghani and DeMaria 2002, Riess 2003).

2.4.2.6. Stabilization by proteins

Early ultrasound contrast agents were coated with an absorbed layer of albumin protein. The albumin coated microbubble Albunex® and Optison™ were the first commercially available FDA approved contrast agents. More recently, protein shelled microbubbles have been functionalized to carry targeting ligands. Albumin shell tends to be rigid and less stable to ultrasound, however, and introduces typical immunogenicity issues associated with animal derived materials. Albumin shells are also known to bind complement proteins (Pomper and Gelovani 2008).

2.4.2.7. Microbubble stiffness

The bulk modulus expresses the stiffness of the whole microbubble, composed of gas-filled interior and surrounding shell. Compared to the free gas bubble, the bulk modulus of the shell-encapsulated bubbles is higher due to the shear modulus of the shell. Polymeric microbubbles are approximately 20 times stiffer than free gas bubbles and are 1000 times compressible than water. When three different contrast agents Albunex, polymeric microbubbles, and Sonazoid (a lipid shelled microbubble) are compared, three agents are different, with the Albunex and polymer microbubbles being the stiffest, and Sonazoid being considerably more flexible with a bulk modulus of 600 kPa, which is about 6 times the stiffness of a free gas bubble (Hoff L, 2001).

Table 2.1. Examples of some ultrasound contrast agents

Agent	Shell material	Gas
Albunex®	Sonicated human serum albumin	Air
Bisphere™	Polymer–protein bilayer	Air
Echovist®	None	Air
Filmix™	Phospholipid	Air
Levovist®	Palmitic acid	Air
Quantison™	Spray dried serum albumin	Air
Sonavist™	Cyanoacrylate	Air
EchoGen®	Surfactant	Perfluoropentane
Aerosomes™	Phospholipid	Octafluoropropane
Definity™	Phospholipid	Octafluoropropane
Optison™	Cross-linked human serum albumin	Octafluoropropane
Imagent®	Stabilized surfactant	Perfluorohexane & Nitrogen
Imavist™	Surfactant	Perfluorohexane & Air
SonoVue®	Phospholipid	Sulphurhexafluoride

2.5. Some ultrasound contrast agent particles

There are a number of commercialized and non-commercialized ultrasound contrast agents available. A selection of them is listed in Table 2.1 giving their material compositions. (Grayburn 2002, Stride and Edirisinghe 2008). The extensive use of PFCs as gas in CAPs is very clear from the above **Table 2.1.**

2.6. Polymer based drug delivery

The development of polymer based drug and gene delivery systems, particularly controlled drug delivery systems, have been practical only in recent years, but within a short time they have had an impact on almost every branch of medicine including cardiology, ophthalmology, endocrinology, oncology, pulmonology and pain management. Some of the major advantages of these systems are continuous maintenance of drug levels in a therapeutically desirable range, reduction of harmful side effects due to targeted delivery to a particular cell type or tissue, potentially decreased amount of drug needed, decreased number of doses and facilitation of drug administration for pharmaceutical use with short in-vivo half lives (for example peptides and proteins). However, these advantages also must be weighed against the following concerns in the development of each particular drug delivery system: (1) toxicity of the materials (or their degradation products) from which the drug is released, or other safety issues such as unwanted rapid release of the drug (dose dumping); (2) discomfort caused by the system itself or the means of insertion; and (3) expense of the system due to the drug encapsulation materials or the manufacturing process (Langer 1998).

Providing control over the drug delivery can be the most important factor at times when traditional oral or injectable drug formulations cannot be used. These include situations requiring the slow release of water-soluble drugs, the fast release of low-solubility drugs, drug delivery to specific sites, drug delivery using nanoparticulate systems, delivery of two or more agents with the same formulation, and systems based on carriers that can dissolve or degrade and be readily eliminated. An ideal drug delivery system should be inert, biocompatible, mechanically strong, comfortable to patient, capable of achieving high drug loading, safe from accidental release, simple to administer and remove, and easy to fabricate and sterilize (Brannon-Peppas 1997).

2.6.1. Polymers used for delivery systems

A range of polymeric materials including polyurethanes, polysiloxanes, polyvinyl alcohol (PVA), polyethylene, polyethylene glycol, polylactides (PLA), polyanhydrides, polyorthoesters, polyglycolides (PGA), poly(lactide-co-glycolides) (PLGA), are employed for drug delivery because of their desirable physical properties such as elasticity, insulating ability, physical strength and transparency, toughness and lack of swelling, suspension capabilities, and free of leachable impurities. Many of these materials are designed to degrade within the body (Langer 1998, Brannon-Peppas 1997).

In the treatment of various diseases or conditions that result from lack of simple hormones or peptides, the use of polymeric nano/micro particles as effective carriers of drugs or genes has been widely accepted as peptide drugs and small peptides can be easily degraded by proteolytic enzymes and hence cannot reach their targeted sites by oral administration (Maysinger and Morinville 1997). The biodegradable polymers such

as polylactide (PLA) homopolymers and copolymers have been extensively investigated as they have shown no adverse tissue reactions when carrying drugs and these biodegradable polymeric carriers can be hydrolyzed in the body to form products that can be easily eliminated and that removing these implants by surgery are not needed. Also, introducing polyethylene glycol (PEG) into polylactic acid homopolymers could increase degradation rate, decrease the acidity of degraded products, and increase hydrophilicity of polymer carriers (Maysinger and Morinville 1997, Huang *et al.*1997).

Enteric polymers such as cellulose acetate phthalate, which are preferentially soluble in the less acidic environment of the intestine, are used to prepare enteric nano/micro particles to deliver a drug to a particular region of intestine or colon as these enteric polymer particles protect the gastric mucosa from drug irritation and prevent drug degradation in the stomach by enzymes or acidic fluids (Dong and Bodmeier 2006).

Biocompatible polymers such as alginate, a linear copolymer, are used in cell technology as encapsulating materials as this permits the transportation of non-human cells that are considered as an alternative to the limited supply of the donor tissues (Marua *et al.* 2008). In order to develop an alternative approach to somatic gene therapy, alginate microcapsules have been used to provide immunological protection to deliver a therapeutic protein by implanting "universal" recombinant cells (Barsoum *et al.* 2003). For the delivery of macromolecular drugs, poly (lactide-co-glycolide) (PLGA) based *in-situ* polymer systems have been used as extended release parenteral drug delivery systems (Korber and Bodmeier 2008).

Polymeric particles used as drug delivery systems are also defined as colloidal systems made of solid polymers that may be classified according to their manufacturing method and size. In this case, particle is a collective term used for capsules and spheres. Nano/micro capsules are composed of a polymeric wall containing a liquid inner core whereas nano/micro spheres are composed of a polymeric porous structure in which the drug can be dispersed throughout (Delie and Blanco-Prieto 2005). The sizes covered by 'nano' ranges from 1 nm to 100 nm and by 'micro' ranges from 100 nm to 1000 μm. Bio-structures that are handled in biotechnology include nano and micro sizes and which size is relevant is decided depending on the application (Whitesides 2003).

2.6.2. Traditional drug dosing and controlled- release drug dosing

The goal of many of the original controlled-release systems was to achieve a delivery profile that would yield a high drug level of the blood over a long period of time. With traditional tablets or injections, the drug level in the blood follows the profile shown in **Figure 2.3**a, in which the level rises after each administration of the drug and then decreases until the next administration. The key point with traditional drug administration is that the drug level of the agent should remain between a maximum value, which may represent a toxic level, and a minimum value, below which the drug is no longer effective. In controlled drug delivery systems designed for long-term administration, the drug level in the blood follows the profile shown in **Figure 2.3**b, remaining constant, between the desired maximum and minimum, for an extended period of time. Depending on the formulation and the application, this time may be anywhere from 24 h (Procardia XL) to 1 month (Lupron Depot) to 5 years (Norplant) (Brannon-Peppas 1997).

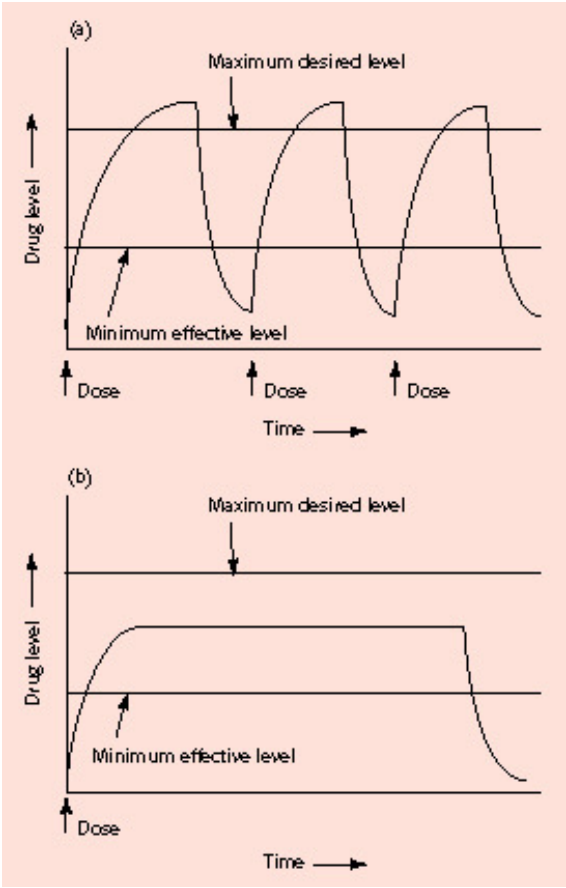

Figure 2.3. Drug levels in the blood with (a) traditional drug dosing and (b) controlled-delivery dosing (Brannon-Peppas 1997).

2.6.3. Drug delivery approaches

There are three general approaches by which drugs are delivered from polymer systems. In one approach (reservoir system, **Figure 2.4**a), drug diffuses through a polymer membrane, the drug is physically entrapped inside a polymer that can then be injected or implanted in the body. Early forms of these systems involved non-degradable polymers such as silicone rubber, which could release low molecular mass lipophilic drugs for extremely long times (Folkman and Long 1964). This type of approach led to the development of Norplant, small silicone capsules containing contraceptives that are slowly released by diffusion through the polymer for 5 years. However, this approach does not permit the slow delivery of either ionic species or molecules with a

relative molecular mass over about 400 g because they are not able to diffuse through such polymers. To address this problem, drugs were physically embedded in polymers at concentrations high enough to create a series of interconnecting polymers (matrix system, **Figure 2.4**b) through which the drug that is evenly distributed could subsequently slowly diffuse through the polymer (Langer and Folkman 1976). The third approach (osmotic system, **Figure 2.4**c), the combination of diffusion through pores as well as polymer matrix degradation, has provided the basis for injectable delivery systems lasting for 1 to 4 months for normally short-lived hormones (Ogawa *et al.*1988)

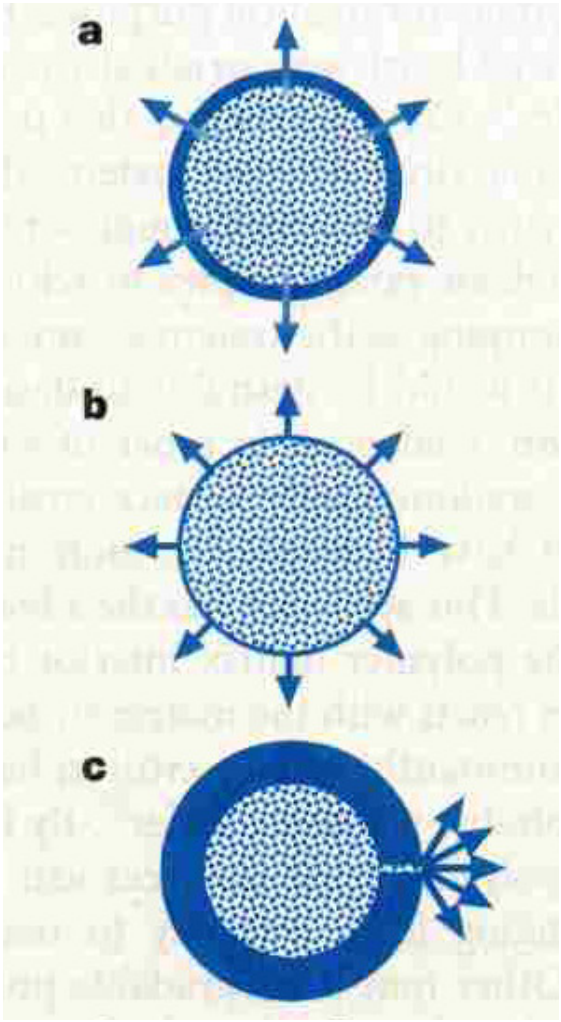

Figure 2.4. Schematics of polymer-based drug delivery systems: (a) Reservoir system, (b) Matrix system and (c) Osmotic system. Small dots represent drug and arrows show the direction in which drug is released (Langer 1998).

2.7. Polymeric microspheres for tissue engineering

Tissue engineering has emerged as a viable alternative to the problem of organ and tissue shortage. The use of microspheres of biodegradable polymers for tissue engineering is an emerging area of application of microspheres in medical engineering (Borden *et al*.2002). As a consequence of our aging and longer-living population, skeletal reconstruction requiring bone grafting has become a routine procedure for the orthopaedic surgeon. For autogenous bone graft (autograft), patient-derived bone tissue is extracted from a healthy site of a patient's body and grafted into a site in need of repair. However, the use of autograft has several distinct disadvantages, including significant postsurgical pain at the site of removal, increased operative time, blood loss, additional costs, and a limited supply (Goulet *et al.*1997). Three dimensional synthetic scaffolds of thermally sintered microspheres of biodegradable polymers are being currently investigated as bone-tissue replacements; however, ideal scaffolds must provide appropriate mechanical support, which is particularly important for bone tissue engineering (Botchwey *et al.*2004, Jones and Boccaccini, 2005,). The issues to be addressed when selecting biodegradable materials are the effect of degradation products in the body, the influence of the body environment on the degradation rates, and the resulting time frame of the degradation process (Borden *et al.* 2002, Botchwey *et al.* 2004).

2.8. Conventional preparation methods of microspheres

Preparation of microcapsules dates back to the early 1950s, when Green and Schleicher produced microencapsulated dyes for the manufacture of carbonless copying paper. Since then, and particularly since the mid-1970s, microencapsulation has become increasingly popular in pharmaceutical technology as well as for many other products

and processes in daily use. For certain products, a single reason may provide sufficient justification for microencapsulation, while for others microencapsulation may have several advantages. In pharmaceutical technology, for example, the overriding reason for microencapsulation is (at present) controlled release. However, increased stability, masking of taste and odour, etc., may also be the primary or contributory reasons for microencapsulation. Microspheres and microcapsules are manufactured from a wide range of monomeric and polymeric materials and by a large number of different polymerization techniques and microencapsulation processes, as indicated in **Table 2.2.** Thus, in practice, appropriate combinations of starting materials and manufacturing methodology can be chosen to produce microspheres and microcapsules having a wide variety of compositional and morphological characteristics. In certain instances, it may be possible to produce practically similar microcapsular products by two different manufacturing techniques. It is also possible to prepare two or more morphological patterns using a single formulation by procedural modification of a single manufacturing process. Suspension cross-linking, coacervation and solvent evaporation are considered most important among the methods tabled (Arshady 1989).

Table 2.2. Major Microencapsulation techniques (Arshady 1989)

From monomeric starting materials	From polymeric starting materials
Suspension polymerization	Suspension cross-linking
Emulsion polymerisation	Coacervation/phase separation
Dispersion polymerization	Solvent evaporation/extraction
Precipitation polymerization	Polymer precipitation
Suspension polycondensation	Polymer chelation
Dispersion polycondensation	Polymer gelation
Precipitation polycondensation	Polymer melt solidification
Interfacial polycondensation	

2.8.1. Suspension cross-linking

Preparation of polymer microspheres/microcapsules by suspension cross-linking is basically similar to suspension polymerization. It involves the formation of a stable droplet suspension of the polymer solution (or melt) in an immiscible liquid, gradual hardening of the droplets by covalent cross-linking, and finally recovery of the resulting cross-linked polymer particles. For the preparation of microcapsules, it is obvious that the core material remains completely within the droplets. This means that the core material (dispersed or dissolved) should have a substantially higher affinity for the droplet phase than the suspension medium. The average size of the droplets must be about one order of magnitude larger than that of the core particles to ensure complete encapsulation (Arshady 1989).

2.8.2. Coacervation/phase separation

This method can be explained by a simple experiment: an aqueous solution of gelatine is prepared and maintained at 40-60^{0}C. Drop-wise addition of ethanol to this solution leads to the formation of a two phase-system, in which the concentration of gelatine in one phase is higher than that of the other phase. This phase separation takes place because the most favourable water-ethanol interactions in the three component mixture gradually reduce gelatine solvation (hydration). This, in turn, leads to increased interactions between polymer molecules themselves, and hence the formation of partially desolvated macromolecular aggregates or coacervates. The individual polymer coacervates formed in this way gradually approach each other and form a macroscopic coacervate phase (i.e., phase separation) (Arshady 1990).

2.8.3. Solvent evaporation/extraction

The method adopted for the production of nanospheres with wide range of polymers can be given as an example to explain this technique. A performed polymer is dissolved in a volatile organic solvent (e.g., chloroform, ethyl acetate, methylene chloride), and the organic solution is dispersed in an aqueous phase to form an oil/water emulsion, in the presence of a surfactant (e.g., polysorbate, poloxamer, sodium dodecyl sulphate) or a stabilizer such as poly(vinyl alcohol) (PVA). Continuous emulsification under stirring prevents coalescence of the organic droplets and can be further improved by sonication or microfluidization with a high pressure homogenizer. The extraction of the solvent from the nanodroplets is achieved by evaporation at room temperature under stirring or in a rotary evaporator under reduced pressure. As a consequence of this extraction, the polymer precipitates leading to the formation of nanospheres (Julienne *et al.* 1992).

2.9. Microfluidic flow focusing technique for microbubbling

In the flow focusing technique, a liquid is injected through a capillary tube whose exit is located close to a small hole drilled on a thin plate. A stream of another fluid (gas or liquid) surrounding the tube is forced through the hole. The mechanical stress exerted by this stream deforms the meniscus attached to the tube exit. Then, the meniscus develops a cusp like shape from whose vertex a thin jet is issued (Loscertales *et al.* 2002).

2.9.1. Formation of microbubbles at high values of Reynolds number

One of the first systems that demonstrated high-throughput formation of monodisperse microbubbles with diameters in the range of tens to hundreds of micrometers was an axi-symmetric flow focusing device (Ganan-Calvo and Gordillo 2001). In this system

(**Figure 2.5),** a gas is continuously supplied through a capillary tube which terminates a few hundred micrometers upstream of an orifice-a hole of diameter D= 100 or 200 µm-fabricated in a metal plate (50 µm thick). The liquid flows around the capillary that delivers gas and into the orifice. The flow of liquid focuses the tip of the stream of gas into a cusp-like geometry with a thin ligament extending into and through the orifice. This ligament bulges into a growing bubble downstream of the orifice and breaks of at a constant frequency. The flow of the fluids typically proceeds at high Reynolds numbers ranging from 50 to 1400 and as such the dynamics of flow is dominated by inertial effects and that the diameter of the bubbles can be calculated on the assumption that viscous effects are negligible. The equation put forward was, $d_b/D = 1.1\ (Q_g/Q_l)^{0.4}$, where d_b is the bubble diameter, D is the orifice diameter, and Q_g and Q_l are gas and liquid flow rates, respectively (Garstecki *et al.* 2005).

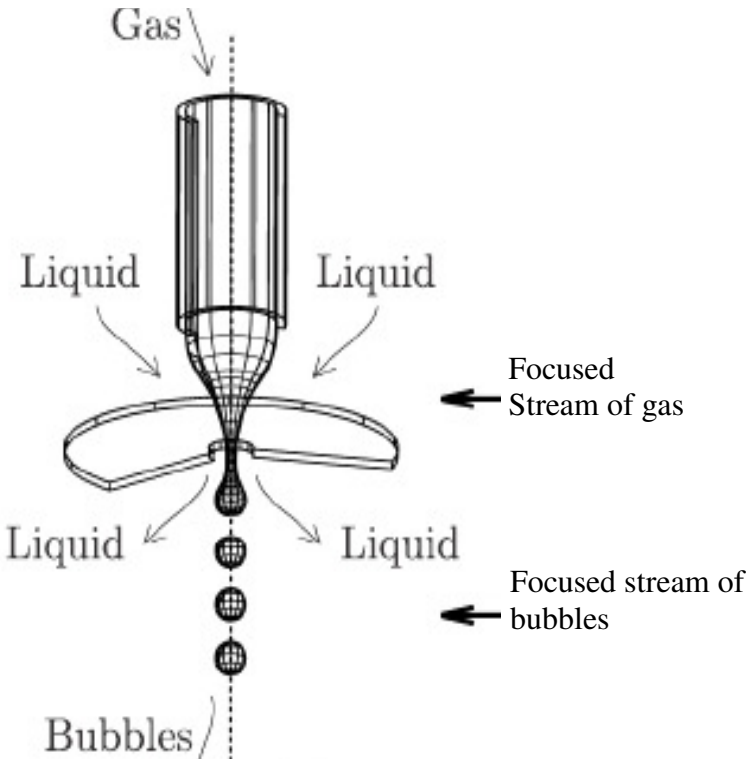

Figure 2.5. Schematic representation of an axi-symmetric microfluidic flow focusing setup for liquids with high Reynolds number (Garstecki *et al.* 2005).

2.9.2. Formation of microbubbles at low values of Reynolds number

Figure 2.6 is the schematic of the microfluidic flow-focusing device that can be operated at low to moderate Reynolds numbers and as such viscous effects are important in this system. The two immiscible phases flow down the inlet channels (one inlet channel for gas, and the two outer channels for liquid) and meet at the junction of these channels upstream of the orifice. The pressure drop along the axis of the system forces the fluids through this orifice; the tip of the stream of gas enters the orifice and inflates a gas cavity downstream of the orifice. This cavity (a growing bubble) displaces and pushes away the liquid in the outer channel. Subsequently, the neck connecting the inlet for the gas with the growing bubble breaks, and the bubble is released in the outer channel. Over a wide range of pressures (p) applied to the stream of gas, and of rates of flow (Q_l) of the liquid, the system establishes a periodic state, in which, in each period, the tip enters the orifice, inflates a bubble, breaks, and retracts upstream of the orifice. For a constant pressure applied to the stream of gas, an increase in the rate of flow of the liquid results in a decrease of the volume of the bubbles. For a fixed rate of flow of the liquid, an increase of pressure results in an increase of the size of the bubbles. The scaling put forwarded was that, $V_b \propto p / Q_l \mu$, where V_b is the volume of the bubbles, and the μ is the dynamic viscosity of the liquid (Garstecki *et al.* 2004).

2.10. Electrohydrodynamic Atomization (EHDA)

Electrohydrodynamic atomization is a phenomenon where a liquid is passed at a controlled flow rate through a capillary needle maintained at several kilovolts relative to a ground electrode few centimetres away (**Figure 2.7**). The disruption of a liquid surface into a spray of charged droplets when subjected to an intense electric field has been known for more than two centuries since Bose recorded the phenomenon in 1745.

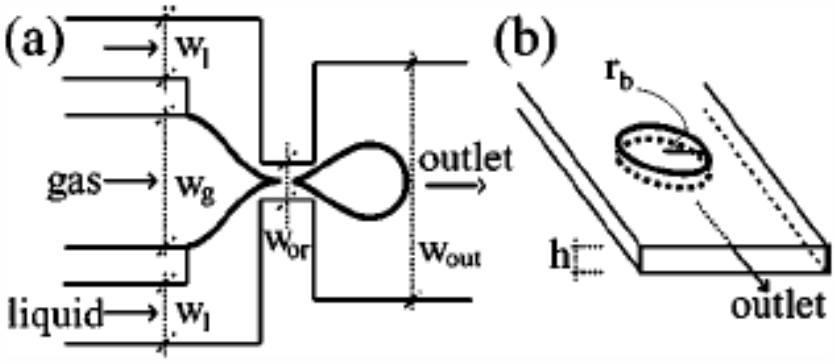

Figure 2.6. Schematic representation of an axi-symmetric microfluidic flow focusing device for liquids with low Reynolds number. (a) Top view of the device, w_l= 250 µm and w_g = 200 µm for the liquid and gas, respectively. w_{or} = 30 or 60 or 90 or 120 µm, and w_{out} = 250 or 500 or 750 or 1000 µm. (b) Illustration of a bubble in the outlet channel, h= 28 µm, r_b= radius of the bubble-wall interface (Garstecki *et al.* 2004).

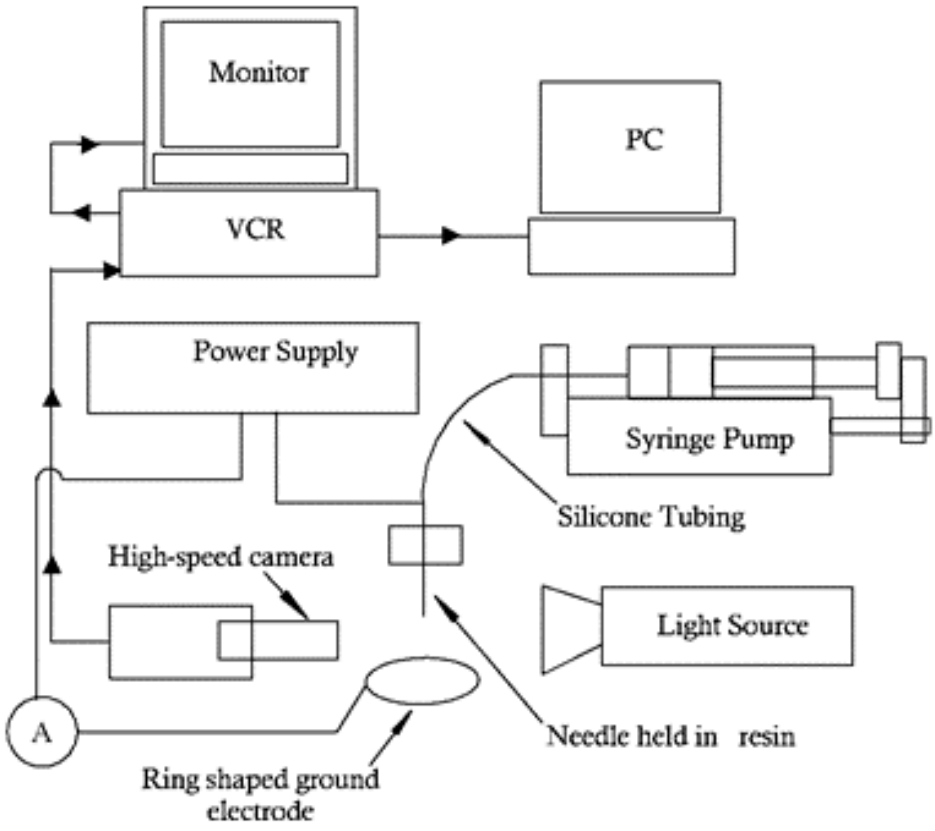

Figure 2.7. Schematic representation of the electrohydrodynamic atomization rig (Jayasinghe and Edirisinghe 2003).

This phenomenon was later explained as the action taking place on a liquid drop of electric forces opposing those of surface tension. Rayleigh (1879) found that when the charge on the drop reaches a certain value, the electric forces become stronger than those of surface tension, and the drop becomes unstable.

Rayleigh made the earliest observation of instability of a droplet due to electric charge. The stability of a drop is dependent upon the balance of forces, between the outward electrical stresses tending to disrupt the drop and the counteracting surface tension forces which tries to hold the drop together (Rayleigh 1882).

Rayleigh calculated the electric charge beyond which a droplet is no longer stable. This charge is given by the following equation and it is called as Rayleigh limit of the charges (Rayleigh 1882):

$$Q_R = 2\pi (16 \gamma \varepsilon_o r^3)^{1/2} \qquad (2.4)$$

where γ is surface tension of the liquid, ε_o is the relative permittivity of the free space and r is the radius of the liquid droplet.

Pioneering experimental studies on the modes of atomization and droplet formation have been carried out since early periods of the last century. The work carried out by Zeleny in 1914 by subjecting a needle carrying liquid and a ground electrode set-up under a high voltage marked a break-through in this area of research.

Drozin (1955) systematically investigated the electrical dispersion of liquid and found that a liquid with negligible dielectric constant cannot be dispersed and liquid dispersion

could take place only if the conductivity is below an upper limit. The first explanation for the conical shape of the liquid spray as a hydrostatic balance between electrical and surface tension forces has been put forward in 1964 (Taylor 1964, Zeleny 1917). Taylor (1964) studied the break-up of a droplet using glycerol and glycerol-water mixture when electric field is applied to the capillary tube carrying the liquid. He noticed in his investigations that a conducting liquid with high viscosity does not vibrate before spraying but rather adopt a conical shape. He noticed that the conical shape was having a sharp apex with an angle ~ 49.3^0 with vertical.

Jones and Thong (1971) found that an electrical dispersion of a jet of kerosene into a spray of monodisperse droplets could only be achieved within a range of applied voltage and the droplet size was a function flow rate but independent of the applied voltage. Mutoh *et al.* (1979) claimed that steady state mode exists only if the conductivity of the liquid lies between certain limits.

The conditions necessary to produce smaller droplets were suggested when Nagorynyi and Bezrukov (1980) investigated the decrease in droplet size with increasing applied voltage. Smith (1986) presented his experimental work on the process in terms of liquid properties such as conductivity, surface tension and viscosity.

After Zeleny (1917) and Taylor (1964), the most significant work presented was the classification of modes of spraying by Cloupeau and Prunet-Foch (1990). They identified four different spraying conditions and defined them as spray modes, and described the specific characteristics of each mode in terms particle size distribution of aerosols emitted and the causes of irregularity in drop sizes. The liquid meniscus at the

outlet of the capillary takes various shapes under the action of the electric field including a conical shape, with a thin jet emerging from the cone tip (Tang and Gomez 1994). Among the distinctive properties of the atomization of a liquid by electrostatic means are (1) monodispersivity of the primary droplets, (2) high net charge on the surface of the generated droplets, and (3) controllable droplet size by varying either the flow rate or the electrical conductivity or the applied voltage (Ganan-Calvo *et al.* 1997).

2.10.1. Modes of electrohydrodynamic atomization

Depending on the flow rate and the applied voltage, various modes of atomization can be observed. In general, the spraying modes can be divided into two groups based on the geometrical form of the liquid at the outlet of the capillary and the type of the jet behaviour in its disintegration into droplets. The first group comprises the modes in which only fragments of liquid are ejected from the capillary, i.e., the dripping, microdripping, spindle, multi-spindle, and ramified-meniscus modes. The second group comprises the modes in which liquid issues a capillary in the form of a long continuous jet which disintegrate into droplets some distance, usually a few mm, from the outlet of the capillary. The modes belong to this group are cone-jet, precession, oscillating-jet, multi-jet, and ramified-jet. The meniscus and the jet in the second group can be stable, can vibrate, and rotate spirally around the capillary axis or whips irregularly (Jaworek and Krupa 1999).

2.10.2. Cone-jet mode

In the cone-jet mode the liquid issues from the capillary in the form of a regular, axi-symmetric cone with a thin jet at its apex (**Figure 2.8**), stretching along the capillary axis and breaking up into fine droplets**.**

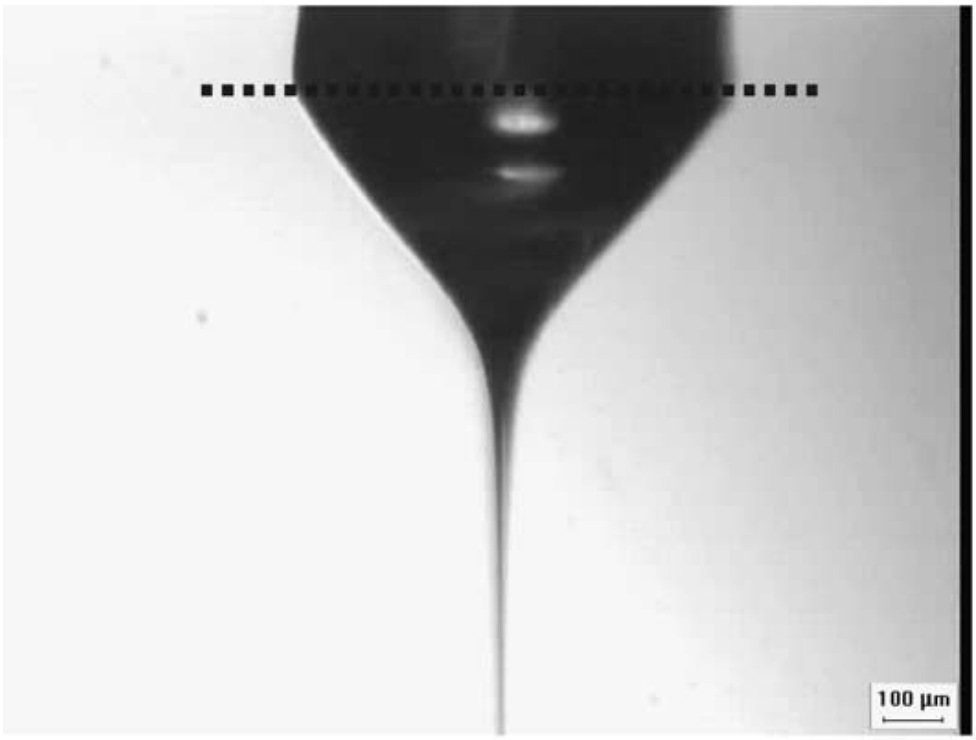

Figure 2.8. Representation of cone-jet mode. An axi-symmetric liquid cone with a thin jet at its apex (Jayasinghe and Edirisinghe 2004).

The liquid is pumped through a nozzle at a low flow rate and a droplet is formed at the tip of this nozzle. An electric field is applied which induces a surface charge in the droplet. As a result of the electric stress, the droplet is transformed into a conical shape. The shape of the liquid cone is a result of the balance of liquid pressure, liquid surface tension, and gravity, electric stress in the liquid surface, the liquid inertia, and the liquid viscosity (Hartman *et al.* 1999a). The applied electric field accelerates the surface charge toward the cone apex. This jet breaks up into a number of primary or main droplets and a number of secondary droplets and satellites (Tang and Gomez 1994).

2.10.3. Process parameters

2.10.3.1. Effect of liquid flow rate on cone-jet mode

The size distribution produced in electrohydrodynamic atomization in the cone-jet mode depends on the diameter of the jet, and on the break-up of this jet into droplets. Every liquid has a minimum flow rate, below which a stable cone-jet mode cannot exist. At this minimum flow rate the jet breaks up due to axi-symmetric instabilities. These instabilities are also called varicose instabilities. At higher flow rates, the current through the liquid cone increases. With increasing current, the surface charge on the jet increases. Above a certain surface charge the jet break-up will also be influenced by lateral or azimuthal instabilities of the jet. These instabilities are also called kink instabilities. When the influence of these kink instabilities increases, then the size distribution of main droplets also becomes wider (Hartman *et al.* 2000).

2.10.3.2. Effect of applied voltage on cone-jet mode

The electric field between the capillary and the ground electrode is an important parameter in controlling the process of electrohydrodynamic atomization. This is

determined mainly by the applied voltage and other factors such as the configuration of the ground electrode and the inter-electrode spacing. The atomization of the liquid takes place mainly due to electrical forces produced by this field, therefore a higher applied voltage leads to a stronger atomization effect on the liquid. Within a well defined voltage range, the meniscus of liquid becomes conical and stationary. Below this voltage range, the spray always operates in pulsating mode (Ganan-Calvo *et al.* 1997).

With a given inter-electrode spacing, different modes of atomization can be observed if the voltage is gradually increased from lower values to higher values. Applied voltage is a key variable in establishing the cone-jet mode and the cone-jet mode can prevail within a range of applied voltages of higher values (Tang and Gomez 1994). Within this range of applied voltage of cone-jet mode, droplet size reduces with the increase of applied voltage from the lower value of range to higher value. As the droplet size decreases with the applied voltage and increases with the flow rate, it is necessary to select the highest possible value of applied voltage and the lowest possible value of flow rate to achieve the minimum droplet size (Jayasinghe and Edirisinghe 2004). For highly conducting and viscous liquids, the sizes of the droplets electrosprayed from the cone-jet mode are found to be relatively insensitive to applied voltages (Ku and Kim 2002).

2.10.4. Liquid properties

The modes of electrohydrodynamic atomization are also influenced by the liquid properties such as surface tension, viscosity, electrical conductivity, relative permittivity, and density (Ganan-Calvo *et al.* 1997, Hartman *et al.* 1999b).

2.10.4.1. Surface Tension

In order to form a stable cone-jet mode, the surface tension has to be overcome by the electric stresses. The higher the surface tension the stronger the electric field strength would be. According to the experimental results obtained by Smith (1986) the onset voltage for the stable cone-jet spray will increase with the liquid surface tension. If the liquid surface tension is large, a stable electrospray may not be established because the field required exceeds that for the electric break down in the gas surrounding the cone Tang and Gomez (1995) used gases with higher electrical breakdown strength as a surrounding fluid instead of air to obtain the stable cone-jet mode for water.

2.10.4.2. Viscosity

The viscosity is another vital liquid property which plays a significant role in the jet break-up process and influence the size of the produced main and secondary droplets. According to Weber (1931) in increase in viscosity will lead to lower dominant wave numbers. The lower dominant wave numbers will lead to increase of droplet size in electrohydrodynamic processing. Jayasinghe and Edirisinghe (2002a) studied the effect of viscosity on the size of relics produced by electrohydrodynamic processing. They found the greatest effect of increased viscosity upon the relic size, which increase dramatically. They found that the increase in viscosity over three orders of magnitude would have a dramatic effect on the electrohydrodynamic processing of liquids and their suspensions.

2.10.4.3. Electrical Conductivity

Among the properties of liquid, conductivity is the most important property for electro spraying in cone-jet mode. Sufficient electrical conductivity is necessary for the liquid

droplet at the capillary exit to be transformed into a conical shape. On the other hand, if the electrical conductivity is too high, electrohydrodynamic processing will be impossible due to the corona discharge before attaining the required applied voltage for the stable cone-jet mode. Liquids with low conductivity (insulators), e.g., olive oil, cannot be subjected to electrohydrodynamic atomization, although they can be electrosprayed in cone-jet mode by artificially increasing their conductivities with additives such as ethanol (Lopez-Herrera 2003). The value of liquid conductivity influences the morphology of the liquid issued in stable cone-jet mode. As conductivity increases, the filament width, length, flow rate for cone-jet mode and droplet size all decrease (Ganan-Calvo *et al.* 1997).

2.10.4.4. Relative Permittivity

Relative permittivity or dielectric constant is a measure of the polarisability of a material in an electric field. The polarization reduces the magnitude of electric field inside the liquid. Relative permittivity along with the vacuum permittivity and conductivity determines the electrical relaxation time, $t_e = \beta\varepsilon_o/K$. Electrical relaxation time is the time required to smooth a perturbation in the electric charge; β being the relative permittivity, ε_o and K are the vacuum permittivity and electrical conductivity, respectively (Ganan-Calvo *et al.* 1997).

2.10.4.5. Density

The density of the liquid also plays a role in determining the jet diameter in the cone-jet mode. When the viscosity and the conductivity of the liquid are large enough, the electrical charge is efficiently transmitted across the jet section by viscous forces. However, the viscous force depends on the density of the liquid (Ganan-Calvo *et al.*

1997). At the cone base, the acceleration of the liquid is very small and does not play an important role. However, the liquid density is of some importance due to the influence of gravity on the cone shape. For large capillaries, diameters larger than 1mm, gravity influence the shape of the cone strongly (Hartman 1998).

2.10.5. Needle size and electrode configuration

With regard to needle size, there is a difference of opinion among researchers. Cloupeau and Prunet-Foch (1989) showed that, for a given liquid, the range of possible flow rates vary with the change of needle size. Tang and Gomez (1996) found that the droplet size is independent of the needle size. However, they showed that the needle size significantly affect the stable cone-jet domain of electrospray. The maximum liquid flow rate needed for the stable cone-jet electrospray decreases dramatically as the needle diameter increases. This shows that in the voltage-flow rate graph, the stable cone-jet domain of the electrospray becomes smaller as the needle size increases.

Jayasinghe *et al*. (2002) showed that the droplet trajectories depend on the configuration of the ground electrode. For a point like ground electrode, the smaller the radius of the point, the higher the concentration of the droplets produced in the spraying pattern. They pioneered the use of a point-like ground electrode for their work by which they focused most of the ceramic suspension droplets. This configuration of the ground electrode was the key to their innovation of electrostatic atomization printing (EAP).

2.10.6. Scaling laws

The scaling laws are established for characterising a defined electrohydrodynamic processing. It enables the produced droplet size and emitted current to be better

correlated with the factors involved in the processing. It provides better understanding of the mechanisms involved in the process. Basically, the droplet size and the emitted current are given by liquid physical properties (electrical conductivity, density, viscosity, surface tension and dielectric constant) and liquid flow rate.

The scaling laws derived by De la Mora and Loscertales (1994) and Ganan-Calvo *et al.* (1997) well correlate the liquid physical properties with the droplet size and emitted current. Before stating these scaling laws, the conditions for classical electrohydrodynamic processing to take place are given below. This is the inequality criteria established by Ganan-Calvo *et al.* (1997). They established the criteria that the hydrodynamic time ($t_h = LD^2/Q$) should be much greater than the electrical relaxation time ($t_e = \beta\varepsilon_o/K$) as a condition that should be satisfied to have a steady state cone-jet structure.

$$t_h >> t_e \tag{2.5}$$

$$LD^2/Q >> \beta\varepsilon_o/K \tag{2.6}$$

where Q is the flow rate, D is the jet diameter and L is the axial length of the jet.

Consequently, the liquids having electrical relaxation time higher than the hydrodynamic time cannot be electrohydrodynamically processed unless their electrical relaxation time is modified well below the hydrodynamic time with the use of some additives (Ganan-Calvo *et al.* 1997).

The scaling laws for the droplet size and the emitted current during electrohydrodynamic processing derived by De la Mora and Loscertales (1994) are given below:

$$D_d = G(\beta)(Q\beta\varepsilon_o/K)^{1/3} \quad (2.7)$$

$$I = f(\beta)(\gamma QK/\beta)^{1/2} \quad (2.8)$$

where D_d is the droplet diameter, I is the emitted current, G(β) and f(β) are functions of liquid relative permittivity.

Ganan-Calvo *et al.* (1997) obtained scaling laws for the spray current and the droplet size based on the theoretical model of charge transport and these are given below.

For liquids with high velocity and conductivity:

$$I \sim (QK\gamma)^{1/2}/(\beta-1)^{1/4} \quad (2.9)$$

$$d \sim [(\beta-1)^{1/2}Q\varepsilon_o/K]^{1/3} \quad (2.10)$$

For liquids with high velocity and conductivity:

$$I \sim [\gamma^3\varepsilon_o K/\rho]^{1/4} \quad (2.11)$$

$$d \sim [\rho\, Q^3\varepsilon_o/\, \gamma\, K]^{1/6} \quad (2.12)$$

where I is the spray current, d is the droplet diameter and ρ is the liquid density.

2.10.7. Electrohydrodynamic atomization of suspensions

In the search for a new micro-fabrication technology for thin films and coatings, electrohydrodynamic atomization in cone-jet mode exhibits much promise with its

inherent capability for producing fine droplets in micrometre and submicrometre range with a narrow size distribution (Tang and Gomez 1994, 1995). In initial stages, although it was possible to synthesize thin films of $LiMn_2O_4$ by electrospray, the particle size was found to be not uniform due to temporary instabilities in the cone-jet and variation in the distance between the nozzle and the electrode (van Zomeren *et al.* 1994). However, Chen *et al.* (1998) showed the use of some additives in the suspension and was able to prepare uniform thin films of TiO_2 and ZrO_2 fine powders using electrospray technique.

Compared with other thin-film deposition technologies like chemical vapour deposition, physical vapour deposition, and plasma spraying, electrostatic atomization is a relatively inexpensive process and also has the added advantage of having the potential to control and deposit multi-layer coatings (Balachandran *et al.* 2001). EHDA technique has also been developed to generate an ultra-fine spray of ZrO_2 and SiC ceramic suspensions with a droplet size of about 4 μm and a narrow size distribution for preparing homogenous thin films of ZrO_2 and SiC (Miao *et al.* 2001).

Electrospray was also used to prepare foams of Al_2O_3 and ZrO_2. The compressive strength and the Young's modulus of the ZrO_2 foams prepared by electrospray were much higher than the ZrO_2 foams prepared by slurry dipping method (Jayasinghe and Edirisinghe 2002b, Chen *et al.* 2006). Biocompatible semi-micrometre sized relics prepared by electrospray offered surface topography and coverage for a favourable cell response (Huang *et al.* 2004). Printing of a pre-determined architecture of ceramic droplets by electrostatic spray in the cone-jet mode was a breakthrough in the direction of controlled deposition of fine droplets of ceramic suspensions (Jayasinghe *et al.*2002). The schematic of the experimental set-up used for this work given **Figure 2.9.**

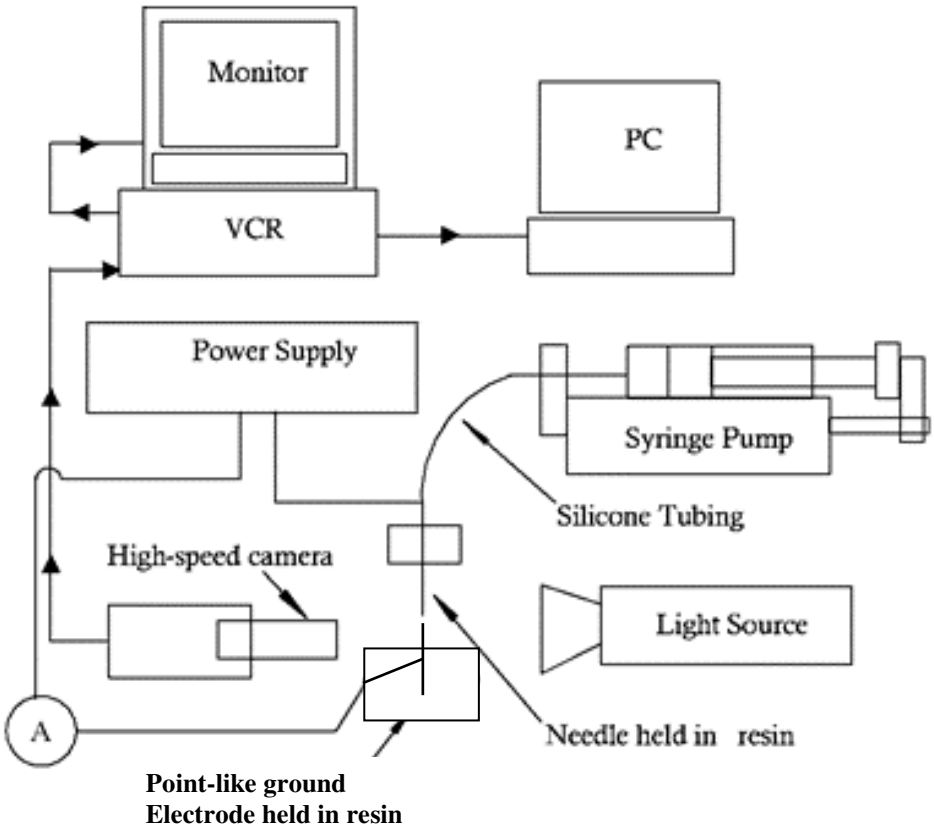

Figure 2.9. Schematic representation of the electrohydrodynamic atomization rig with point-like ground electrode (Jayasinghe and Edirisinghe 2004).

2.10.8. Microencapsulation by electrohydrodynamic atomization

Xie *et al.* (2006) have reported the preparation of polymeric particles by modified EHDA set-up using solutions of Paclitaxel, an anticancer drug, and variety of polymers, for drug delivery applications. The particles have shown controllable morphologies such as spheres, doughnut shapes and corrugated shapes with sizes from several tens of microns to hundreds of nanometres. The reduction of particle size had been achieved by decreasing the polymer concentration and the surface of the microparticles had also changed from a smooth surface to rough corrugated surface with the change of concentrations. The modifications made to the EHDA set-up and the results Xie *et al.* 2006) have achieved are extremely promising for future applications of EHDA for the preparation of microcapsules for drug delivery purposes.

2.11. Co-axial electrohydrodynamic atomization (CEHDA)

2.11.1. The mechanism of co-axial electrohydrodynamic atomization

Co-axial electrohydrodynamic atomization (CEHDA) is a further development of EHDA. The technique uses electrohydrodynamic forces to generate co-axial jets of immiscible liquids or suspensions. The schematic of basic experimental set-up of CEHDA is given in **Figure 2.10.** Two immiscible liquids or suspensions (T1 Outer Liquid, T2 Inner Liquid) are passed through two concentrically placed capillaries. The outer and inner needles are connected to the same electrical potential of several kilovolts relative to an earthed ring electrode. For a certain range of values of the applied voltage and flow rates, a cone-jet is formed at the exit of needles with an outer meniscus surrounding the inner one **(Figure 2.11).** A liquid thread is issued from the

vertex of each one of the two menisci, giving rise to a compound jet of two co-flowing liquids or suspensions **(Figure 2.12)** (Loscertales *et al.* 2002)

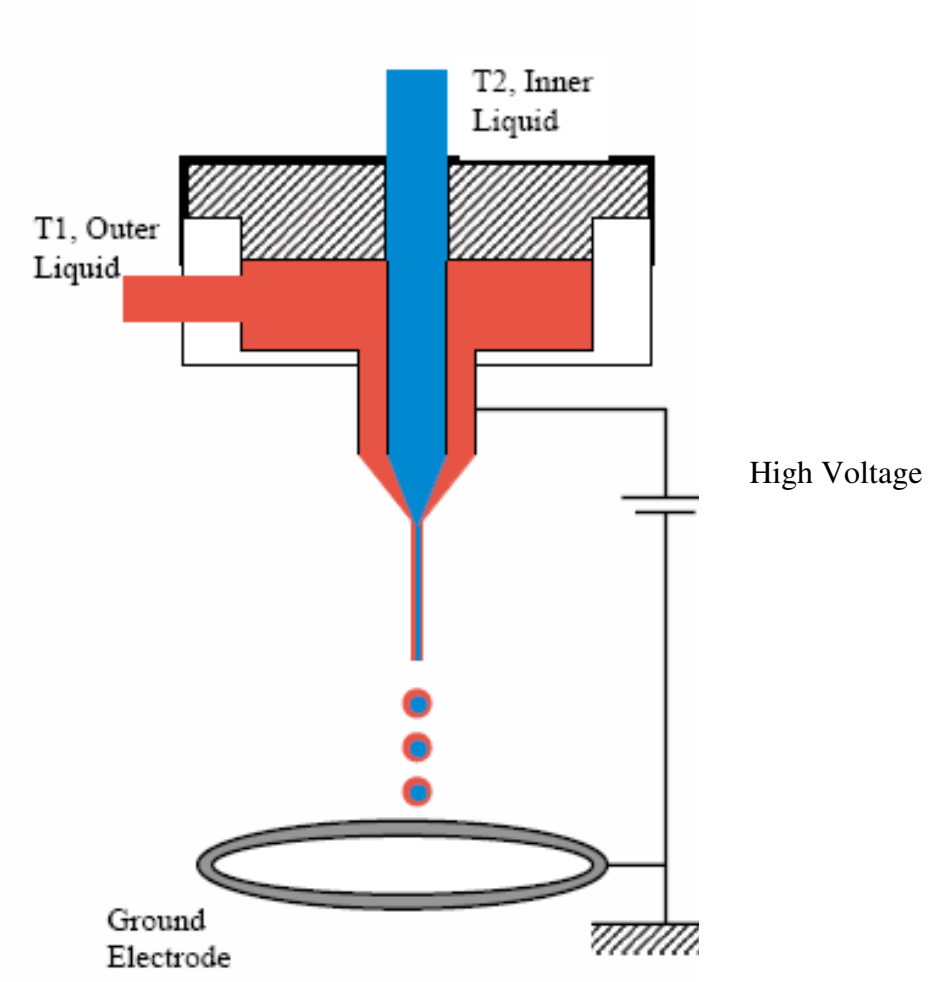

Figure 2.10. Schematic representation of the conventional CEHDA setup (Loscertales *et al.* 2002)

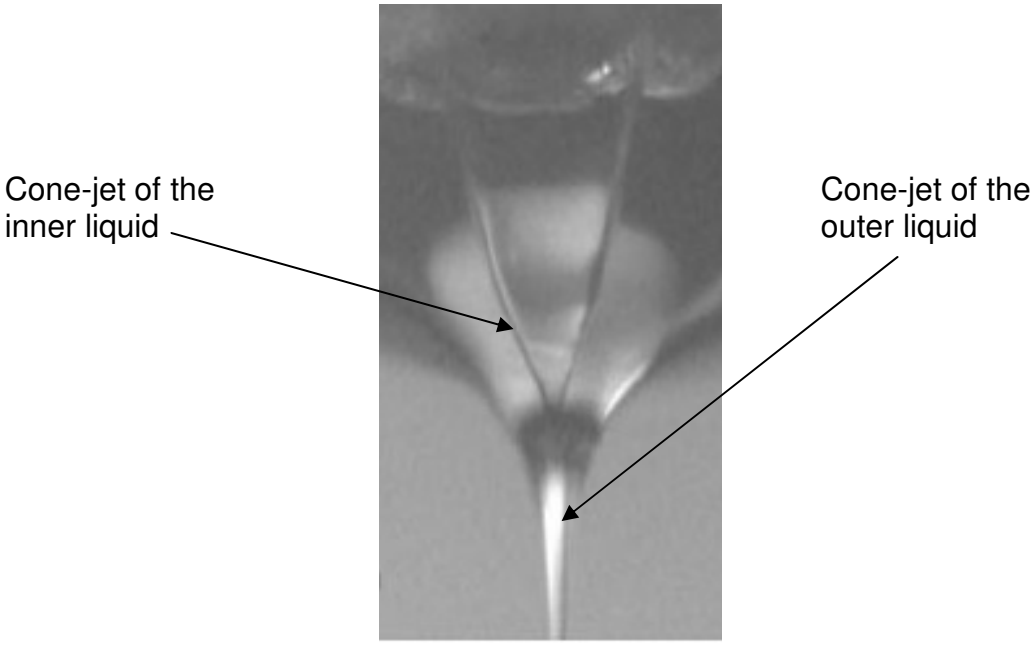

Figure 2.11. Formation of a cone-jet in CEHDA with outer meniscus surrounding the inner one (Loscertales *et al.* 2002)

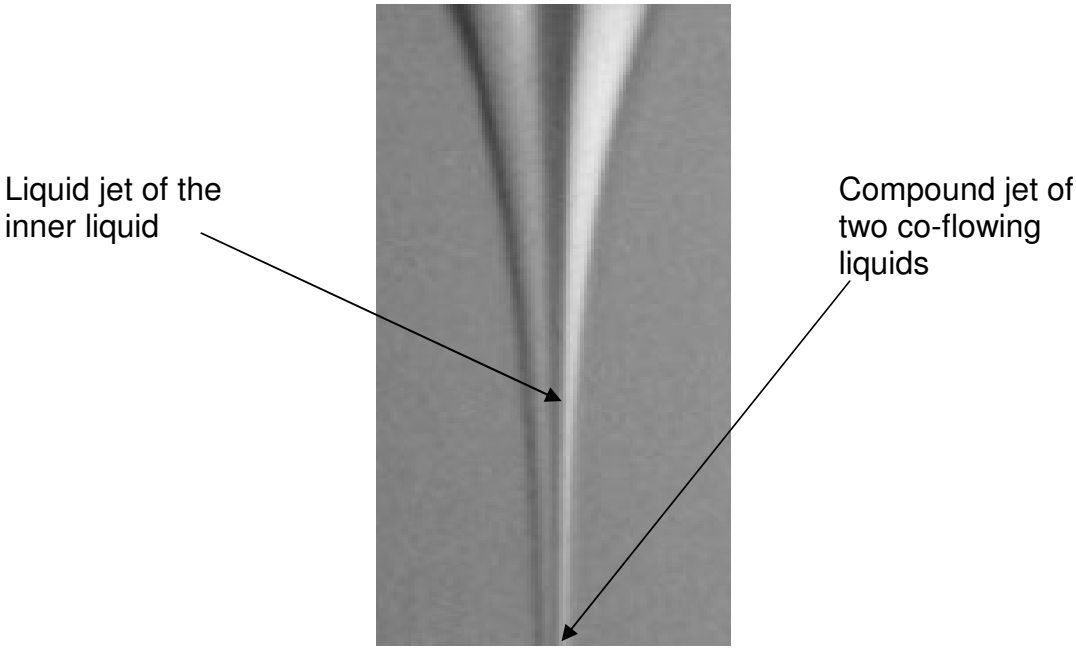

Figure 2.12. Formation of a compound jet in CEHDA (Loscertales *et al.* 2002)

2.11.2. The concept of driving liquid

To obtain a structured cone-jet, electrohydrodynamic forces must act on at least one liquid, although they may act on both. The liquid upon which electrohydrodynamic forces act to form a cone-jet is called the driving liquid. The driving character of one of the liquids of the couple can also be explained by a comparison of their electrical relaxation times. The electrical relaxation time, $t_e = \beta\varepsilon_o/K$, is the time required to smooth a perturbation in the electric charge; ε_o being the vacuum permittivity, β is the dielectric constant of the liquid, and K is the electrical conductivity. If the electrical relaxation time of the outer liquid is much smaller than that of the inner one, charges are located at the outer interface and they are supplied to the outer interface much more efficiently from the outer liquid bulk than from the inner one (Loscertales *et al.* 2002).

The driving character of one of the liquids can be lost in favour of other if the electrical conductivity of the latter is enhanced sufficiently by adding a suitable additive to it. When charges are located at the outer interface, the tangential electrical stresses which point towards the vertex of the conical interface must be efficiently transmitted throughout the liquid bulk by viscous diffusion. This requires that the viscosity of the outer liquid be high enough to play an important role in the liquid motion. Moreover, the use of less viscous liquids outside would give rise to intense re-circulations in the electrified meniscus and these re-circulatory motions are incompatible with steady compound jets. However, liquids with lower viscosity can be used as drivers when they are used inside, even when a non conducting liquid such as olive oil is used outside. This is also one way of electrospraying liquid insulators. The other way is to artificially increase their conductivity via additives (Lopez-Herrera *et al.* 2003)

2.11.3. Scaling of droplet size with flow rates of co-flowing liquids

Scaling laws discussed in **Section 2.10.6** that govern EHDA also apply to CEHDA. However, in this case, the flow rate used in the equations must be that of the driving liquid. The measurements of the current emitted through the co-axial jet when made dimensionless fit satisfactorily the current scaling law of EHDA. The mean diameter of droplets resulting from the break-up of a conducting-insulator liquid couple is determined by whether the driving liquid is flowing outside or inside. Droplet size is dependent on the liquid viscosities and on the ratio of the liquid flow rates (Lopez-Herrera *et al.* 2003).

2.11.4. Co-axial electrohydrodynamic atomization of suspensions

An exploratory work has successfully been carried out to prepare annular structures of advanced ceramic materials using the suspensions of alumina and zirconia via CEHDA. The speed of jetting in the nozzles has played an important role on the microstructure prepared. The results offer promising possibilities for encapsulating advanced materials in one another to produce composite structures (Balasubramanian *et al.* 2006).

2.11.5. Preparation of microspheres with solid core via CEHDA

The ability of CEHDA was demonstrated for the first time for the preparation of polymer-coated microspheres containing a protein, and subsequently controlled release of protein. Thus Starch/bovine serum albumin (BSA) microspheres coated with polydimethylsiloxane (PDMS) were prepared using CEHDA for controlled release of BSA. About 75% of the protein was released over a period of 7 days. This single step and relatively simple process can be exploited for the preparation of biodegradable microspheres for protein drug release (Pareta and Edirisinghe 2006). In the similar

fashion described above, Bovine serum albumin (BSA) was encapsulated with poly (lactide) (PLA) using CEHDA. Bovine serum albumin as the driving liquid due to its high electrical conductivity, while the high viscosity of the PLA and low interfacial tension of the PLA and BSA solutions favoured the formation of stable cone-jets. The morphology of the particles was changed from irregular to fully spherical with smooth surfaces when the PLA concentration increased from 1% to 5%. The effects of the PLA concentration and flow rate and applied voltage on particle size were statistically significant. Particle size increased as PLA concentration increased from 2% to 3.5% and decreased as the applied voltage was increased from 15 to 19 kV (Xu and Hanna 2008).

CHAPTER 3

EXPERIMENTAL DETAILS

3.1. Introduction

This chapter details the materials used and methodologies followed in conducting experiments for the investigations. The details of suppliers of materials, apparatus, equipment and software are provided appropriately. The methods used to characterise the materials are described. A detailed description about the accessories and equipment used in the co-axial electrohydrodynamic processing is also given. Finally, the experiments conducted on characterising the suspensions of microbubbles, suspension of microspheres and dried microspheres are also discussed.

3.2. Materials

The main materials used in the experiments were Glycerol (**Chapter 4**), L-α-phosphatidylcholine (**Chapter 5**), and Polymethylsilsesquioxane (**Chapter 6**). Other subsidiary materials used were ethanol, Tween 80, zircon, PEG 40 stearate, and Propane-1,3 diol. While glycerol and polymethylsilsesquioxane were used as model materials to study the processes, L-α-phosphatidylcholine was used to represent phospholipids.

3.2.1. Glycerol

Pure glycerol [$C_3H_5(OH)_3$, purity 99.9 %, density 1260 kg m^{-3}, molecular weight 92, melting point 18^0C, boiling point 290^0C, surface tension 65 mN m^{-1}, electrical conductivity $2x10^{-5}$ Sm^{-1}, relative permittivity 40, viscosity 1100 m Pa, Sigma-Aldrich Co.Ltd., Dorset, UK], a liquid with no colour and odour, widely used in pharmaceutical

formulations, was used as the main material for microbubbling investigations detailed in **Chapter 4**.

3.2.2. L-α-phosphatidylcholine

L-α-phosphatidylcholine ($C_{42}H_{82}NO_8P$, molecular weight 760, purity >99 %, Avanti Polar Lipids, Inc., Alabama, USA) which is a major phospholipid in the outer plasma membrane of mammalian animals, was used as a main ingredient in our investigations described in **Chapter 5**. Structure of the material is given below in **Figure.3.1.**

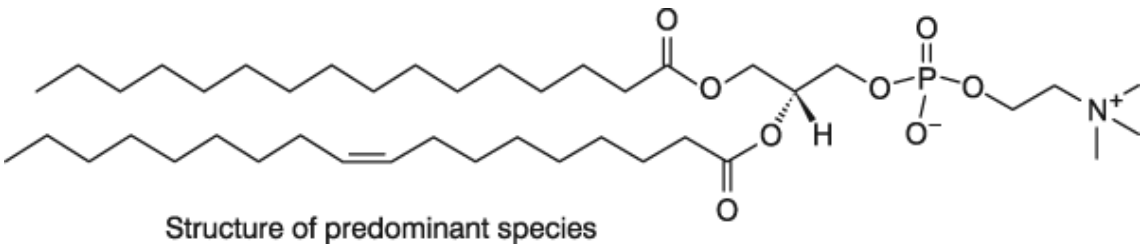

Figure 3.1. Molecular structure of the L-α-phosphatidylcholine showing the hydrophobic tail group and the hydrophilic head group.

3.2.3. Polymethylsilsesquioxane

Polymethylsilsesquioxane (MK powder, density 1240 kg m^{-3}, Wacker Chemie AG, Germany), a preceramic polymer, was used in our investigations described in **Chapter 6** as a main ingredient. This polymer is hydrophobic, chemically stable and unreactive and has been used *in-vivo* on account of its bio durability and biocompatibility for several decades.

3.2.4. Ethanol

General purpose research grade ethanol (C_2H_5OH, density 790 kg m^{-3}, molecular weight 46, electrical conductivity $3.4x10^{-5}$, viscosity 1.3 mPa s, surface tension 23 mN m^{-1}, BDH Laboratory Supplies, UK) was used as the solvent medium in preparing a polymer suspension used in our research described in **Chapter 6**. In addition, ethanol was also used for the calibration of characterisation apparatus and for the cleaning of capillary needles which were essential components of the experimental set-up.

3.2.5. Tween 80

Tween 80, also known as Polysorbate 80 and chemically known as polyoxyethylene sorbitan monooleate ($C_{64}H_{124}O_{26}$, density 1070 kg m^{-3}, molecular weight 1307, LindChem Ltd., Norfolk, UK) was used in our investigations described in **Chapters 4 and 5** as a surfactant. Tween 80 is also used in the manufacture of protein solution formulations to help solubilize and stabilize protein. It is one of a series of materials (including Tween 20, 40 and 60) which are fatty acid esters of sorbitan polyethoxylates.

3.2.6. Zirconia

Zirconia, also known as zirconium oxide (ZrO_2, Grade HSY3, mean particle diameter 0.5 μm, density 6,000 kg m^{-3}, Min-Chem Limited, Aldershot, UK). This material was selected for its smaller size in stabilizing microbubbles with initial diameter of 45 μm (**Chapter 4).** The use of zirconia for the deposition of thin films via electrohydrodynamic atomization and for the preparation of a composite via co-axial electrohydrodynamic atomization has also been mentioned elsewhere (Balasubramanian *et al.* 2006).

3.3. Preparation of suspensions and solutions

3.3.1. Glycerol suspensions and solutions

For the investigations described in **Chapter 4**, in addition to using glycerol in its pure form, a glycerol solution with Tween 80 and a glycerol suspension with zirconia were also used.

3.3.1.1. Glycerol-Zirconia suspension

A 2 wt. % zirconia suspension was prepared by adding 5 g of zirconia powder to 245 g of glycerol (purity 85 %, density 1217 kg m^{-3}, viscosity 740 mPa s, surface tension 63 mN m^{-1}) and leaving the mixture on a roller mixer for a minimum period of 12 h in order to prepare a homogeneous suspension.

3.3.1.2. Glycerol-Tween 80 solution

A 2 wt. % Tween 80 solution was prepared by adding 5 g of Tween 80 to 245 g of glycerol and leaving the mixture on a roller mixer for a minimum period of 12 h in order to prepare a homogeneous solution.

3.3.2. Phospholipid suspensions

For the investigations described in **Chapter 5**, we used two different suspensions of phospholipid. Initially the suspension was prepared without the involvement of Tween 80 and then the suspension was modified for further investigations with the addition of 2 wt. % Tween 80.

3.3.2.1. Phospholipid suspension without Tween 80

The phospholipid suspension was prepared by mixing 0.25 g of hydrogenated L-a-phosphatidylcholine with 0.071 g of polyethylene glycol 40 stearate (Sigma-Aldrich Co. Ltd, UK; density 1300 kg/m^3), 5 ml of glycerol and 25 ml of propane-1,3-diol (density 1000 kg m^{-3}; Sigma-Aldrich Co. Ltd) in a conical flask containing 50 ml of distilled water with slow magnetic stirring. The flask was then topped up with distilled water up to the 250 ml mark and the mixture was stirred for a further 300 s. The dispersion of the phospholipid was achieved by sonicating the suspension using a Misonix ultrasonic cell disruptor XL200 (Labcare Systems Ltd, Somerset, UK) operating at 12W for 60 s. The sonicator probe was placed deep in the suspension to avoid the generation of gas bubbles. To ensure the homogeneous dispersion of the phospholipid in the suspension, a smaller volume of the suspension was transferred to a test tube and was sonicated in the same manner for 120 s before removing 6 ml of the samples for our investigations.

3.3.2.2. Phospholipid suspension with Tween 80.

In order to prepare a phospholipid-Tween 80 suspension, 196 g of the phospholipid mixture described in **Section 3.2.2.1.** and 4 g of Tween 80 were transferred to a conical flask and stirred for a 300 s. A homogeneous suspension was then obtained by sonicating using a Misonix ultrasonic cell disruptor XL200 (Labcare Systems Ltd. Somerset.UK) operating at 12 W for 60 s. The sonicator probe was placed deep in the suspension to avoid the generation of gas bubbles. Smaller volumes of this phospholipid-Tween 80 suspension were then taken for our investigations. Combination of phospholipid and Tween 80 is treated in this instance as a mixture of two different surfactants.

3.3.3. Polymer solutions

For the investigations described in **Chapter 6**, a solution with 60 wt. % polymer was prepared in a conical flask by dissolving polymethylsilsesquioxane in ethanol and by subsequently magnetic stirring. This parent-solution was subsequently diluted to prepare solutions containing 40, 24 and 18 wt. % polymer. These percentages of polymer were decided on trial and error basis. Each time the contents of polymer and ethanol in remaining solutions were calculated carefully just before diluting the solution by further addition of ethanol.

3.4. Characterisation of liquid, suspensions and solutions

3.4.1. Density

The density of the liquid/suspension/solution was measured using a 25 ml standard density bottle (VWR International, Lutterworth, UK). The mass of the empty bottle and the mass of the bottle filled with liquid/suspension/solution were obtained using an electronic balance (AND HF-1200G A&D Instruments Ltd., Japan) which is capable of giving values up to four decimals. The density was calculated as follows:

The mass of the empty density bottle = W_1 g

The mass of the density bottle filled with liquid/suspension/solution = W_2 g

Therefore, the mass of liquid/suspension/solution only = (W_2-W_1) g

Therefore, the density of liquid/suspension/solution = (W_2-W_1)/25 g cm^{-3}

The mean value of five such consecutive calculations was taken as the density of liquid/suspension/solution and reported in this thesis. Measurements were taken at

ambient temperature and pressure conditions and the density bottle was calibrated using ethanol.

3.4.2. Viscosity

Dynamic viscosity of transparent fluids such as ethanol etc. was determined using a U-tube viscometer (BS/U type, Schott Instruments GmbH, Germany). For thicker fluids such as glycerol etc. the dynamic viscosity was determined using VISCOEASY rotational viscometer (CamLab Ltd, Cambridge, UK) by following the instructions provided in the operation manual of this equipment.

3.4.2.1. Determination of viscosity using VISCOEASY rotational viscometer

For the determination of viscosity of glycerol, glycerol-Tween 80 solution, glycerol-zirconia suspension, phospholipid suspensions, and 60 wt. % polymer suspension, VISCOEASY rotational viscometer was used. An appropriate spindle was selected only after few trials. Rotational viscometers use the idea that the torque required to turn an object in a fluid is a function of the viscosity of that fluid. The torque required to rotate a spindle in a fluid is measured at a known speed.

3.4.2.2. Determination of viscosity using U-Tube viscometer

For the determination of viscosity of 18, 24, and 40 wt. % polymer suspensions, a calibrated U-tube (size C, nominal constant 0.03) viscometer was used. The time taken for a standard volume of fluid to pass through the capillary of the u-tube was noted for five times and the mean value of the time (s) was calculated. Then, the kinematic viscosity (ν) was obtained by multiplying the nominal constant (C) by the time (t):

$$v = Ct \tag{3.1}$$

Then, the dynamic viscosity (η) was then calculated by multiplying the kinematic viscosity by the density (ρ) of the suspension:

$$\eta = v\rho \tag{3.2}$$

If equations (3.1) and (3.2) are combined,

$$\eta = Ct\rho \tag{3.3}$$

Ethanol was used to calibrate the viscometer. The mean value of five readings was taken as the dynamic viscosity of the sample. For U-tube viscometers that are not calibrated by manufacturers, use of a calibrating liquid is essential as the viscosity value cannot be calculated without comparing with another liquid.

3.4.3. Surface tension

Surface tension of the liquid/suspension/solution was measured using a Kruss Tensiometer K9 (Standard Wilhelmy's plate method). The plate was hung from the hook and the beaker containing the sample was placed on the platform. The plate was completely immersed into the sample whose surface tension was to be measured. The plate was then gradually lifted and the surface tension value was directly read when the plate was just about to detach from the liquid surface. In order to minimize errors, the plate was cleaned thoroughly and dried in a drier before each measurement. The mean value of five readings was taken as the surface tension of the sample.

3.4.4. Electrical Conductivity

Electrical conductivity was measured using a HI-8733 (Hanna Instrument, USA) conductivity probe. The electrode was always cleaned with distilled water and dried before measurements. The electrode was kept immersed in the solution up to the correct length of the electrode for 10 min and the reading shown on the meter was recorded.

The mean value of five consecutive readings was taken as the electrical conductivity of the sample.

3.5. Equipment used for Co-axial electrohydrodynamic atomization microbubbling

3.5.1. Needle set-up

The experimental setup used for all our investigations described in **Chapters 4**, **5**, and **6**, is shown in **Figure 3.2**. The co-axial nozzle used for microbubble generation was made up of an inner stainless steel capillary needle (inner diameter 150 μm and outer diameter 300 μm) carrying the air flow surrounded by an outer stainless steel needle (inner diameter 685 μm and outer diameter 1100 μm) carrying the liquid/suspension/solution. The tip of the inner needle was positioned ~2 mm inside the outer needle in order to allow the air to be pushed by liquid/suspension/solution. The schematic of the needle configuration is given in **Figure 3.3**.

3.5.2. Ground electrode

A ring (inner diameter 15 mm and outer diameter 20 mm) electrode was placed ~12 mm below the tip of the outer needle as shown in **Figure 3.2.** The electric stress is determined by the electric field between the needle and the ground electrode configuration.

3.5.3. High voltage power supply

The needles and the ground electrode were connected to a high voltage DC power supply unit (FC30 P4 12w, Glassman Europe Limited, Bramley, UK) using a high

voltage power cable. The output voltage range of the unit was 0-30 kV and the output current range was 0-4 mA.

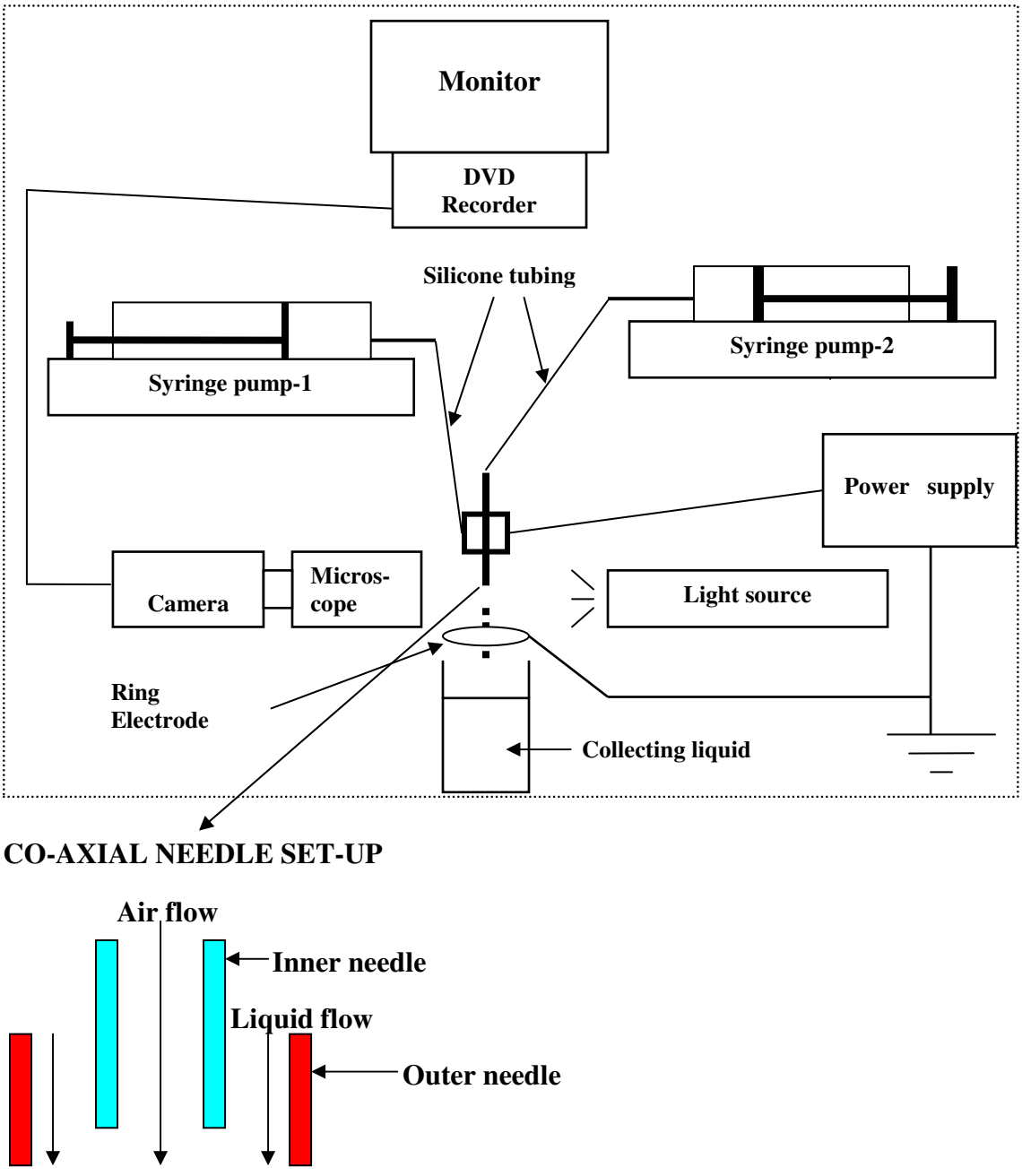

Figure 3.2. Schematic representation of the new experimental set-up used for co-axial electrohydrodynamic microbubbling (Farook *et al.* 2007a).

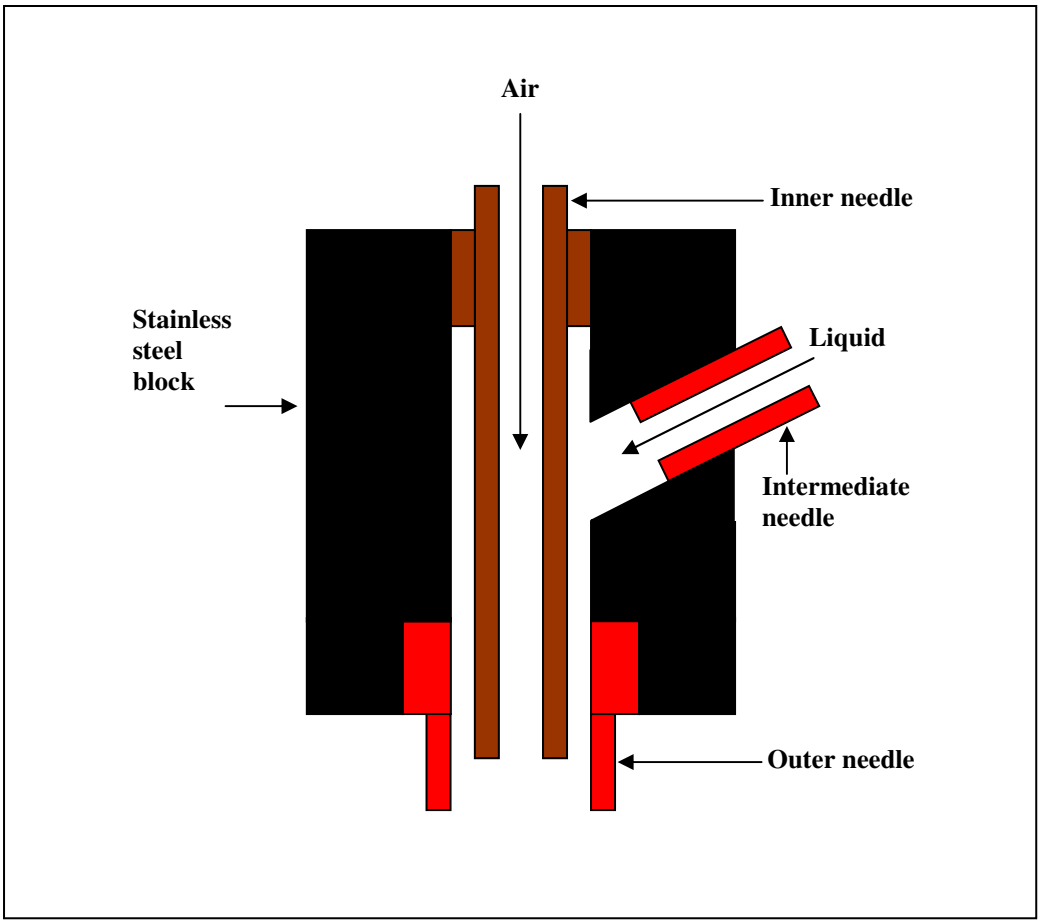

Figure 3.3. Schematic of the needle configuration of CEHDA microbubbling set-up.

3.5.4. Syringe pumps

The inner needle and the outer needle were connected by silicone tubings with plastic syringes (BD Plastic^{TM}, VWR, Lutterworth, UK) containing the air and liquid/suspension/solution. The flow rates of the air and the liquid/suspension/solution through the needles were controlled by high precision Harvard syringe pumps (Infuse/Withdraw PHD 4400 Hpsi programmable syringe pump, Harvard Apparatus Ltd., Edenbridge, UK). The capacity of the syringes used for the air and liquid/suspension/solution were 10 ml and 5 ml, respectively. The pumps were calibrated frequently using glycerol.

3.5.5. Data recording unit

The flow of material exiting the needles was observed/recorded using a LEICA S6D JVC-colour video camera attached to a zoom lens and a data DVD video recorder MP-600 using CDV Recorder/Editor DN-100 with a video screen for real time monitoring.

3.6. Characterisation of suspensions of microbubbles and microspheres

The microbubbles prepared during investigations described in **Chapter 4** were characterized only using the optical microscope and the Sympatec laser diffractometer. The microbubbles prepared during investigations described in **Chapter 5** were subjected to optical microscopy, ultrasound attenuation analysis, and ultrasound imaging. The microspheres prepared during investigations described in **Chapter 6** were subjected to optical microscopy, ultrasound attenuation analysis, scanning electron microscopy, and transmission electron microscopy.

3.6.1. Optical microscopy

An optical microscope (Nikon Eclipse ME 600, Nikon, Japan) was extensively used for all our investigations described in chapters 4, 5, and 6. For each observation, 1 ml sample of suspension of microbubble/microspheres was applied to a microscopic glass slide and the observation was made using the bottom light. During optical microscopy, the diameters of the microbubbles were measured using standard Image-Pro Plus software (Media Cybermatics, L.P.Del Mar, CA, USA).

3.6.2. Sympatec Laser diffractometry

The size distribution of the microbubbles generated during our investigation was obtained using a computer controlled Sympatec helos Model KF (helium laser optical spectrometer) sizing system (Sympatec Ltd., System-Partikel-Technik, Bury, UK), which recorded and subsequently plotted the data collected (**Chapter 4**). A sample of microbubble suspension was transferred to a spectrophotometer cell containing pure glycerol such that the bubbles were in the Z dimension of the cell for the 2.2 mm diameter laser beam to pass through. The sympatec system is based on the diffraction of light occurring when a laser beam impinges on the particles. The droplet detection capability of the lens used was 0.5-175 μm. The measurements were carried out in ambient conditions and reference background data was taken prior to the measurements. The experiment was repeated 5 times on the same sample and 5 sets of size distribution data were also obtained.

3.6.3. Ultrasound attenuation measurement

For the ultrasound attenuation measurement, which ensures the presence of microbubbles in the suspension, 1 ml of the microbubble suspension was added to a

specially designed chamber filled with distilled water. The chamber was constructed using polymethylmethacrylate tubing (inner diameter 60 mm, wall thickness 5 mm, length 30 mm) with acoustic "windows" made from a thin polyethylene film (thickness 50 μm) at either end. The tubing was held between two square aluminium plates into which recessed circular holes had been cut to hold the tubing in place. The chamber was suspended in a water bath, also filled with distilled water, to enable transmission of the ultrasound through the chamber and to minimise temperature fluctuations. The schematic of the experimental apparatus for the ultrasound attenuation measurements is given **Figure 3.4.**

Measurement of ultrasound attenuation through the microbubble suspension in the chamber was made using a custom made broadband transducer having a nominal centre frequency of 1 MHz, diameter 20 mm and a 3 dB bandwidth of 60%. This was aligned co-axially with the chamber 20 mm from one of the windows of the chamber so that the ultrasound beam passed through the chamber on to a stainless steel reflector and back to the transducer. The distance between the transducer face and the steel plate was 60 mm. The transducer was activated using a pulser/receiver unit (Panametrics model 5055 PR) which was set to give an output peak negative pressure in water of ~50 kPa. Signal capture was performed using a digital oscilloscope (LeCroy 9310M Dual 300 MHz) which was connected via a general purpose interface bus (GPIB) to a computer. Subsequent data analysis was performed in MATLAB (Version 7 of 2006, The Mathsworks, Natick, MA, USA).

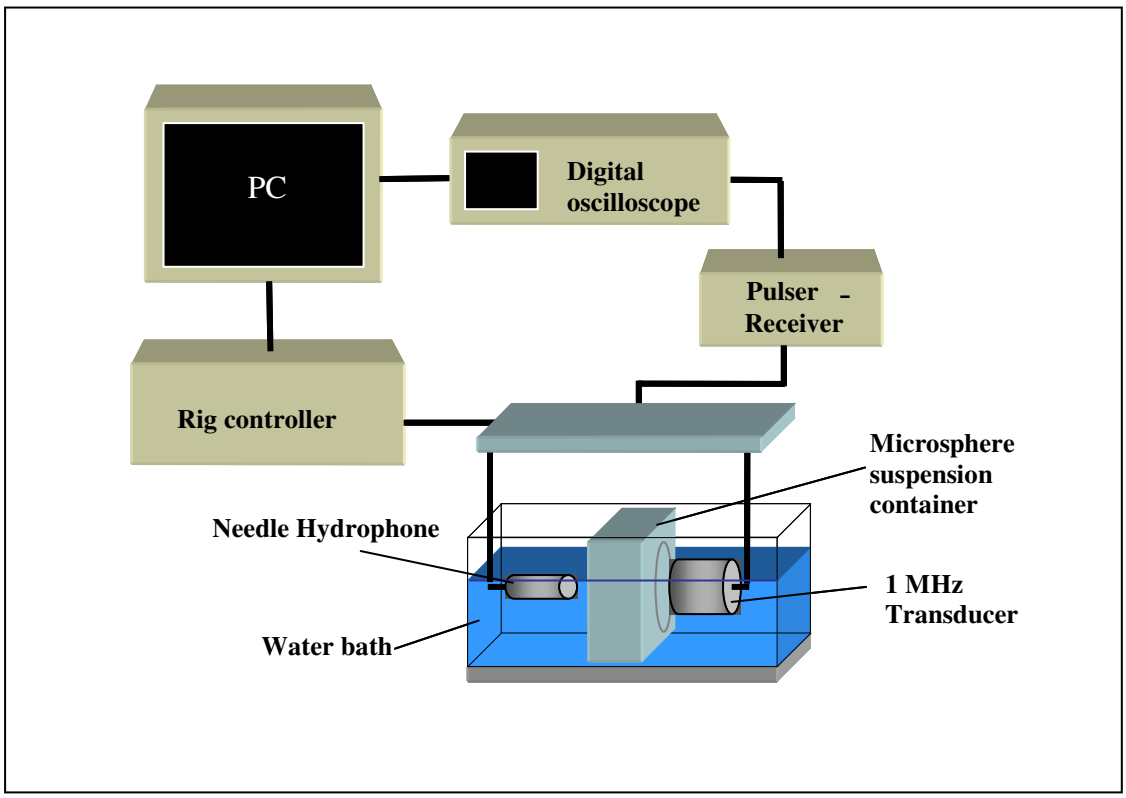

Figure 3.4. Schematic of the experimental apparatus for the ultrasound attenuation measurements.

3.6.4. Scanning electron microscopy (SEM)

The samples of suspensions of microspheres prepared during investigations described in **Chapter 6** were also subjected to scanning electron microscopy in order to characterise the morphology of the microspheres. A Jeol JSM 6301F field emission scanning electron microscope (FE-SEM, JEOL Ltd., Herts, UK) was used, which is equipped with an emitter that can achieve a resolution of ~ 1.5 nm. The accelerating voltage was

set at 6 kV and the working distance between the emitter and the sample was 20 mm. Samples of 0.05 ml of microbubble suspension were taken onto gold coated glass slides and dried under ambient conditions for 2 h. After that, the glass slides were placed inside a desiccator for further drying for at least two days under ambient conditions before the SEM examination.

Since the polymer used for the preparation of microspheres is an insulator, the SEM sample was gold coated for 2 min using a sputtering machine (Edwards sputter coater S 1 50B) in order to release electrons so that sample surface will not be charging during examination. The sample was then placed on an aluminium stub and stuck with a carbon sticker and was placed in the SEM chamber. In the SEM, electrons from the electron gun are focused to a fine point at the specimen surface by means of the lens system. This point is scanned across the specimen under the control of currents in the scan coils situated within the final lens. Secondary electrons are emitted from the specimen surface and are attracted to the detector. The detector relays signals to an electronic console, and the image appears on a television screen.

3.6.5. Ultrasound imaging equipment

Microbubble suspensions prepared during the investigations described in **Chapter 5** were also examined by ultrasound imaging in order to confirm that gas bubbles had been successfully prepared. Gelatine cubes (25 mm x 25 mm x 25 mm) with a central cylindrical cavity (diameter ~ 9 mm) were prepared as simple phantoms. Grayscale images were acquired using a Philips ATL HDI 5000 scanner (L7-4 probe) for cubes filled with distilled water only and subsequently with each of the suspension samples. When ultrasound probe is pressed against the gelatine phantoms as shown in **Figure 3.5**

(a & b), grayscale images could be obtained on the monitor due to the backscattering of ultrasound waves that are sent into the gelatine phantoms from the ultrasound probe. It is expected to compare the grayscale images obtained with and without microbubble suspension in the central cavity of the gelatine phantoms and to observe difference due to the presence of microbubbles.

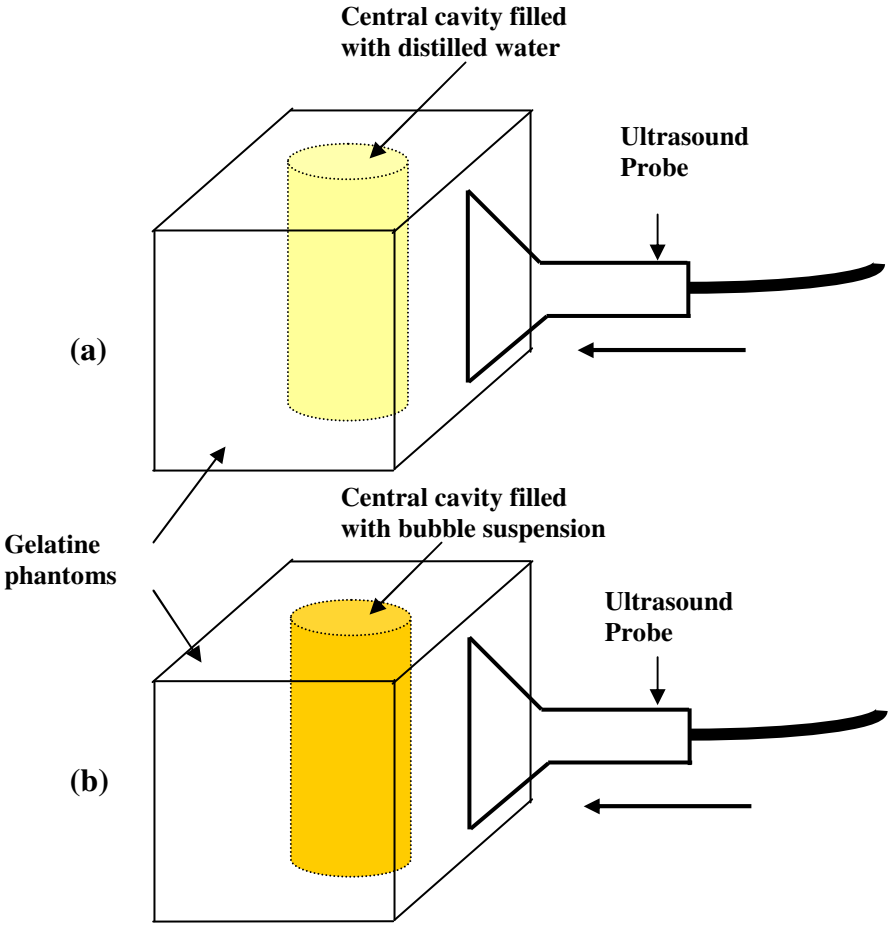

Figure 3.5. Schematic of the experimental set-up for the ultrasound imaging using a gelatine phantom. Central cavity of the gelatine phantom filled with **(a)** distilled water **(b)** microbubble suspension.

3.6.6. Transmission electron microscopy (TEM)

The suspension of microparticles prepared during investigations described in **Chapter 6** was also subjected to examination under a transmission electron microscope. A 0.05 ml volume of suspension was taken for examination under TEM after placing a drop of suspension on carbon coated grid and air dried. The TEM used was a high resolution JEOL JEM 2010, operated at 200 keV accelerating voltage, fitted with EDS (Energy Dispersive X-ray Spectroscopy) analytical attachment, by Oxford Instruments.

In TEM, a beam of electrons is focused on a single pinpoint spot or element on the sample being studied. The electrons interact with the sample and only those that go past unobstructed hit the phosphor screen on the other side. At this point, the electrons are converted to light and an image is formed. The dark areas of the image correspond to areas on the specimen where fewer electrons were able to pass through; the lighter areas are where more electrons did pass through, although the varying amounts of electrons in these areas enable the user to see structures and gradients. The TEM operates on the same basic principles as the light microscope but uses electrons instead of light. What we can see with a light microscope is limited by the wavelength of light. TEM use electrons as "light source" and their much lower wavelength make it possible to get a resolution a thousand times better than with a light microscope.

CHAPTER 4

MICROBUBBLING BY CO-AXIAL ELECTROHYDRODYNAMIC ATOMIZATION USING A MODEL GLYCEROL-AIR SYSTEM

4.1. Introduction

This chapter describes an innovative investigation that enabled co-axial electrohydrodynamic atomization (CEHDA), to be used for the first time to prepare microbubbles, and showed that diameters < 10 μm and a narrow size distribution could be achieved. The reasons behind considering CEHDA for this purpose were, primarily, a need in ultrasound medical imaging for a viable technique to prepare stabilized microbubbles with required size and size distribution, secondarily, the capability of CEHDA to prepare micro/nano capsules with near monodispersivity.

4. 2. Conceptualization of new experimental set-up for CEHDA

Although CEHDA is capable of forming coaxial jets of immiscible liquids which eventually break up into droplets with the outer liquid encapsulating the inner one, the same cannot be achieved by conventional CEHDA when a gas and a liquid are flowing through inner and outer needles, respectively. The main reason for this limitation was the inability of the set-up to pump gas into the liquid stream flowing through the annular gap. An important feature that is available in microfluidic flow focusing systems is that a gas stream flowing through a capillary can be pushed through an orifice by a liquid stream flowing outside the capillary to generate microbubbles (Ganan-Calvo 2004). This principle of microfluidic flow focusing systems has been incorporated into the new experimental CEHDA set-up by raising the inner needle by a few millimetres (~ 2 mm) above the tip of outer

needle promoting a co-flow of liquid and gas in the form of a jet as a result of electrohydrodynamic forces.

The liquid flowing through the outer needle has to be a liquid with sufficient conductivity and viscosity in order to form a cone-jet as in the case of conventional EHDA and CEHDA. The jet diameter at which bubble break-up takes place in CEHDA can be compared with the diameter of the orifice available in the microfluidic flow focusing systems. The novelty in the new experimental set-up is that it combines the features of both, microfluidic flow focusing systems and conventional co-axial electrohydrodynamic atomization to prepare microbubbles. **Figure 4.1** illustrates how conventional CEHDA and microfluidic flow focusing have been combined to form new CEHDA.

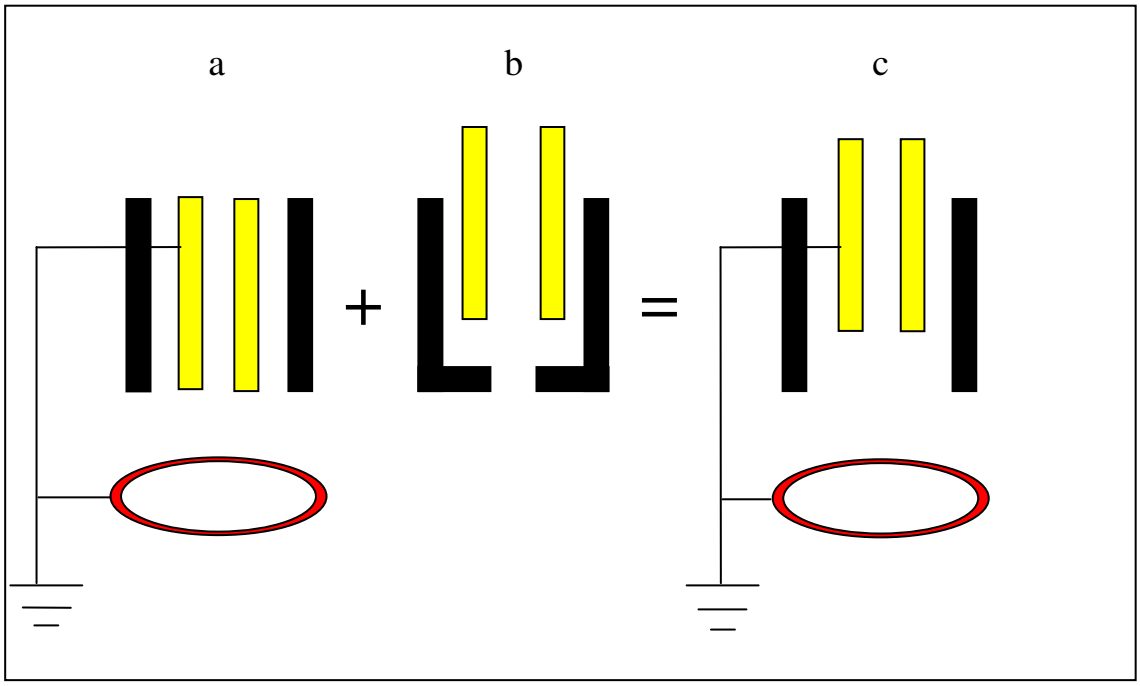

Figure 4.1. Schematic of new CEHDA needle configuration by combining conventional CEHDA with microfluidic flow focusing: (a) conventional CEHDA (b) microfluidic flow focusing (c) new CEHDA.

4.3. Initial investigations with a model glycerol-air system

With the modification of conventional CEHDA, after some trials with various liquids such as silicone oils, a glycerol-air system was selected to generate microbubbles for the first time through the new CEHDA set-up. Glycerol was selected as the encapsulating liquid for its high values of electrical conductivity and viscosity. Since glycerol can dissolve in water, it was also decided to collect microbubbles in a container of glycerol itself.

4.3.1. First formation of microbubbles

At lower values of flow rates of air and glycerol and at zero voltage, there was no sign of microbubbling. Glycerol was flowing through the needle exit in droplets. However, with the gradual increase of flow rates of air and glycerol and at a flow rate combination of 1.66 µl s^{-1} (air): 4 µl s^{-1} (glycerol), a large number of air bubbles were seen collecting in the liquid meniscus. **Figure 4.2** shows how a plain glycerol meniscus transformed into a meniscus containing a large number of air bubbles. With the increase of applied voltage, the glycerol meniscus with air bubbles turned into a shape of partial cone. With further increase of applied voltage and at 8.8 kV, a steady near cone-jet was formed and started emitting a thread of microbubbles from the apex of the cone and the microbubbles were able to be collected in a container of glycerol. The analysis of optical micrographs obtained using the suspension of microbubbles prepared at the above combination of flow rates resulted in a multimodal size distribution (**Figure 4.3** a) showing a large population (~ 94%) of microbubbles with diameters > 10 µm. (For both air and glycerol, flow rates were increased by 0.08 µl s^{-1} from an initial value of 0.5 µl s^{-1}).

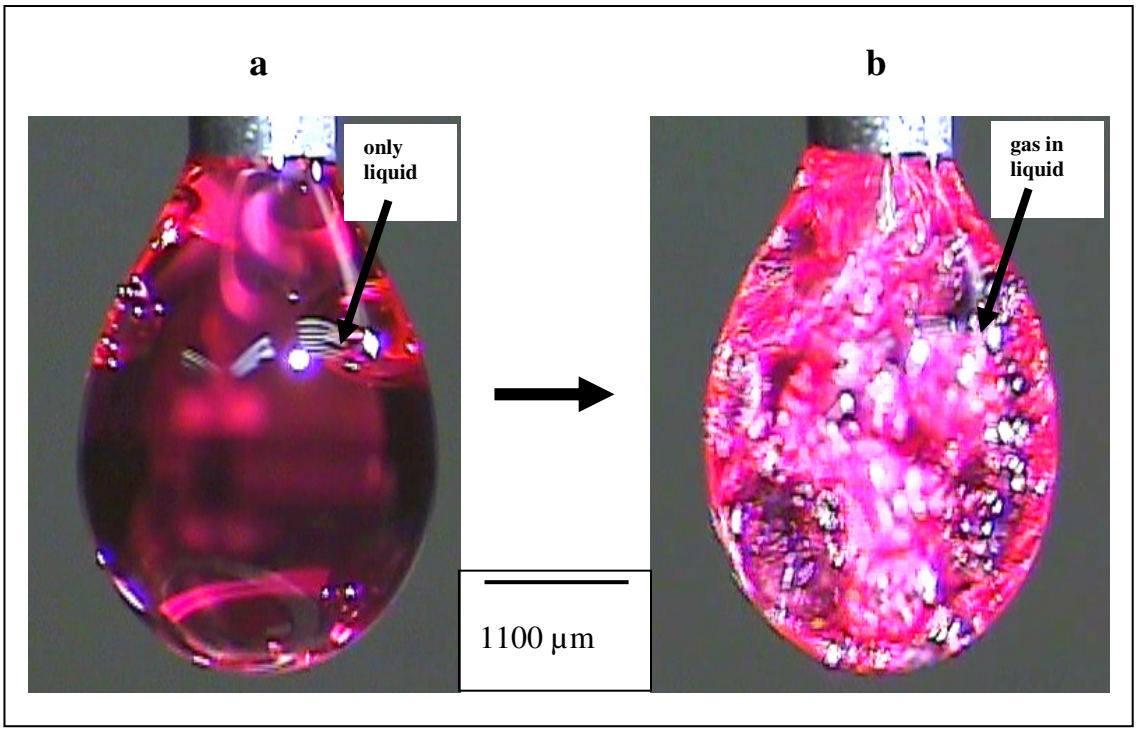

Figure 4.2. Transformation from liquid dripping to bubble dripping. At zero voltage (**a**) liquid drop with no gas bubbles at lower values of air flow rate (**b**) liquid drop with gas bubbles at increased values of air flow rate.

4.3.2. Effect of flow rates

Since reducing the microbubble diameter to a size < 10 µm was one of the major concerns, further changes were made to the values of flow rates to see the effect on the microbubble diameter. Microbubbling was conducted at a second combination of flow rates by changing the initial air flow rate to 2.08 µl s^{-1} and the glycerol flow rate to 2.5 µl s^{-1}. The analysis of the optical micrographs obtained using the suspension of microbubbles prepared at this new combination of flow rates showed a monomodal size distribution (**Figure 4.3**b) showing 80% of microbubbles with diameters < 10 µm. Microbubbling was further conducted at a third combination of flow rates reducing the air flow rate to 1.66 µl s^{-1} once again and maintaining the glycerol flow rate at the previous level of 2.5 µl s^{-1}. The size distribution analysis of relevant micrographs (**Figure 4.4**) showed a microbubble population with 94% of bubbles having diameters

≤ 10% (**Figure 4.3**c). The relevant gas ratio, λ, (gas flow rate/liquid flow rate) values are tabulated in **Table 4.1** along with the respective flow rate values.

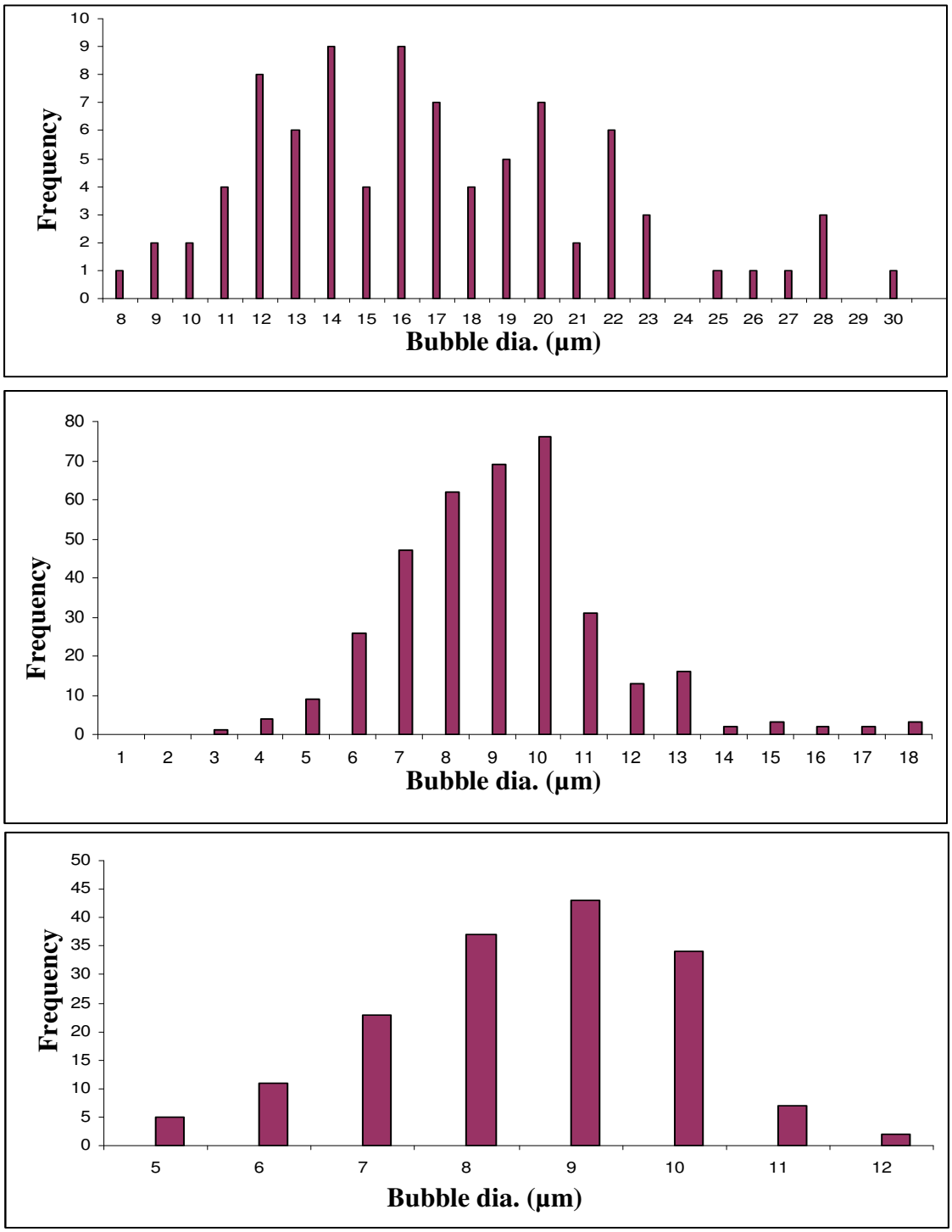

Figure 4.3. Size distribution of microbubbles obtained at: (a) flow rates 1.66 µl s^{-1} (air): 4 µl s^{-1} (glycerol) (b) flow rates 2.08 µl s^{-1} (air): 2.5 µl s^{-1} (glycerol) (c) flow rates 1.66 µl s^{-1} (air): 4 µl s^{-1} (glycerol).

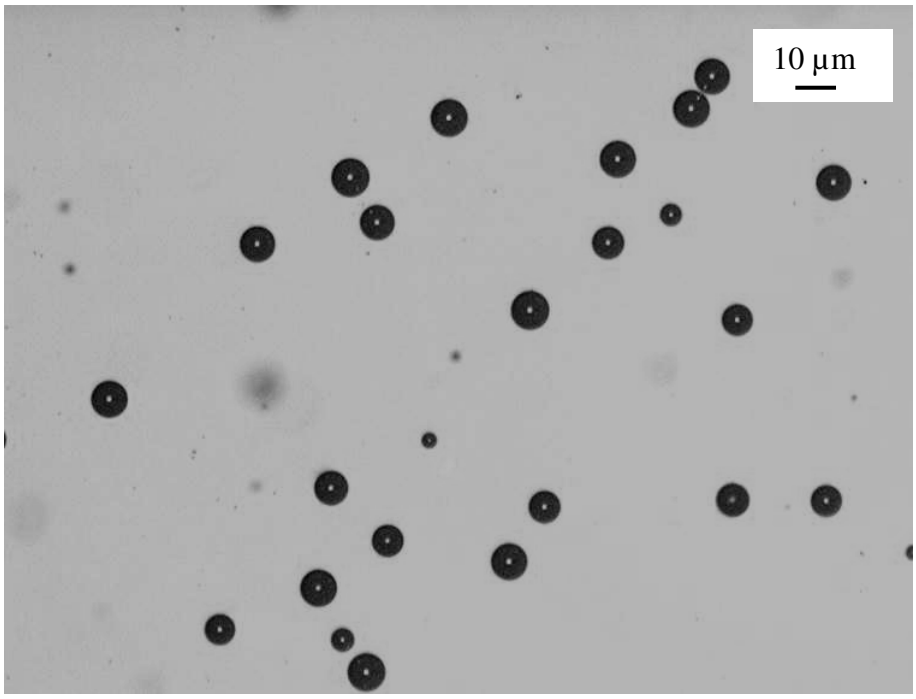

Figure 4.4. A micrograph of suspension of microbubbles prepared at flow rate combination 1.66 µl s^{-1} (air): 2.5 µl s^{-1} (glycerol) and at applied voltage 8.8 kV.

Table 4.1. Pattern of change in gas ratio at different combinations of flow rates

Air flow rate (µl s^{-1})	Glycerol flow rate (µl s^{-1})	Gas ratio (λ)
1.66	4.0	0.4
2.08	2.5	0.8
1.66	2.5	0.7

4.3.3. Characterization with Sympatec Laser difractometry.

The suspension of microbubbles obtained at flow rate combination of 1.66 µl s^{-1} (air): 2.5 µl s^{-1} (glycerol) was also studied by laser diffractometry. The results (**Figure 4.5**) confirmed that of the optical microscopy having a size distribution of 2-8 µm with a median value of 5 µm.

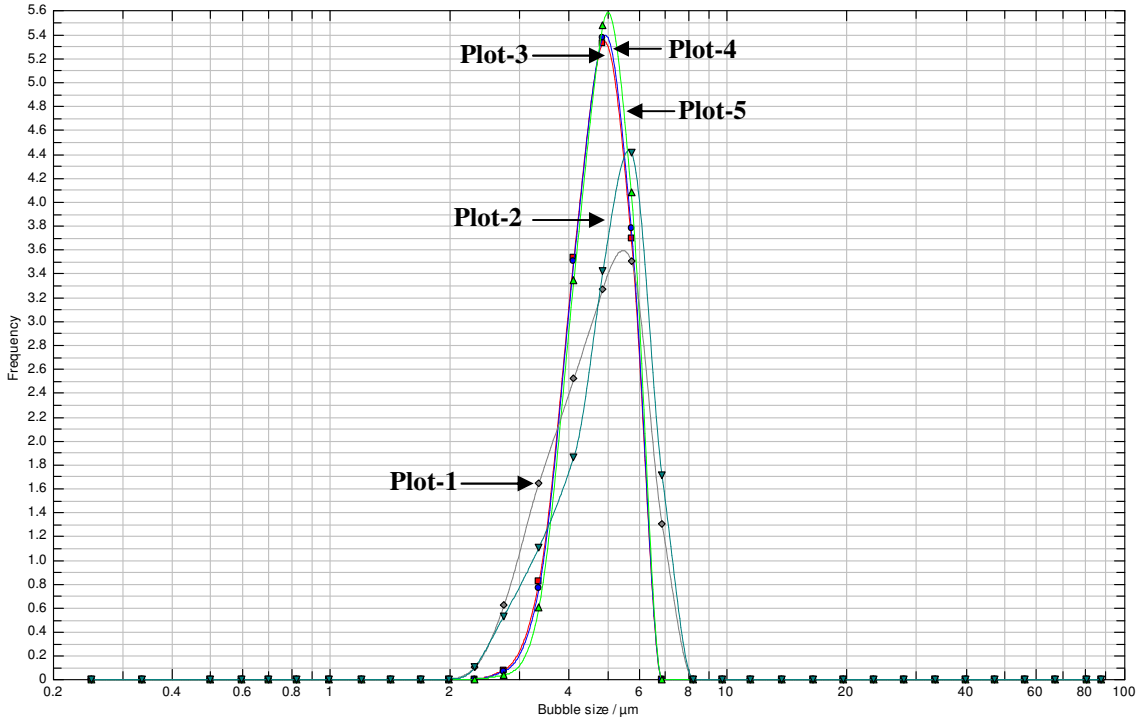

Figure 4.5. Laser diffractograph of microbubble suspension prepared at flow rate combination 1.66 µl s^{-1} (air): 2.5 µl s^{-1} (glycerol). Results of five experiments are given. Each Plot shows the bubble size distribution.

4.4. In-depth investigations on the effects of flow rates

The results obtained from initial investigations suggest that it is only at certain combinations of flow rates that microbubbling is possible and that these combinations also have a direct impact on the mean microbubble size and size distribution. The mean microbubble size at λ= 0.4 was much larger than the mean microbubble size at λ=0.8 for entirely different combinations of flow rates. However, when the glycerol flow rate was fixed at 2.5 µl s^{-1} and the air flow rate was reduced to 1.66 µl s^{-1}, microbubble size also reduced with the reduction of gas ratio value (λ=0.7). These observations led to a detailed flow rate mapping study with the view to identifying regimes of flow rates for microbubbling.

4.4.1. Modes of microbubbling

Identifying the modes of microbubbling for liquid-air systems in CEHDA microbubbling was an essential requirement in pursuing this research work. This is because the modes of microbubbling were different from the modes of atomization in conventional EHDA and CEHDA (Jaworek and Krupa 1999). In this work three distinct modes were identified as discussed below: bubble dripping, coning and microbubbling.

At zero voltage, when the glycerol flow rate and the air flow rate were reached a suitable combination, numerous large air bubbles were seen collecting in the glycerol meniscus. As the gravitational force overcame the surface tension forces, a glycerol drop full of air bubbles was detached from the tip of the outer needle and immediately after that a new drop began to form at the tip of the needle. The appearance of this phenomenon of the bubble dripping mode at zero voltage is the initial stage for microbubbling (**Figures 4.6**a **& 4.6**b).

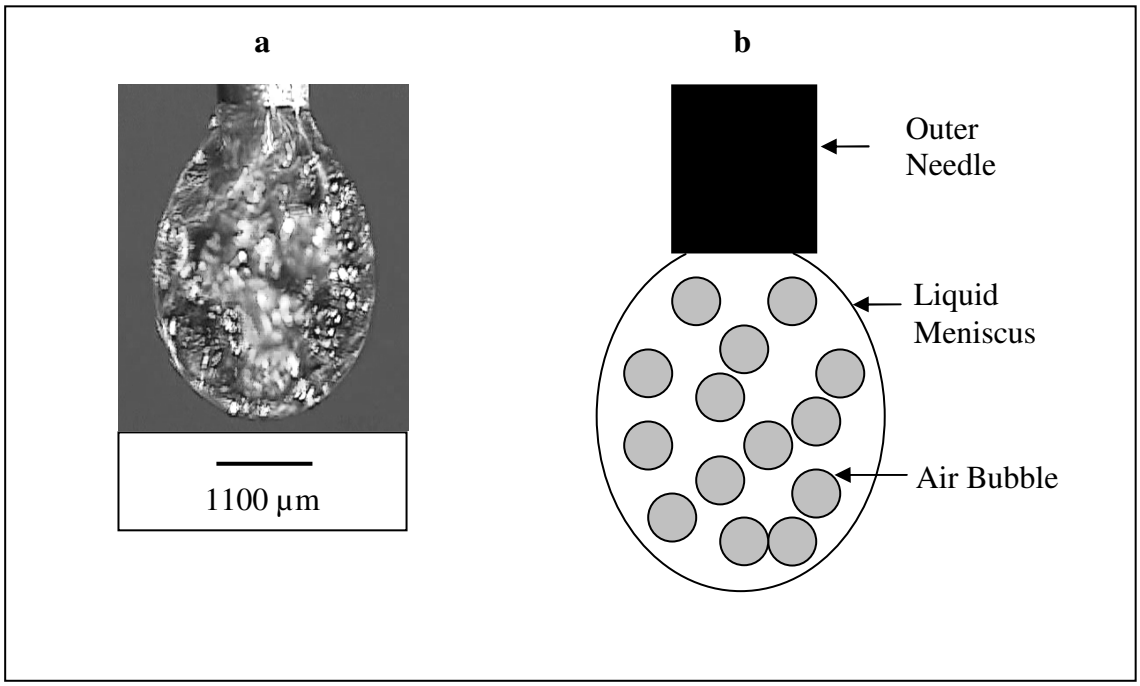

Figure 4.6. Bubble dripping mode at a flow rate combination 1.66 µl s^{-1}(air) : 2.5 µl s^{-1} (glycerol) and at zero voltage (**a**) actual and (**b**) schematic.

With a gradual increase in applied voltage, the bubble filled drop starts to take the shape of a partial cone (**Figures 4.7**a **& 4.7**b). This is identified as the coning mode and with further increase in applied voltage it gradually changes into the microbubbling mode, which can be compared with the cone-jet mode in conventional electrohydrodynamic atomization (**Figures 4.8**a **& 4.8**b). The applied voltage requirement for these three different modes of CEHDA microbubbling for six different combinations of flow rates was studied and the results are tabulated in **Table 4.2** indicating the presence of the three modes in different ranges of applied voltage.

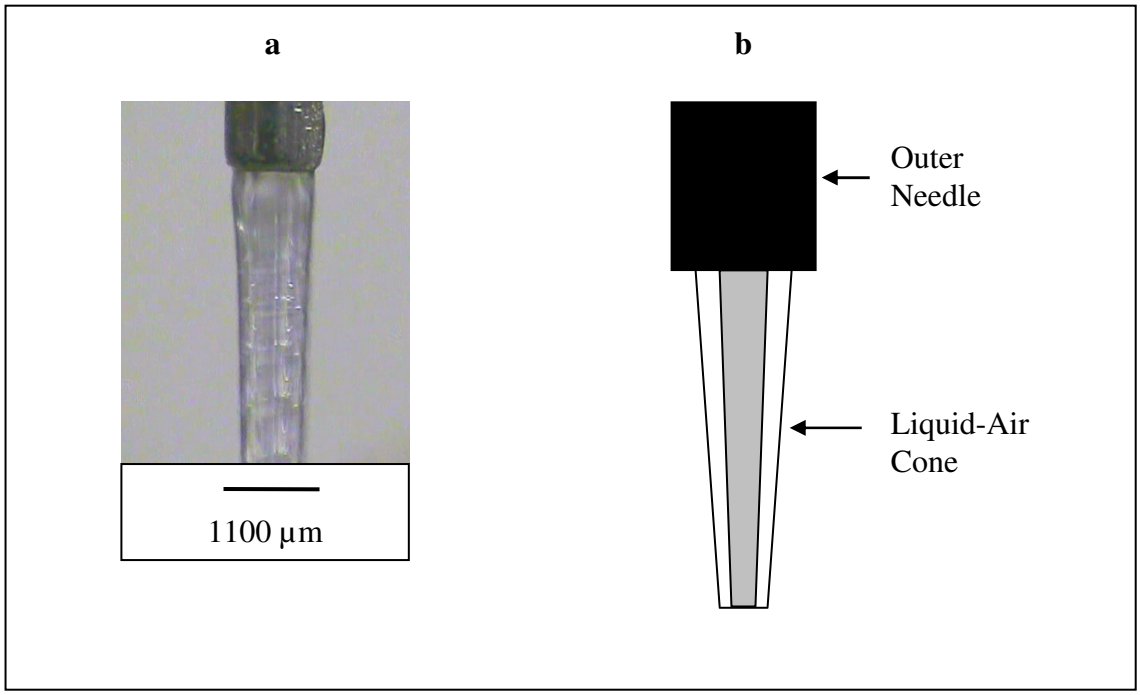

Figure 4.7. Coning mode at a flow rate combination 1.66 µl s^{-1}(air) : 2.5 µl s^{-1} (glycerol) and at 5.5 kV (**a**) actual and (**b**) schematic.

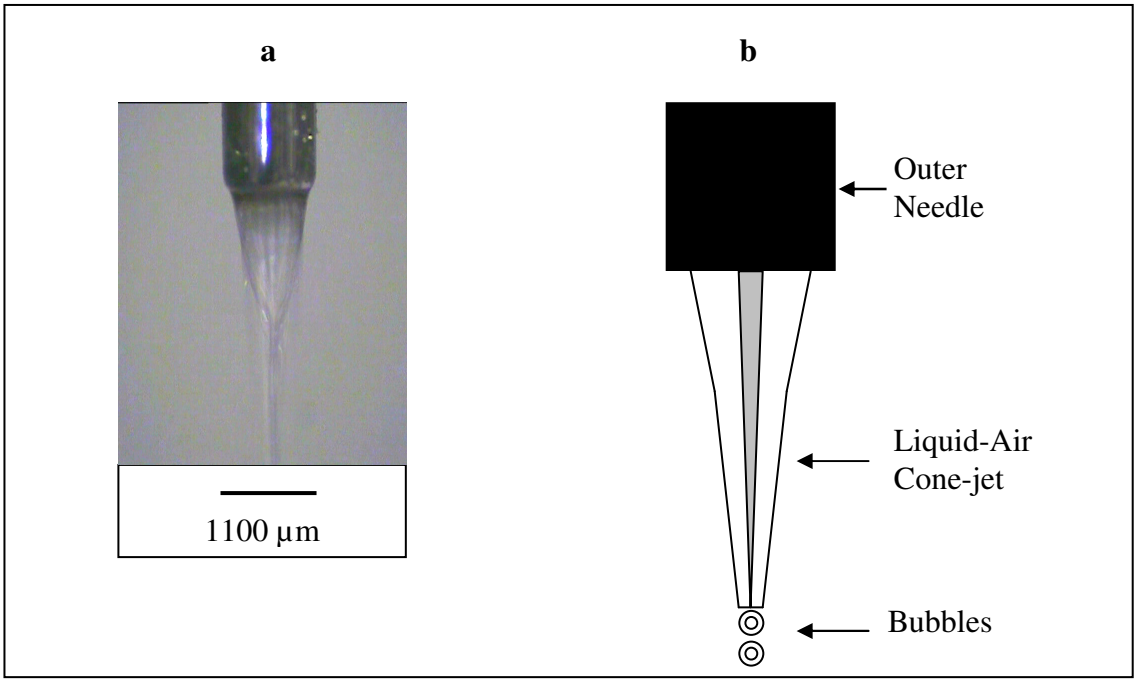

Figure 4.8. Microbubbling mode at a flow rate combination 1.66 µl s^{-1}(air) : 2.5 µl s^{-1} (glycerol) and at 8.8 kV (**a**) actual and (**b**) schematic.

Table 4.2. Ranges of applied voltage for different modes of microbubbling at various combinations of flow rates (no measurement of bubble size was undertaken).

Air Flow rate (µl/s)	Glycerol Flow rate (µl/s)	Voltage range for Bubble dripping (kV)	Voltage range for Coning (kV)	Voltage range for Microbubbling (kV)
3.33	3.33	0-5.2	5.2-8.2	8.2-12.5
3.33	2.50	0-5.3	5.3-8.0	8.0-12.5
4.16	3.33	0-5.2	5.2-8.3	8.3-12.5
4.16	5.00	0-3.9	3.9-8.5	8.5- 9.4
4.16	5.83	0-4.1	4.1-8.3	8.3- 9.3
5.00	5.00	0-4.8	4.8-9.2	9.2-12.5

4.4.2. Flow Rate mapping

Figure 4.9 shows a parametric plot constructed for the microbubbling of a glycerol-air system as a function of glycerol flow rate and air flow rate. The range of air flow rate from 0.4 μl s^{-1} to 6.8 μl s^{-1} demanded the liquid flow rates to be increased up to 12 μl s^{-1} to construct this map.

This map (**Figure 4.9**) reveals that there can be four notable regimes of material discharge when glycerol and air are allowed to flow in a new co-axial electrohydrodynamic flow needle set up (**Figure 3.2**). Below a critical minimum flow rate (~0.8 μl s^{-1}) of air, glycerol behaved as a liquid subjected to conventional electrohydrodynamic atomization showing the conventional modes of atomization on application of voltage (Jaworek and Krupa 1999) and this zone has been identified as **Zone-1** in **Figure 4.9.**

For air flow rates above this critical minimum level, until a first threshold value of glycerol flow rate was reached, the microbubbling mode was not detected upon applying a voltage although the bubble dripping mode appeared at zero voltage at much higher values of air flow rate. The region below this first threshold value where air flow dominates and no microbubbling is noticeable is identified as Zone-2 in **Figure 4.9.**

Above this first threshold value, intermittent microbubbling was noticeable until a second threshold value was found at a higher liquid flow rate. The region between these two threshold values where microbubbling is intermittent is named as Zone-3 in **Figure 4.9.** Above the second threshold value, continuous microbubbling occurs and this region has been identified as Zone-4 (**Figure 4.9).**

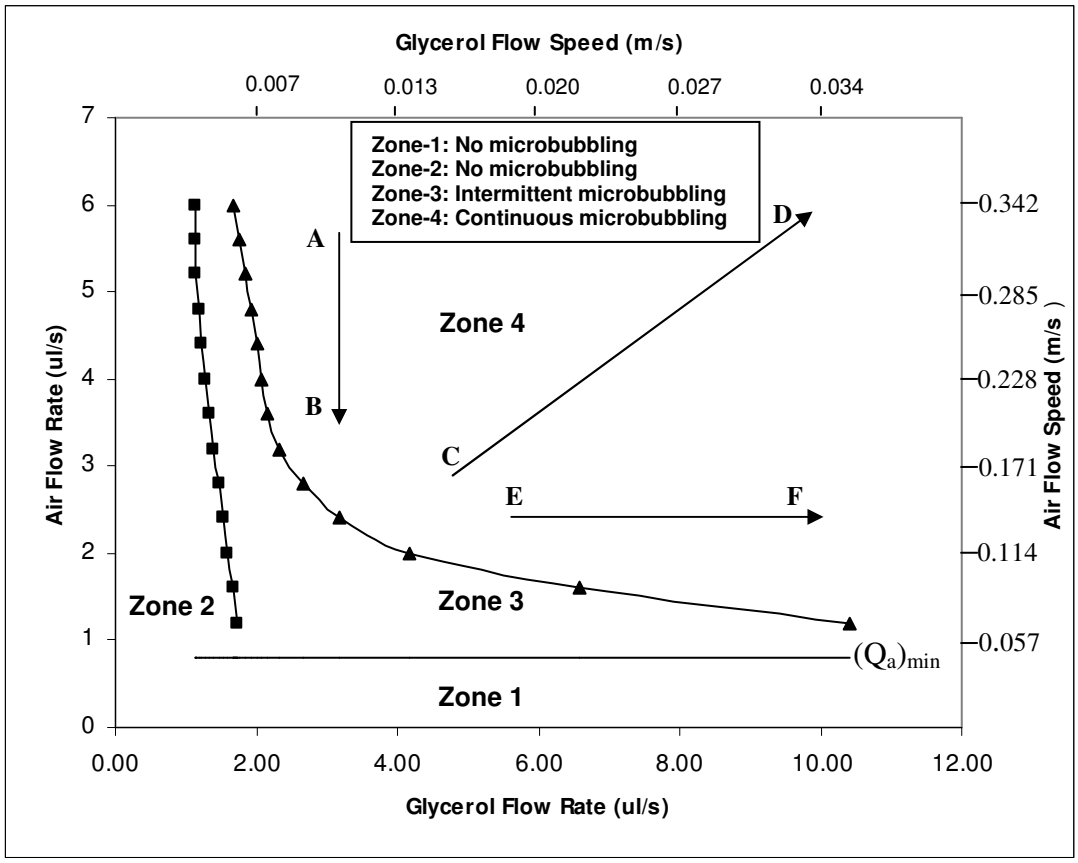

Figure 4.9. Graph of air flow rate versus glycerol flow rate showing various regions encountered. On line AB, gas ratio (λ) reduces with the reduction of jet diameter. On CD, λ is constant with increase of jet diameter. On EF, λ reduces with the increase of jet diameter.

Zone-1, where the conventional modes of EHDA occur, corresponds to a result of a very low air flow rate and, in this region; air has no influence on the atomization of glycerol. The absence of microbubbling in Zone-2 can be attributed to the low flow rates of liquid and the fact that the flow of air is dominant and so generates, at zero voltage, large air bubbles at the tip of the outer needle as in **Figure 4.10.** In Zone-3, microbubbling takes place intermittently and there is wastage of liquid under these conditions. Zone-4 is important as microbubbling in this region is continuous and hence, the yield of microbubbles is high.

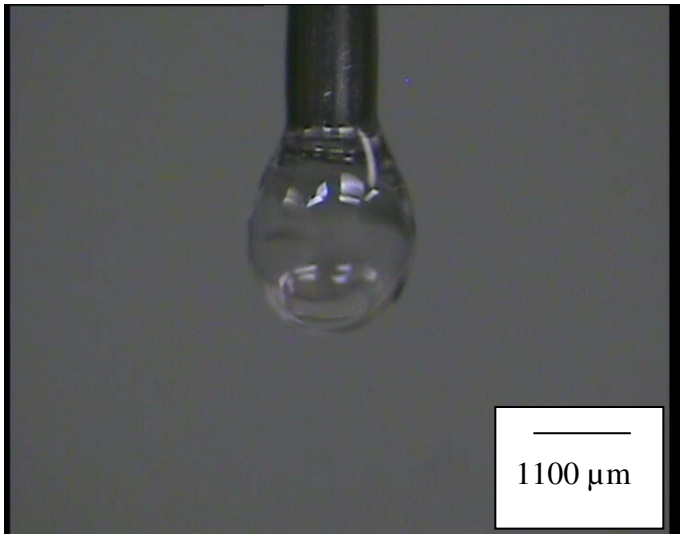

Figure 4.10. A large bubble at the tip of the outer needle during the domination of air flow rate over the liquid flow rate.

4.5. Microfluidic flow focusing systems vs CEHDA microbubbling

The process of microbubbling in co-axial electrohydrodynamic flow can be compared with that of microbubbling in microfluidic systems as the gas pumped through the inner needle is surrounded by the liquid pumped through the outer needle and focused through the formation of a cone and jet (**Figures 4.11**a **& 4.11**b). However, in CEHDA, the liquid that surrounds the gas acts as a driving liquid with electrical and hydrodynamic forces acting upon it to form the cone-jet (Loscertales *et al.* 2002, Lopez-Harrera 2003). In a microfluidic system, the bubble diameter has been correlated with flow rates of liquid and gas, orifice diameter, liquid pressure and the liquid viscosity (Ganan-Calvo and Gordillo 2001, Ganan-Calvo 2004, Garstecki *et al.* 2004, 2005, Gordillo *et al.* 2004).

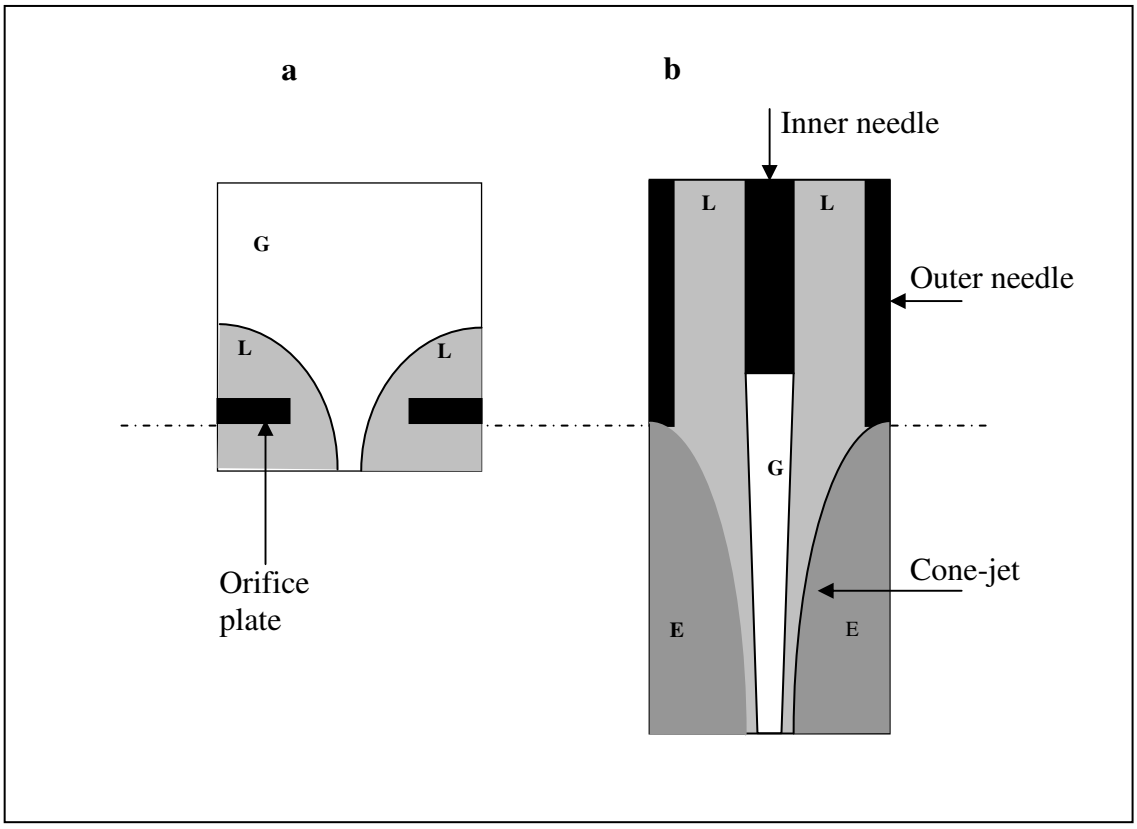

Figure 4.11. Schematic diagrams comparing microbubbling by (a) microfluidics and (b) co-axial electrohydrodynamic atomization. L= Liquid, G= Gas, and E= Electric field

For microbubbling in a capillary flow focusing device (Ganan-Calvo 2004), where the liquid Reynolds number ranges from 40 to 1000, equation (4.1) has been put forward for the determination of bubble diameter (d_b), which is a function of the orifice diameter (D), gas flow rate (Q_g), and the liquid flow rate (Q_l).

$$\frac{d_b}{D} = 1.1\left(\frac{Q_g}{Q_l}\right)^{0.4} \tag{4.1}$$

For a microfluidic flow focusing device associated with much lower Reynolds numbers than the above range; scaling for the bubble diameter (d_b) involves gas pressure(p), liquid flow rate (Q_l) and liquid viscosity (μ) (Garstecki *et al.* 2004, 2005) leading to:

$$d_b = k\,(p/Q_l\mu)^{0.5} \tag{4.2}$$

where k is a constant.

It is clear from eq. (4.1) & (4.2) that in a laminar flow situation, bubble diameter is inversely proportional to liquid flow rate and viscosity and directly proportional to gas flow rate and orifice diameter. Bubble diameter is also proportional to the ratio between gas flow rate and liquid flow rate (λ).

The orifice diameter D in eq. (4.1) for microfluidics can be compared with the steady jet diameter in CEHDA at a point such as 'O' in **Figure 4.12**, where microbubbles are collected in a container of glycerol. It has been amply demonstrated that in the steady cone-jet mode, the jet diameter can be increased or decreased with the increase or decrease of flow rates or with decrease or increase of applied voltage resulting in larger droplets from a larger jet diameter and smaller droplets from a smaller jet diameter (Jayasinghe and Edirisinghe 2004).

The phenomenon of jet diameter reduction due to the decrease of flow rate at a constant applied voltage can be attributed to the obvious reduction in the mass content of the flowing materials and the resulting inertia forces being overtaken by the electric force. Similarly, the electric force will overtake the inertia forces when the applied voltage is increased at a constant flow rate resulting in a smaller jet diameter. For microbubbling

in CEHDA, the best practice is to achieve a steady cone-jet mode at the highest possible applied voltage and then reduce the flow rates to achieve a minimum possible jet diameter at a point 'O' (**Figure 4.12**) if the objective is to reduce bubble size.

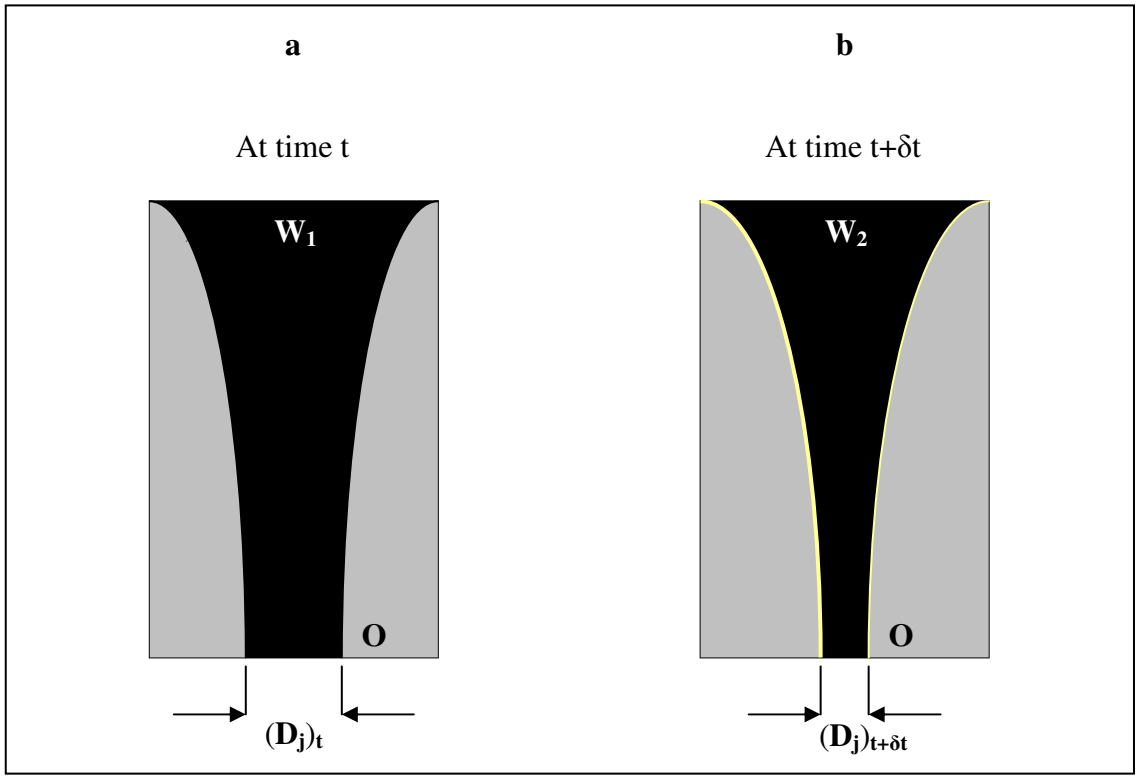

Figure 4.12 Schematic of diagrams showing jet diameter D_j at time (a) t and (b) t +δt. Jet diameter reduces from time t to t +δt either with the increase of voltage or with the decrease of flow rate.

For jet diameter $(D_j)_{t+\delta t}$ < jet diameter $(D_j)_t$ when $V_1 = V_2$,

$$W_1 > W_2 \tag{4.3}$$

where, V_1 and V_2 are applied voltages at time t and $t + \delta t$, respectively. Similarly, W_1 and W_2 are the mass flow rates of throughput at time t and time $t + \delta t$, respectively.

$$W_1 = Q_{l1}\rho_l + Q_{g1}\rho_g \tag{4.4}$$

and

$$W_2 = Q_{l2}\rho_l + Q_{g2}\rho_g \tag{4.5}$$

where, Q_{l1} and Q_{g1} are liquid and gas flow rates at time t. Q_{l2} and Q_{g2} are liquid and gas flow rates at time $t + \delta t$. ρ_l is the liquid density and the ρ_g is the gas density. Combining equations (4.3), (4.4) and (4.5) gives:

$$Q_{l1}\,\rho_l + Q_{g1}\,\rho_g > Q_{l2}\,\rho_l + Q_{g2}\,\rho_g \tag{4.6}$$

A vigorous swirl can be observed within the cone when liquid of poor electrical conductivity and low viscosity are electrosprayed (Barrero *et al.* 1998). In the case of microbubbling using CEHDA in a liquid-air system, which overall has a low electrical conductivity and viscosity, creating less turbulent conditions within the cone is a difficult but an important objective. Reducing the flow rates from time t to time $t + \delta t$ is therefore an important stage to allow viscous forces to be more dominant in the flow of materials. This requires that:

$$R_{l1} + R_{g1} > R_{l2} + R_{g2} \tag{4.7}$$

and

$$R_{g1} > R_{g2} \tag{4.8}$$

where, R_{l1} and R_{l2} are liquid Reynolds numbers at time t and time $t + \delta t$, respectively. R_{g1} and R_{g2} are gas Reynolds numbers at the corresponding times. Since Reynolds number = $R = 4\rho Q / \pi D \mu$, where, ρ is the density, Q is the flow rate, D is the diameter of the cylinder through which material flows, and μ is the viscosity, equation (4.8) leads to:

$$4\rho_g Q_{g1} / D_g \mu_g > 4\rho_g Q_{g2} / D_g \mu_g \tag{4.9}$$

and

$$Q_{g1} > Q_{g2} \tag{4.10}$$

Equations (4.6) and (4.10) both show the importance of reducing the gas flow rate to achieve a smaller bubble size. The initial investigations described in **Section 4.3.2** and the results tabulated in **Table 4.1** also confirm this view, where the bubble diameter was reduced to < 10 µm by maintaining the liquid flow rate at 2.50 µl s^{-1} and reducing the air flow rate from 2.08 µl s^{-1} to 1.66 µl s^{-1} (Farook *et al.* 2007a). In this case, the gas ratio λ was also reduced from 0.8 to 0.7.

The observations in CEHDA microbubbling tallies with eq. (4.1) developed for microfluidics, where reducing the gas ratio λ leads to smaller bubble diameters. However, reducing the gas flow rate or increasing the liquid flow rate in microfluidics can only be done within a limited range. Beyond a certain point, reduced gas flow rate or increased liquid flow rate can lead to no bubble generation due to the liquid completely filling the bubbling chamber (Gordillo *et al.* 2004). Even in CEHDA

microbubbling, bubble generation changes from continuous to intermittent (**Figure 4.9**) when the flow rate combination changes, for example, from 3.0 μl s^{-1} (air) : 3.0 μl s^{-1} (glycerol) to 2.0 μl s^{-1} (air) : 3.0 μl s^{-1} (glycerol). Further reduction in air flow rate would also lead to a no microbubbling situation. On the other hand, increase in liquid flow rate will naturally increase the jet diameter resulting in larger bubble diameters.

On a horizontal line such as EF on **Figure 4.9**, just above the critical minimum air flow rate $(Q_g)_{min}$, microbubbling is vigorous with the increase of liquid flow rate and decrease of λ. However, in CEHDA, the increase of liquid flow rate will affect the inequalities shown in equations (4.6) and (4.10) adversely leading to larger jet diameters and therefore, reduction in λ alone does not mean reduction in bubble size. Similarly, on a line such as CD in **Figure 4.9**, where λ is constant, bubbles are shown to be of the same size in microfluidics (Ganan-Calvo 2004). In contrast in CEHDA microbubbling, maintaining a constant λ for various pairs of liquid and gas flow rates does not keep the bubble size at a constant value as it varies with the change in jet diameter with the increase or decrease of flow rates.

The best option in CEHDA microbubbling is to reduce the bubble size with the reduction of λ by moving downward on a suitable vertical line such as AB in **Figure 4.9**. When moving downward on AB, λ will be decreasing as the gas flow rate is reduced while the liquid flow rate is kept constant and simultaneously the jet diameter will also be reducing as the overall flow rate is reduced with the reduction in gas Reynolds number. The effects of important parameters such as gas flow rate, liquid flow rate and applied voltage are summarized in **Table 4.3**.

Table 4.3. Effects of important parameters on the bubble diameter

Gas Flow Rate	Liquid Flow Rate	Applied Voltage	Gas Ratio	Jet Diameter	Bubble Diameter
Fixed	Increases	Fixed	Decreases	Increases	Increases
Increases	Fixed	Fixed	Increases	Increases	Increases
Decreases	Fixed	Fixed	Decreases	Decreases	Decreases
Decrease	Decrease	Fixed	Fixed	Decreases	Decreases
Increases	Increases	Fixed	Fixed	Increases	Increases
Decreases	Decreases	Increases	Fixed	Decreases	Decreases

The fundamental difference between microbubble preparation by microfluidics and CEHDA is that, in the former, the orifice size is independent of the change in flow rates whereas in CEHDA the jet diameter, which determines the bubble size, is dependent on the change in flow rates, applied voltage and the electrical conductivity of the materials, thus the CEHDA technique offers more opportunities for process control.

4.6. Stability of microbubbles

In order to observe the dissolution behaviour of the microbubbles, the variation in diameter of a single bubble prepared using CEHDA was studied at time intervals of 300s using an optical microscope and standard Image-Pro Plus software. A (0.05 ml) sample of microbubble suspension collected in the glass container was taken onto a glass slide immediately after preparation using a syringe. It took 300 s to single out a bubble with a known diameter before starting to measure its diameter until it disappeared.

The stability of the bubble prepared by CEHDA can be analysed using the equations developed by Epstein & Plesset (1950). If D_o is the bubble diameter at $t = 0$ and D is the diameter of the bubble at $t > 0$;

$$D^2 = D_o^2 - 8\,\alpha t \tag{4.11}$$

α depends on the coefficient of diffusivity, initial dissolved air concentration of liquid, saturated dissolved air concentration and the density of the air inside the bubble. The first two measured values of bubble diameters at t =300 and t=600, respectively, were substituted in eq. (4. 11) to calculate the values of D_o and α, giving D_o= 9.61 μm α = 0.0016 $\mu m^2 s^{-1}$.

The calculated variation of D with t can now be compared with the measured values (**Figure. 4.13**). Except for the fact that the calculated rate of shrinkage is smaller than the actual rate of shrinkage, Epstein & Plesset's equation can represent the dissolution of the bubble prepared by CEHDA. However, it has been noted that the Epstein & Plesset equation does not fully represent larger bubbles as these tend to maintain a minimum size for a longer period before their dissolution (Duncan and Needham 2004) but our work is focused on smaller < 10 μm size bubbles and this is why this particular size was selected in the above analysis. It must also be noted that eq. (4.11) does not consider surface tension effects and if these are taken into account, the gap between the measured dissolution behaviour of the bubble and the accompanying calculated scenario will narrow.

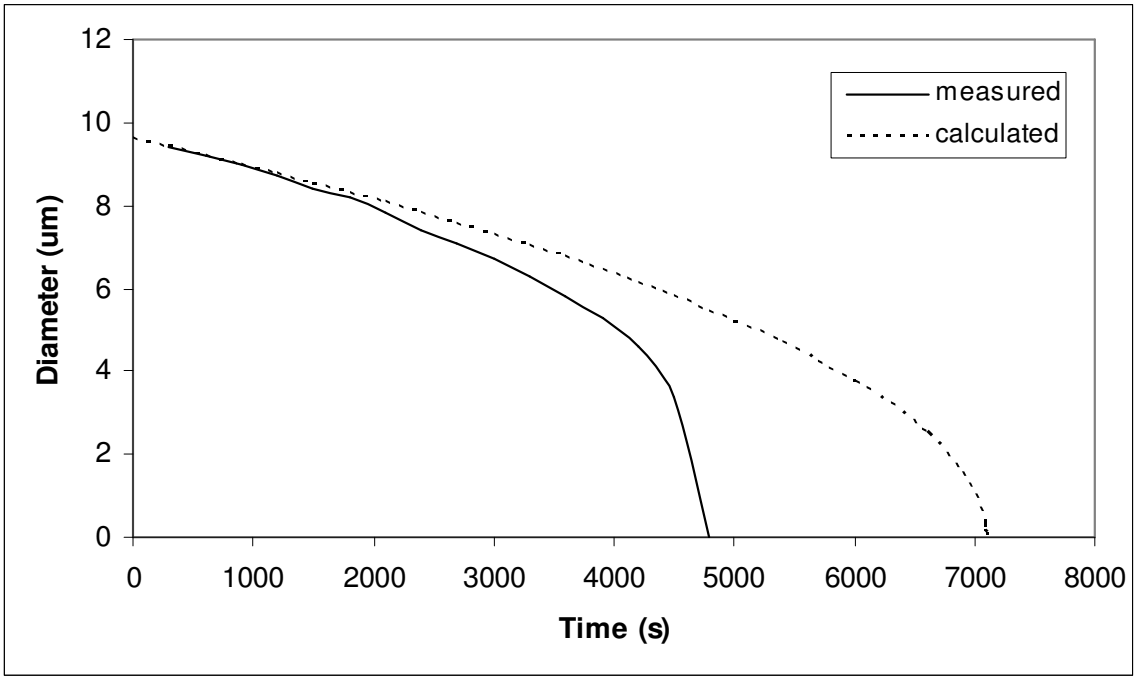

Figure 4.13. Variation of the diameter as a function of time for a microbubble of starting diameter 9.4 µm prepared by CEHDA microbubbling (Relative error is 5%).

The measured microbubble survival time of ~4800 s needs to be considerably improved in actual microbubble suspensions used as ultrasound contrast agents in medical engineering. The prolonged survival of microbubbles can be achieved by restricting the outward diffusion of air by the use of shells or bubble surface modifying agents, and by the substitution of high density high molecular weight gas for air (Borden and Longo 2002, Krasovitski and Kimmel 2006, Raisinghani and DeMaria 2002, Soetanto and Chan 2000).

Since the investigations discussed in this thesis are limited to using air as the gas component of microbubbles, for reasons of cost, attempts have been made, firstly, to modify the bubble surface using a surfactant and a fine solid particle, secondly, to

compare bubbles prepared by CEHDA with those obtained via a different preparation method. The results are discussed in following **sections 4.7.1** and **4.7.2.**

4.6.1. Effect of coating material upon microbubble stability

The material properties measured for the different liquid media are shown in **Table 4.3.** The glycerol used in these experiments had a water content of 15 %. The rates of dissolution for microbubbles prepared by electrohydrodynamic atomisation using the glycerol-air, glycerol-Tween-air and glycerol-zirconia-air systems are shown in **Figure 4.14.** It is clear from this that the microbubbles prepared from the glycerol-air system dissolved at a greater rate than the microbubbles prepared from the other two systems.

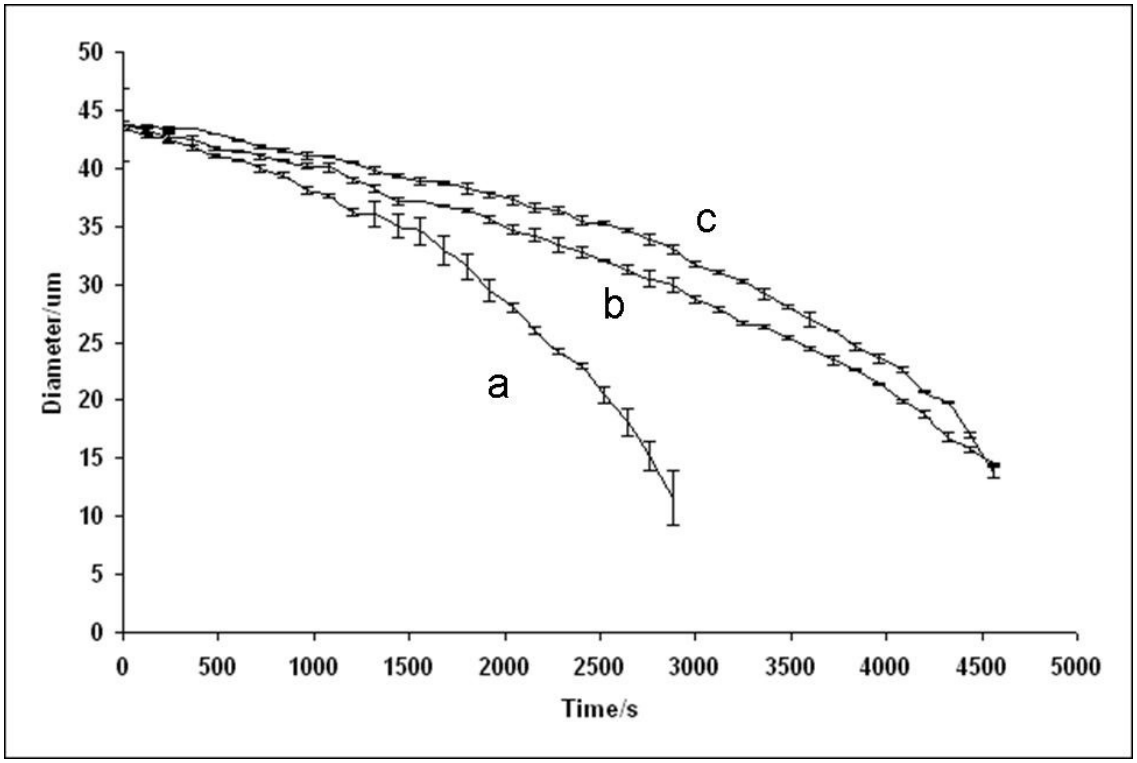

Figure 4.14. Comparison of dissolution behaviour of microbubbles prepared by CEHDA using **a** glycerol-air system **b** glycerol-2 wt % zirconia-air system **c** glycerol-2 wt % Tween 80-air system.

Table 4.4 Measured material properties for the different liquid media used

Material	Density ($Kg\ m^{-3}$)	Surface tension ($mN\ m^{-1}$)	Viscosity mPa s
Glycerol	1217	63	740
Tween 80	1214	25	435
Glycerol with 2 wt % Tween 80 (A model solution)	1214	33	690
Glycerol with 2 wt % zirconia (A model suspension)	1240	34	760

From eq. (3.3), there are 3 factors which may potentially affect the stability of gas bubbles: (i) surface tension at the gas/liquid interface (ii) the gas concentration in the surrounding liquid and (iii) the diffusivity of the gas through the microbubble coating and/or in the surrounding liquid. Since the microbubbles from all three systems were collected in glycerol from the same source, the initial dissolved air concentration in the collecting medium (c_i) should have been the same for all three systems.

As shown in **Table 4.3**, however, the surface tension values were different for each bubble and the observed behaviour (**Figure 4.14**) of microbubbles with respect to the surface tension values is in qualitative agreement with eq. (3.3). Similarly, the presence of the particles and/or surfactant at the bubble surface would also have modified the effective diffusivity at the bubble surface. In the absence of accurate measurements of this latter quantity, it is not possible to draw definite conclusions as to the relative influence of surface tension and diffusivity in this case, although it is clear from eq.(3.3) that the rate of bubble dissolution has much stronger dependence upon *k* than *r*. Tween 80 is a well known surfactant and, as such, would be expected to reduce both surface tension and the effective diffusivity (Singhal *et al.* 1993).

The stabilization of bubbles by solid particles is an interesting phenomenon, first observed by Pickering (1907) with the stabilization of emulsions by fine solid particles instead of surfactants and is widely known as 'Pickering stabilization'. It is used in the recovery and separation of mineral ores, cleaning of crude oil, water treatment and in the food industry. However, since many of the underlying mechanisms were poorly understood, the topic has recently drawn the attention of many researchers once again (Dickinson *et al.* 2004; Binks and Lumsdon 2000; Du *et al.* 2003) and it has been demonstrated that stabilization is dependent on the hydrophobicity of the particles and hence their tendency to adsorb on to the bubble surface rather than disperse in the liquid medium.

The results from this study (**Figure 4.14**) show that microbubbles can similarly be successfully stabilized with solid particles which affect a reduction in surface tension (**Table 4.3**) and will reduce the surface area of the bubble available for diffusion (the size of the effect depending upon the size of the particles relative to that of the bubble and their concentration on the surface). Thus, it may be concluded that CEHDA does not affect the inherent ability of surfactants and/or particle suspensions to improve bubble stability.

4.6.2. Effect of the preparation method upon microbubble stability

In **Figure 4.15**, the curves corresponding to the microbubbles prepared by CEHDA and agitation are denoted by lower and upper case letters, respectively (a/A refer to the glycerol air system and c/C to the glycerol-Tween80-air system). As may be seen, a similar stabilizing effect was observed in the presence of surfactant in both cases, but it is clear that the microbubbles prepared by agitation were more stable. This is in

agreement with previous observations (Pancholi *et al.* 2008a) and there are a number of possible explanations. Firstly, CEHDA may bring about an increase in surface tension and/or diffusivity which makes the bubbles less stable than those prepared by shaking (i.e. r and k are larger for microbubbles prepared by CEHDA). Secondly, there may be insufficient time during atomisation for adsorption of a surfactant coating to take place, or the adsorption process is somehow inhibited (again leading to larger values of r and k due to the lack of a complete coating). Thirdly, shaking may simply introduce more gas into the surrounding liquid so that the diffusion gradient is smaller, than for microbubbles prepared by CEHDA (i.e. the value of c_i - c_s is lower).

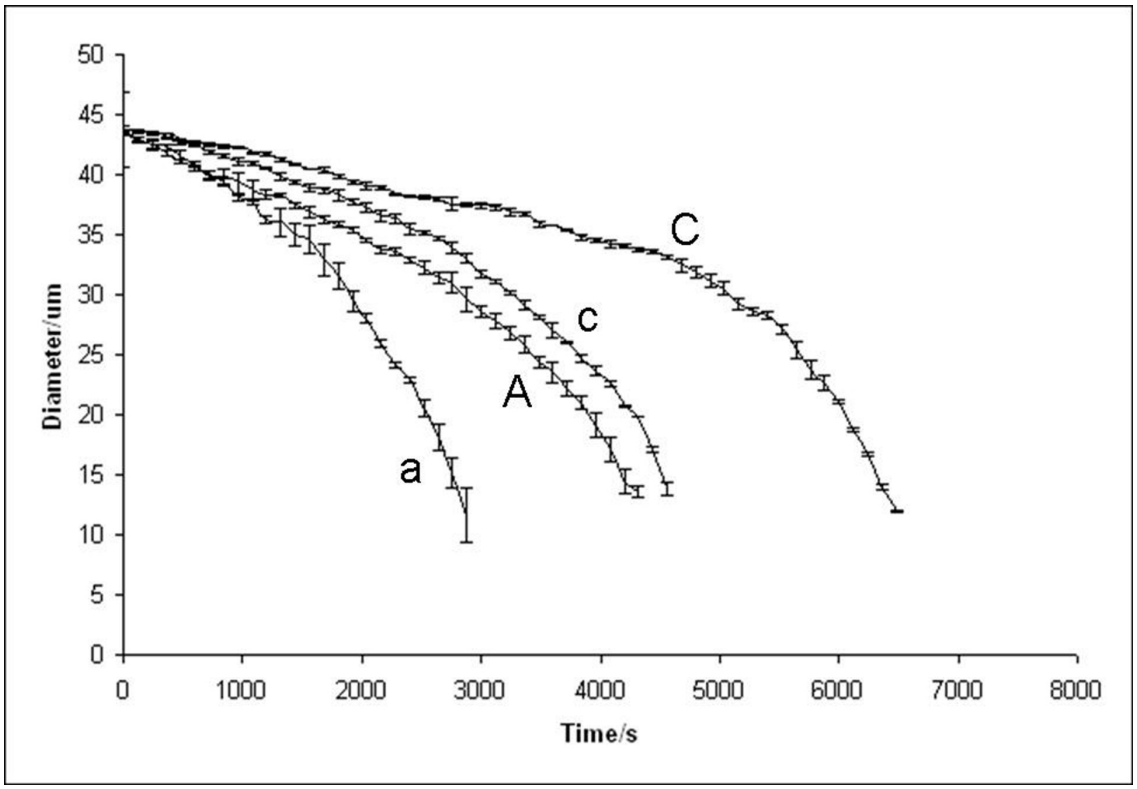

Figure 4.15. Comparison of dissolution behaviour of microbubbles prepared by CEHDA and agitation **a** microbubble by CEHDA using glycerol-air system **A** microbubble by agitation using glycerol-air system **c** microbubble by CEHDA using glycerol-Tween 80-air system **C** microbubble by agitation using glycerol-Tween 80-air system.

The results in the previous section indicate that CEHDA does not alter the qualitative effect of either surfactants or particles upon microbubble stability. Moreover, as mentioned above, it has previously been reported that the effect of an electric field is to reduce surface tension rather than increase it (Sato *et al.* 1998). Similarly, if CEHDA affected the process of surfactant absorption, then the curves for the glycerol–air system in the absence of surfactant (a and A) should still coincide, which they clearly do not. Thus the third hypothesis would seem to be the most likely explanation. Since there is a deliberate attempt to disperse air in the aqueous medium during shaking, the initial dissolved air concentrations for A and C will certainly have been higher than for a and c. This would also account for the greater stability of the microbubbles prepared by microfluidic processing and sonication observed in the previous study (Pancholi *et al.* 2008a).

On account of the nature of the microfluidic device and the bubble monodispersivity, the bubbles were much more closely packed in the collection vial in the case of the former and were also larger than those produced by CEHDA. Similarly, sonication involves both the entrapment of air in the solution during processing and produces much higher concentrations of microbubbles, so, again, stability would be expected to be higher on account of the higher gas concentration in the surrounding liquid (Binks and Lumsdon 2000). Given that it is the collection and storage of the microbubble suspensions which appears to be more important than the actual bubble formation process, improving the stability of microbubbles prepared by CEHDA should be relatively straightforward. Firstly, as shown in this study, both surfactants and particle suspensions can have a stabilizing effect and, thus, selection of the appropriate coating material is important. Particle stabilization may have other benefits in certain

applications (Stride *et al.* 2008), although of course biocompatibility of the particles will be an essential requirement if these bubbles are to be used in biomedical applications. Collecting the microbubbles in high concentrations will also be beneficial, as will saturating the collecting liquid with the filling gas to reduce the concentration gradient. Although the shell thickness of the microbubbles has a major role to play, it has not been investigated in this study.

CHAPTER 5

PREPARATION OF STABILIZED PHOSPHOLIPID-COATED MICROBUBBLES WITH LOW POLYDISPERSIVITY BY CO-AXIAL ELECTROHYDRODYNAMIC ATOMIZATION MICROBUBBLING

5.1. Introduction

This chapter describes an investigation that was carried out on the preparation of suspensions of phospholipid-coated microbubbles, applying the CEHDA microbubbling technique that has been described in **Chapter 4**. The use of amphiphilic molecules, particularly phospholipids, as coating materials has the particular advantage that they self assemble around the gas core, providing a strong shell architecture suitable for the addition of functional molecules such as drugs and genes (Borden and Longo 2002, Raisinghani and DeMaria 2002, Stride and Saffari 2003). In this investigation, we have used a combination of a phospholipid (L-α-phosphatidylcholine) and an emulsifier, PEG 40, to aid lipid dispersion and prevent microbubble coalescence (Borden and Longo 2002, Borden *et al.* 2004 a, b). The method of preparation and the composition of the phospholipid suspension used for our initial investigation have been described in **Section 3.2.1.**

5.2. Characterisation of phospholipid suspension

The phospholipid suspension was characterized at atmospheric pressure and ambient temperature to determine its density, viscosity, surface tension and electrical conductivity. The measured properties of the phospholipid suspension are given in **Table 5.1**. These are important since the suspension acts as the driving liquid during the CEHDA microbubbling process. Viscosity and electrical conductivity play a major role

as these properties are responsible for the electrical charge transport through the liquid mass and for the formation of the cone jet, which determines the final size distribution of the sprayed product (Jayasinghe *et al*.2002; Ku and Kim 2002; Lopez-Herrera *et al*. 2003; Loscertales *et al*. 2002).

Table 5.1. Properties of the phospholipid suspension prepared for microbubbling experiments

Density ($kg\ m^{-3}$)	**Viscosity** (mPa s)	**Surface tension** ($mN\ m^{-1}$)	**Electrical conductivity** ($\mu S\ m^{-1}$)
1030	2.6 ± 0.05	43 ± 0.2	8.8 ± 1

5.3. Modes of microbubbling for the phospholipid-air system

In this process microbubbling succeeds dripping of larger bubbles and subsequent narrowing or coning of the liquid stream as in the case of glycerol-air system described in **Chapter 4**. The bubble dripping, coning and microbubbling modes observed during CEHDA of the phospholipid-air system are shown by **Figures 5.1**a, **5.1**b, and **5.1**c, respectively. The evolution of these modes is discussed in detail in **Chapter 4** and in Farook *et al*. (2007b). With the increase of applied voltage and hence the intensity of the magnitude of electric field, the bubble dripping mode transforms to the microbubbling mode via the coning mode. For the phospholipid-air system used in this work, the bubble dripping mode was observed between 0 to 2.5 kV. The coning mode existed between 2.5 kV and 5.7 kV and the microbubbling mode was observed between 5.7 kV and 6.1 kV.

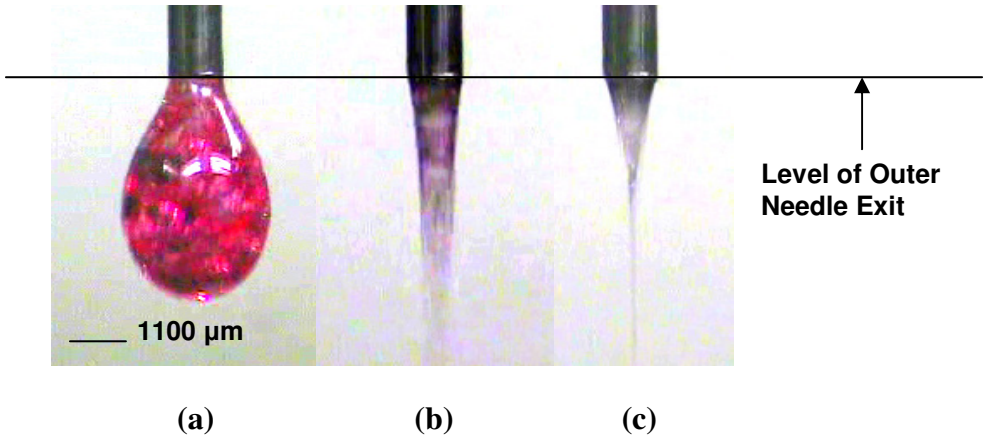

Figure 5.1. Modes of microbubbling, **(a)** bubble dripping mode **(b)** coning mode and **(c)** microbubbling mode, observed for the phospholipid suspension.

5.4. Parametric plot between the flow rate of air and the flow rate of phospholipid suspension

The air flow rates considered for this study ranged from 8.0 µl s^{-1} to 0.8 µl s^{-1}. For each value of air flow rate, the threshold values of intermittent microbubbling and continuous microbubbling were determined by gradually increasing the suspension flow rate and observing the transition from one mode to another on the video screen (Farook *et al.* 2007b). The applied voltage was maintained at 6.1 kV throughout this study. In this way a parametric plot between the flow rate of air and the flow rate of suspension was constructed (**Figure 5.2**).

The horizontal straight line in the plot shows the level of critical minimum air flow rate, $(Q_a)_{min}$, below which there is no microbubbling due to the dominance of the suspension flow. Similarly, Zone 2 shows no microbubbling due to the dominance of the air flow. Zone 3 shows intermittent microbubbling and Zone 4 shows continuous microbubbling.

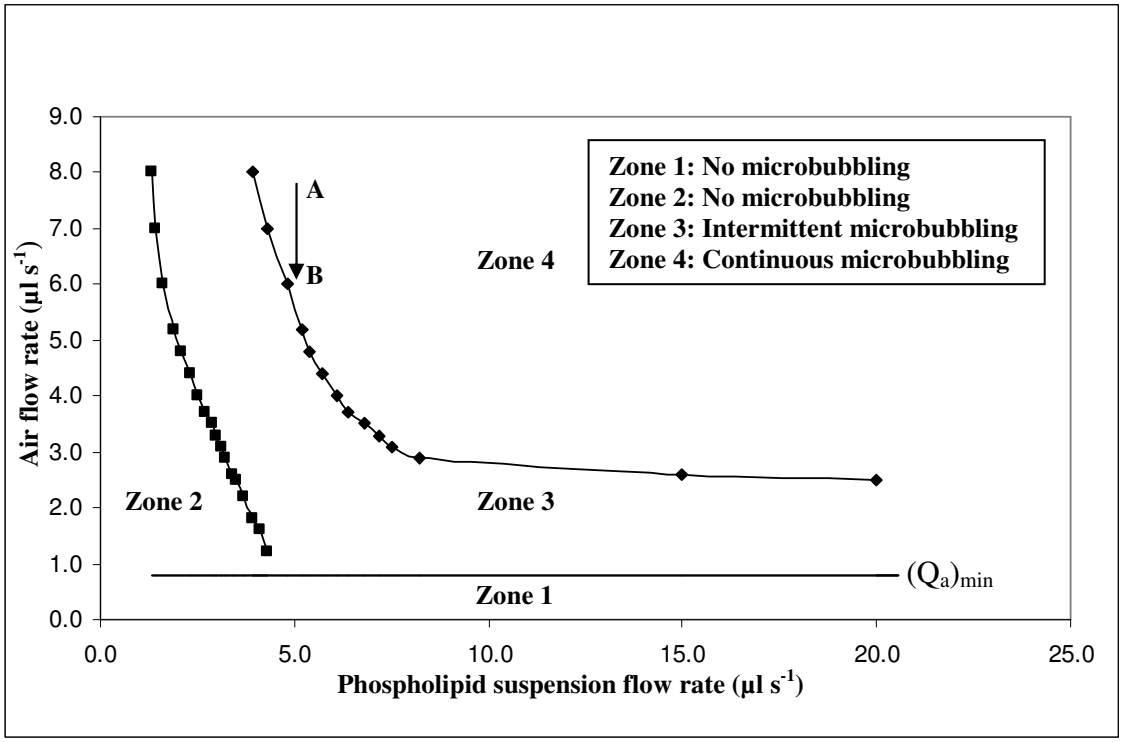

Figure 5.2. Parametric plot between the flow rate of air and the flow rate of phospholipid suspension to show the onset of microbubbling. **Zone 1** and **Zone 2:** No microbubbling, **Zone 3:** Intermittent microbubbling and **Zone 4:** Continuous microbubbling. AB corresponds to a phospholipid suspension flow rate of 5 µl s^{-1}. Horizontal line in the plot represents the critical minimum flow rate of air (0.8 µl s^{-1})

In **Figure 5.3**, the continuous microbubbling zone of the phospholipid-air system has been compared with that of the model glycerol-air system that has been described in **Chapter 4** of this thesis and in Farook *et al.*(2007 b). Curves L & G in **Figure 5.3** represent the onset of continuous microbubbling of the phospholipid-air system and the glycerol-air system, respectively. In the case of the latter, continuous microbubbling begins at lower values of flow rates whereas for the phospholipid suspension, continuous microbubbling begins at higher values of flow rates. The reason for this shift is the difference in physical properties, such as viscosity, surface tension, and dielectric behaviour between glycerol and the phospholipid suspension; and thus this type of plot is material specific. The applied voltage necessary for the microbubbling mode also therefore varies from system to system.

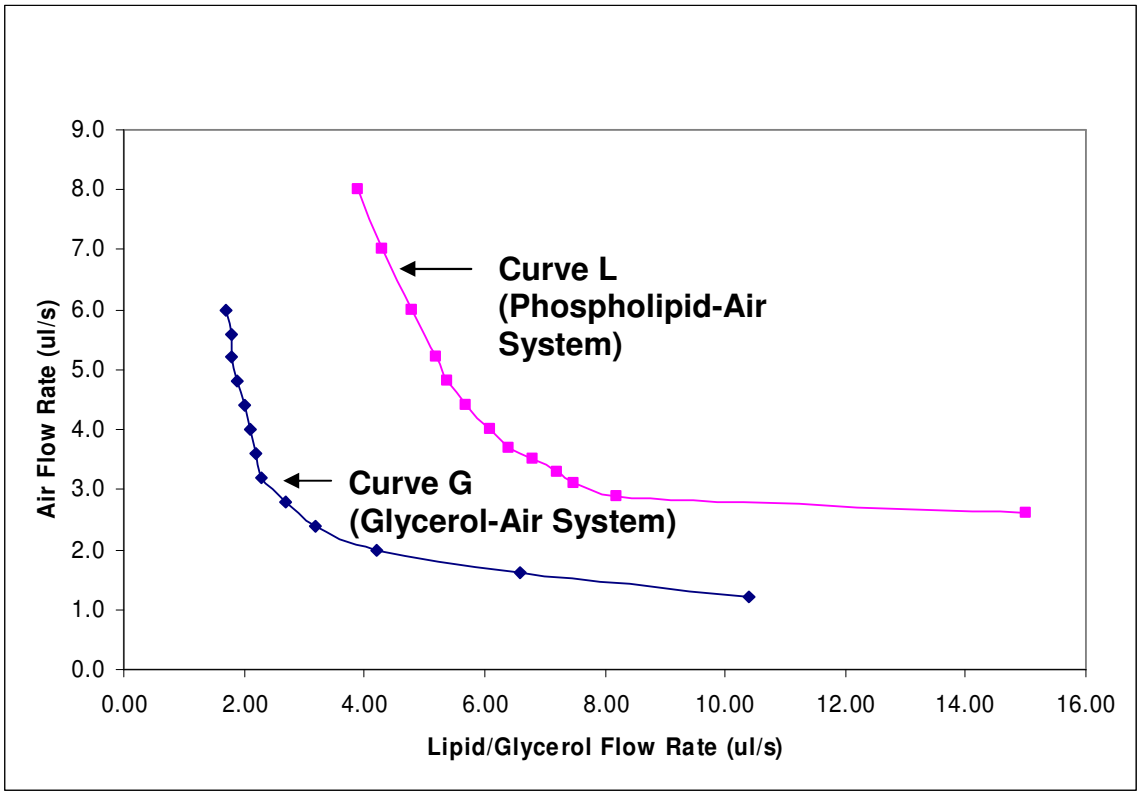

Figure 5.3. Comparison of the onset of continuous microbubbling in the phospholipid-air system and the model glycerol-air system.

5.5. Characterisation by optical microscopy

Phospholipid-coated microbubbles were studied by optical microscopy at ambient temperature (22^{o}C) as well as at human body temperature (37^{o}C). At the ambient temperature, 6 ml of lipid suspension was microbubbled while collecting the microbubble suspension in a glass vial containing 2 ml of distilled water. A sample of 0.05 ml of the microbubble suspension was immediately transferred using a 1 ml syringe from the glass vial to a glass slide and optical microscopic examinations were conducted. The experiments on the behaviour of microbubbles prepared by CEHDA at 37^{o}C were conducted in two stages. Firstly, a glass vial containing 1 ml of distilled water was placed on a hot plate below the ring electrode and the temperature of the distilled water was maintained at 37^{o}C while microbubbling only 3 ml of phospholipid suspension into the glass vial. The bubble concentration was kept constant in all experiments by maintaining a fixed ratio between the phospholipid suspension, volume of water and the injection time. After microbubbling, the vial was removed to ambient conditions and then samples of 0.05 ml were taken at 10, 20, 30, 40, 50 min and after 40 h for microscopic examination. Secondly, 3 ml of phospholipid suspension was microbubbled into a glass vial containing 1 ml of distilled water at the ambient temperature and then the glass vial was transferred on to a hot plate and the temperature of the microbubble suspension was maintained at 37^{o}C for 1 h while samples of 0.05 ml were taken at 10, 20, 40 and 50 min duration for optical microscopy. All the micrographs were prepared using standard Image-ProPlus software (Media Cybernetics, L.P. Del Mar, CA, USA).

Table 5.2. Microbubble sizes obtained by co-axial electrohydrodynamic flow at 22°C. For calculation of mean diameters and standard deviation 100 bubbles were taken from respective micrographs.

Zones From Figure 5.2	Air Flow Rate (µl s^{-1})	Phospholipid Suspension Flow Rate (µl s^{-1})	Gas Ratio (λ)	Mean diameter (µm)	Standard Deviation (µm)	Polydispersivity Index (P.I) (%)
Zone 4	25	5	5	7.5	2.4	32
Zone 4	20	5	4	7.1	2.7	38
Zone 4	15	5	3	6.8	2.1	31
Zone 4	10	5	2	6.6	2.5	39
Zone 3	5	5	1	5.5	1.8	33

5.6. Effect of flow rate on microbubble size and size distribution

Table 5.2 shows the bubble size distribution obtained for five different combinations of flow rates selected from the parametric plot on a downward vertical line AB (**Figure 5.2**), corresponding to a suspension flow rate of 5 µl s^{-1}. With the decrease in air flow rate, a marked decrease in bubble diameter is achieved. The smallest bubble diameter was obtained only at a flow rate combination of 5 µl s^{-1}(air) : 5 µl s^{-1}(suspension), within the intermittent microbubbling zone just below the threshold of continuous microbubbling. **Figure 5.4**a shows the optical micrograph of the microbubbles prepared at this flow rate combination. The smallest size achieved within the continuous microbubbling zone, i.e. Zone 4, at a flow rate combination 10µl s^{-1} (air): 5µl s^{-1} (phospholipid suspension) also satisfies the requirements in terms of bubble size for intravenous use (< 8 µm diameter). **Figure 5.4**b shows an optical micrograph of the

microbubbles prepared at the flow rate combination of 10 µl s^{-1} (air) : 5 µl s^{-1} (phospholipid suspension).

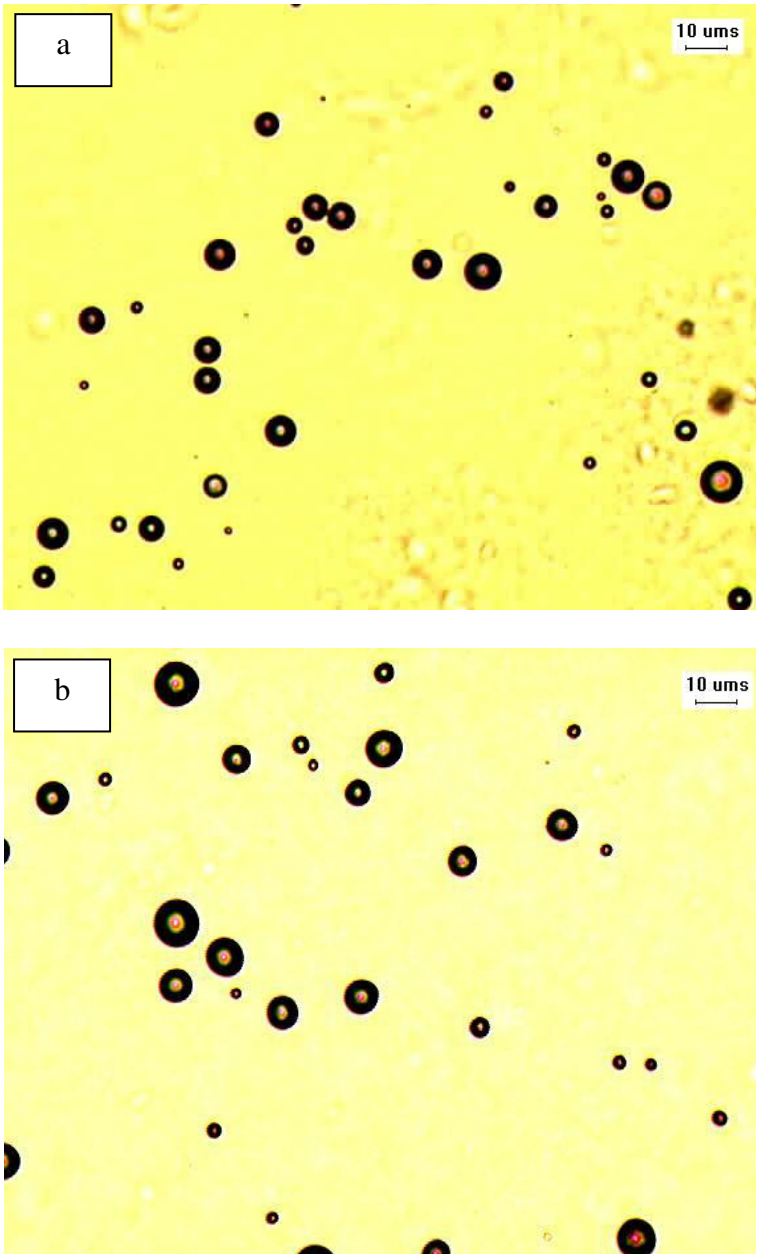

Figure 5.4. Optical micrographs of phospholipid-coated microbubbles collected at the ambient temperature at a flow rate combination of (a) 5µl s^{-1}: 5 µl s^{-1} (b) 10 µl s^{-1}: 5 µl s^{-1}, respectively.

The microbubbling time for a 6 ml lipid suspension was 20 min and the microbubbles were collected in a glass vial containing 2 ml distilled water to make the total volume to 8 ml. The reduction in bubble size with the reduction of gas flow rate at a constant phospholipid suspension flow rate indicated in **Table 5.2** agrees with the previous observations in microbubbling by both microfluidic techniques and CEHDA microbubbling for other liquids (Ganan-Calvo 2004, Garstecki *et al.* 2005, Farook *et al.* 2007b).

5.7. Effect of temperature on the stability of microbubbles

The stability of the of microbubbles prepared at 22^0C at the flow rate combination 10 μl s^{-1}(air): 5 μl s^{-1} (phospholipid suspension) was evaluated by taking samples for optical microscopy examination at time intervals of 10 min, 40 min, 70 min, 100 min and 160 min following collection. The mean bubble diameter 10 min after preparation was 6.6 μm with a standard deviation of 2.5 μm. After 160 min, the bubble diameter was 6 μm with a standard deviation of 1.8 μm. The effect of different shell materials and gases in the bubble core upon stability has been investigated previously (Soetanto and Chan 2000; Krasovitski and Kimmel 2006, Klibanov *et al.* 2002). However, there have been relatively few *in-vitro* investigations of the stability of microbubbles at the human body temperature (37^oC). **Table 5.3** shows the size variations of microbubbles prepared at 37^oC of the samples taken up to 40 h after preparation. The relevant micrographs of these samples were taken after allowing the microbubble suspension to cool to ambient temperature. The results show that within 50 min the mean microbubble size dropped rapidly to ~ 2 μm but then this size is retained for a very long period of time.

Table 5.3. Microbubble sizes obtained from the samples collected at 37^{o}C at a flow rate combination of 10 µl s^{-1} (air): 5 µl s^{-1} (phospholipid suspension).

Time interval (min)	Bubble mean diameter (µm)	Standard deviation (µm)
10	4.7	1.6
20	4.1	1.4
30	3.3	1.3
40	2.8	1.0
50	2.0	1.0
2400	1.9	1.0

Table 5.4 shows the size variations of microbubbles maintained at 37^{o}C up to 50 min after preparation. The relevant micrographs of these samples were taken while maintaining the microbubble suspension at 37^{o}C. These results indicate that at 37^{o}C, the microbubble size rapidly decreases to a mean diameter ~2 µm and subsequently the reduction in size is much slower. Thus, a stable microbubble diameter of 1-2 µm has been achieved and this compares well with the stable microbubble sizes prepared using other techniques such as flow focusing microfluidics (Talu *et al*. 2006), agitation/sonication (Borden *et al.* 2007) and by selective acoustic pulsing (Borden *et al*. 2005).

Table 5.4. Microbubble sizes obtained from the samples collected and maintained at 37°C at a flow rate combination of 10 µl s^{-1} (air): 5 µl s^{-1} (phospholipid suspension).

Time interval (min)	Bubble mean diameter (µm)	Standard deviation (µm)
10	2.1	0.7
20	1.7	0.6
40	1.3	0.5
50	1.3	0.4

The size reduction of the phospholipid-coated microbubbles at 37°C is potentially significant because the bubble's resonance frequency is directly related to its size and it is desirable that this should fall in the range of ultrasound frequencies used for medical imaging (1-10 MHz). It is likely that there would be less of a reduction if a higher molecular weight gas such as perfluorocarbon was used instead of air (Krasovitski and Kimmel 2006).

5.8. Characterisation by ultrasound attenuation measurement

The microbubble suspension collected at the ambient temperature was also characterised ultrasonically in order to confirm that gas filled bubbles had been successfully prepared. The aim in measuring the attenuation of ultrasound through the prepared suspension was to determine whether or not gas-filled microbubbles were present. The attenuation coefficient in a bubbly liquid is significantly higher than in a suspension of solid or liquid particles due to the large acoustic impedance contrast between liquid and gas and the high compressibility of gas bubbles (Stride and Saffari 2005). Hence this is a convenient way of confirming the presence of microbubbles **Figure 5.5** shows the frequency spectra for ultrasound pulses transmitted through water

and the suspension prepared by CEHDA. The large reduction in signal amplitude for the latter confirms the presence of air filled microbubbles in the suspension.

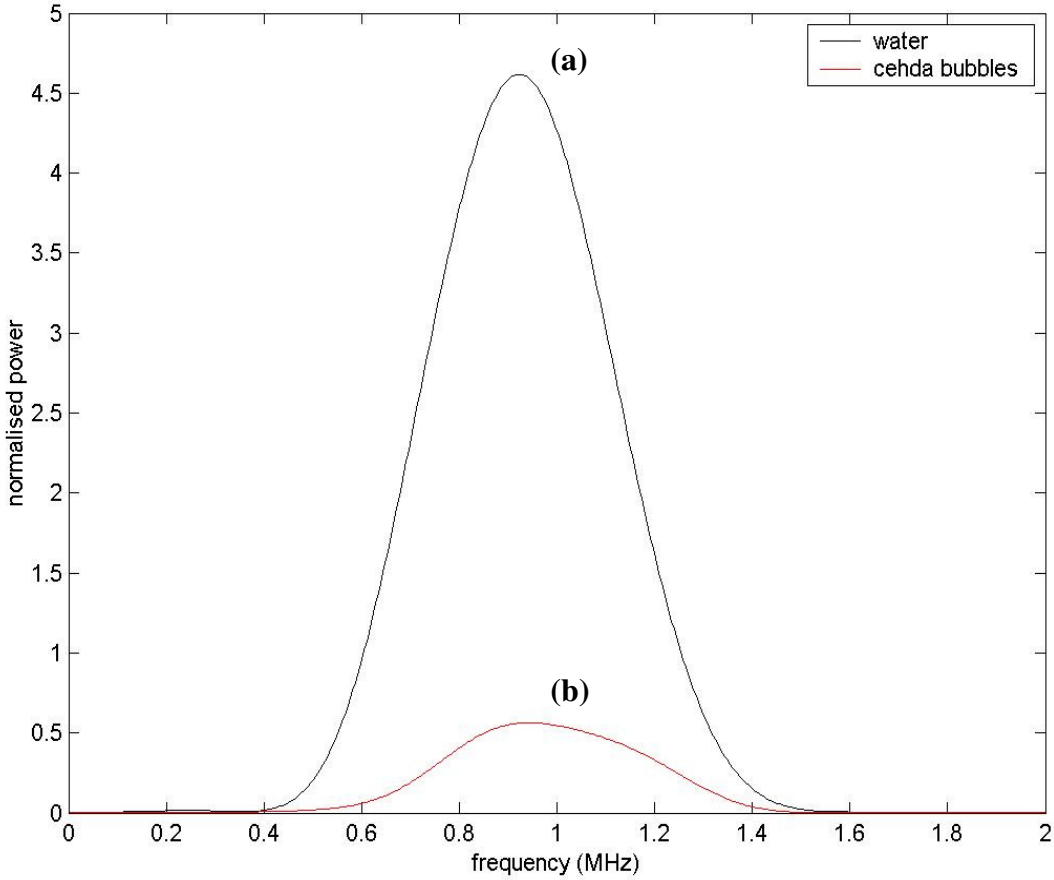

Figure 5.5. Frequency spectra for a 1 MHz ultrasound pulse transmitted through (a) water (b) CEHDA microbubble suspension.

5.9. Controlling the size and size distribution of phospholipid-coated microbubbles

The polydispersivity indices (standard deviation/mean expressed as a percentage) of the microbubbles prepared at 22^0C at various flow rate combinations fall within the range of 30-40% (**Table 5.2**), whereas in the case of flow focusing microfluidic devices this index can be < 2%. Nevertheless, as explained by Hettiarachchi *et al.* (2007), microfluidic devices suffer from the fact that the high gas pressures and liquid flow rates needed to increase bubble production rates result in a significant increase in the polydispersivity index (>50%), whereas, in the electrohydrodynamic device used in this current investigation, variation in air and phospholipid flow rates (**Table 5.2**) does not result in a dramatic change in the polydispersivity index during continuous microbubbling.

Phospholipid-coated microbubbles with diameters <10 μm and a low polydispersivity index are favoured as ultrasound contrast agents, drug and gene delivery vehicles, and blood substitutes due to their structure and nearly identical echo signature (Talu *et al.* 2008). An FDA approved ultrasound contrast agent, DEFINITY® (Bristol-Myers Squibb Medical Imaging, NY, USA), has been reported as having a mean diameter between 1.1 and 3.3 μm with a maximum bubble diameter as large as 20 μm (Hettiarachchi *et al.* 2007) Differential centrifugation has recently been used to successfully isolate fractions of microbubbles with diameters 1-2 μm and 4-5 μm from a multimodal suspension of sonicated lipid-coated microbubbles with a low polydispersivity ranging from 2-15 % (Feshitan *et al.* 2009). These isolated microbubbles have also been shown to be stable for more than two days.

The use of a commercially available surfactant such as Tween 80 (polyoxyethelene sorbitan monooleate) for stabilizing microbubbles has been described in **Chapter 4** and in Farook *et.al.* (2009c). Tween 80 is a surfactant commonly used in microbubble preparation and the investigations carried out to study the effect of Tween 80 on the polydispersivity of phospholipid-coated microbubbles are described in the following sections.

5.9.1. Phospholipid suspension with Tween 80

The method of preparation and the composition of the phospholipid suspension with Tween 80 have been described in **Sections 3.2.1** and **3.2.2**. The measured physical properties of the phospholipid suspension with and without Tween 80 are given in **Table 5.5**.

Table 5.5. Physical properties of phospholipid suspensions with and without Tween 80

Phospholipid suspension	**Electrical conductivity ($\mu S\ m^{-1}$)**	**Surface tension ($mN\ m^{-1}$)**	**Viscosity (mPa s)**	**Density ($kg\ m^{-3}$)**
Without Tween 80	8.8 ± 1	43 ± 0.2	2.6 ± 0.05	1030
With Tween 80	8.8 ± 1	47 ± 0.2	2.7 ± 0.04	1070

5.9.2. Modes of microbubbling of the phospholipid-Tween 80 system

Three distinct modes of microbubbling were noted (**Figure 5.6)** over an applied voltage range of 0-6.7 kV (**Table 5.6**)**.** The initial stage of bubble formation in the form of bubble dripping mode is shown in **Figure 5.6**a**.** With the increase of applied voltage,

bubble dripping takes a shape of a partial cone giving rise to the coning mode (**Figure 5.6**b). With further increase of applied voltage, coning mode converts to a thin jet of microbubbling mode (**Figure 5.6**c). Although the physical properties of the suspension with and without Tween 80 are not significantly different, the small increase in surface tension of the suspension with Tween 80 is reflected in the increase in applied voltage needed to achieve the microbubbling mode (**Table 5.6**).

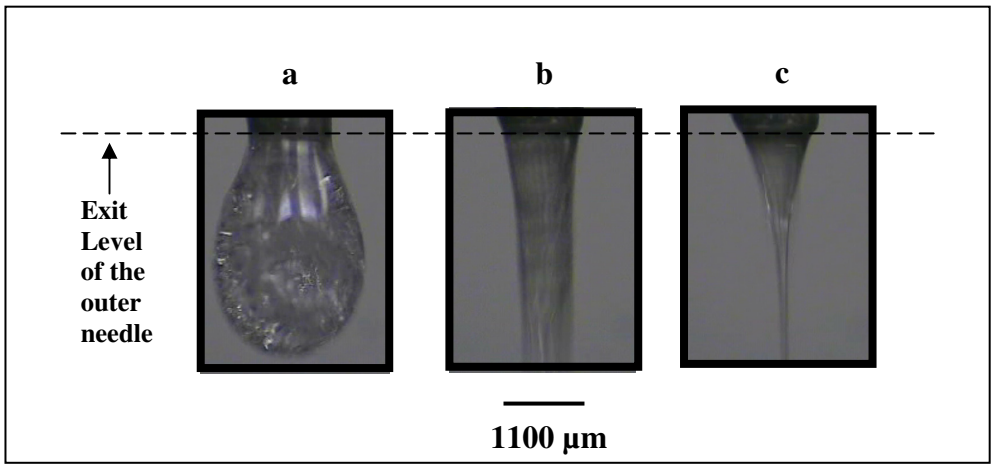

Figure 5.6. Microbubbling modes of the phospholipid-Tween 80 system: (**a**) Bubble dripping mode, (**b**) Coning mode, and (**c**) Microbubbling mode.

Table 5.6. Applied voltage ranges of modes of microbubbling of phospholipid suspensions with and without Tween 80

Phospholipid suspension	Voltage range for Bubble dripping (kV)	Voltage range for Coning (kV)	Voltage range for Microbubbling (kV)
Without Tween 80	0 - 2.5	2.5 - 5.7	5.7 - 6.1
With Tween 80	0 - 1.8	1.8 - 5.9	5.9 - 6.7

5.9.3. Parametric plot between the flow rate of air and the flow rate of phospholipid-Tween 80 suspension

The parametric plot constructed between the flow rate of air and the flow rate of phospholipid-Tween 80 suspension is shown in **Figure 5.7.** The continuous microbubbling zones for the phospholipid suspension with and without Tween 80 are compared in **Figure 5.8.** The use of Tween 80 has enlarged the continuous microbubbling zone by shifting the boundary line between the continuous microbubbling zone and the intermittent microbubbling zone downward, enabling the choice of more combinations of flow rates with lower values of gas ratio (flow rate of air / flow rate of suspension).

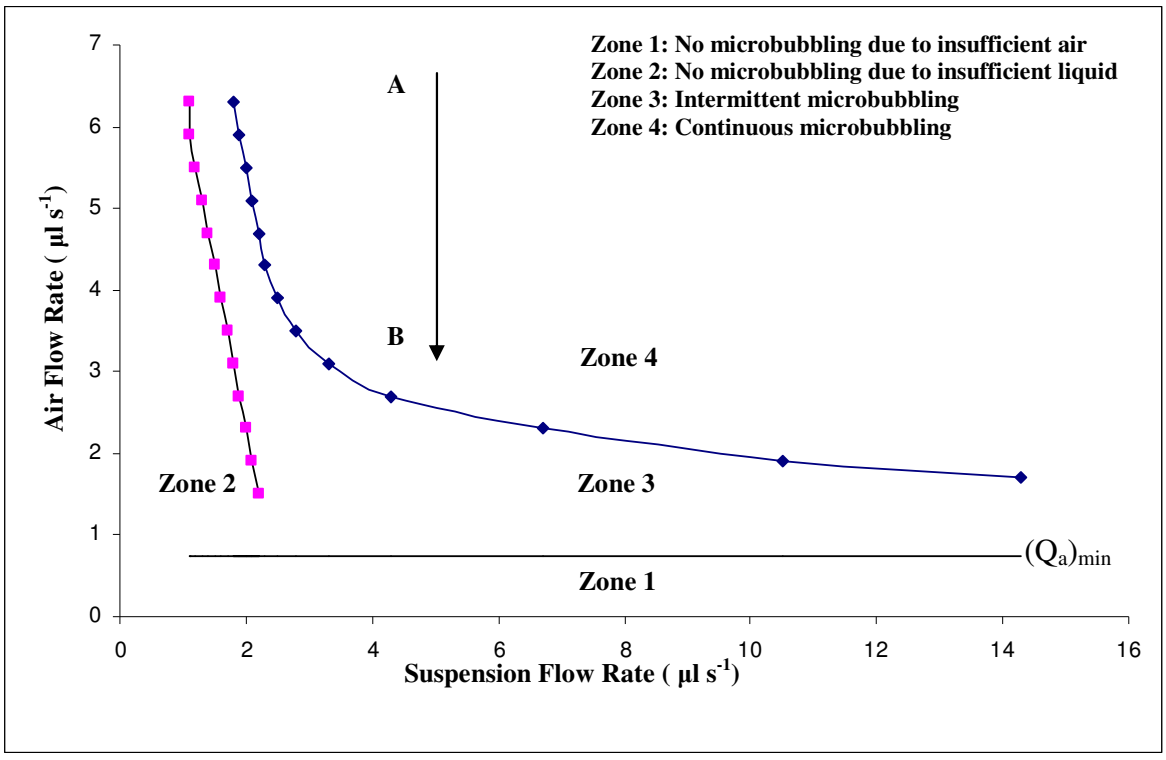

Figure 5.7. Parametric plot between the flow rate of air and the flow rate of phospholipid-Tween 80 suspension.

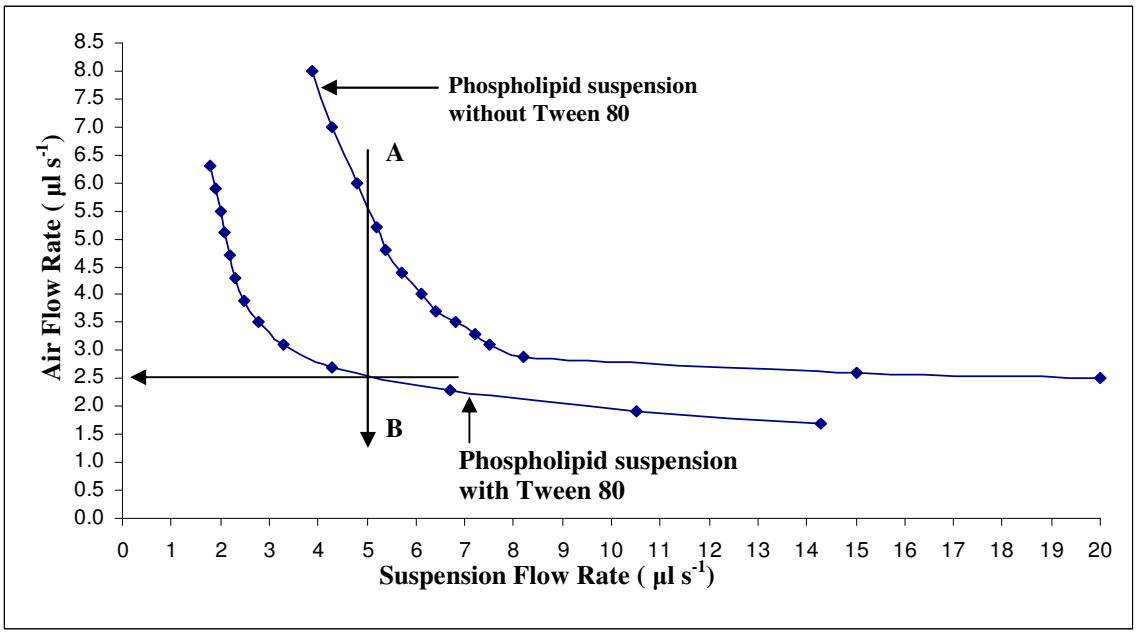

Figure 5.8. Comparison of the Zone 4-Zone 3 boundary of the parametric plots of phospholipid suspensions with and without Tween 80.

5.9.4. Effect of flow rates on the size and size distribution of microbubbles

Table 5.7 shows the bubble size distribution obtained for six different flow rate combinations selected from the parametric plot on a downward vertical line AB (figures 3 and 4) in the continuous microbubbling zone, corresponding to a suspension flow rate of 5 µl s^{-1}. This particular value of phospholipid-Tween 80 suspension flow rate was selected with a view to comparing the bubble size variation observed in our previous work where a phospholipid suspension was used with no addition of Tween 80. As shown in **Table 5.7**, the use of Tween 80 has enabled the polydispersivity index to be reduced to ~ 9 %, compared with previous values of 30-40 % for the phospholipid suspension without Tween 80 (Farook *et al.*2008, Farook *et al.*2009b). With the decrease in air flow rate and gas ratio, not only was the mean size of the bubbles reduced but also the polydispersivity index. The reduction in size of the microbubbles with reducing values of gas ratio has already been reported in the preparation of

microbubbles via microfluidic flow focusing and co-axial electrohydrodynamic atomization (Farook *et al.* 2009 a, Ganan-Calvo 2004, Garsteki *et al.* 2005).

Table 5.7. Microbubble sizes obtained by co-axial electrohydrodynamic microbubbling of the phospholipid-Tween 80 suspension at ambient temperature at different combination of flow rates. 100 bubbles were used and there was a 600 s lapse between bubble generation and examination by optical microscopy.

Air Flow rate ($\mu l\ s^{-1}$)	Phospholipid-Tween 80 suspension Flow rate ($\mu l\ s^{-1}$)	Gas ratio (λ)	Mean diameter (μm)	Standard deviation (μm)	P.I (%)
12.5	5	2.5	7.1	0.8	11
10.0	5	2.0	6.7	0.7	10
7.5	5	1.5	6.5	0.6	10
5.0	5	1.0	5.7	0.6	10
4.0	5	0.8	5.5	0.5	9
3.0	5	0.6	5.3	0.5	9

5.9.5. Microfluidic vs CEHDA microbubbling of phospholipid suspensions

For microbubbling in microfluidic flow focusing systems, Ganan-Calvo (2004) put forward an empirical Eq. (1) for liquids with Reynolds number in the range 40 to 1000.

$$d_b = 1.1D\lambda^{0.4} \quad (1)$$

Where, d_b is the microbubble diameter in μm and the gas ratio $\lambda = Q_g/Q_l$; Q_g and Q_l are air and liquid flow rates, respectively. D is the orifice diameter.

Interestingly, within the continuous microbubbling zone, Zone 4, the microbubble mean diameter d_b, for the air-phospholipid suspension system, scales with the gas constant λ in the form of the following equation (see **Figure 5.9):**

$$d_b=5.95\lambda^{0.14} \quad (2)$$

There are number of similar features between microbubbling in microfluidic flow focusing systems and CEHDA microbubbling. For example, d_b decreases with the decrease in λ and with the decrease of D in microfluidic systems or jet diameter (D_j) in CEHDA. However, in CEHDA microbubbling the change in d_b due to variation in λ is small (**Table 5.7)** and this helps to increase the bubble generation frequency. The essential feature in CEHDA is the importance of the parametric plot between the gas flow rate and the liquid (or suspension) flow rate as suitable combinations of these two parameters should be chosen in order to achieve continuous microbubbling. In addition to this a thin jet at a higher applied voltage helps to decrease D_j and d_b.

For the phospholipid suspension with Tween 80 (this work), d_b scales with λ as given by eq.2 (**Figure 5.10**).

$$d_b=5.77\lambda^{0.21} \quad (3)$$

The graphs plotted between d_b and λ for phospholipid suspension with and without Tween 80 shows the effect of Tween 80 on the bubble size (**Figure 5.11**). The bubble size and the polydispersivity index achieved at a flow rate combination of 3µl s^{-1} (air): 5µl s^{-1} (phospholipid-Tween 80) could be considered as the best possible (lower) values within the continuous microbubbling zone, as further reduction of air flow rate would lead the process into the intermittent microbubbling zone of the parametric plot (**Figure 5.7 & Figure 5.8**).

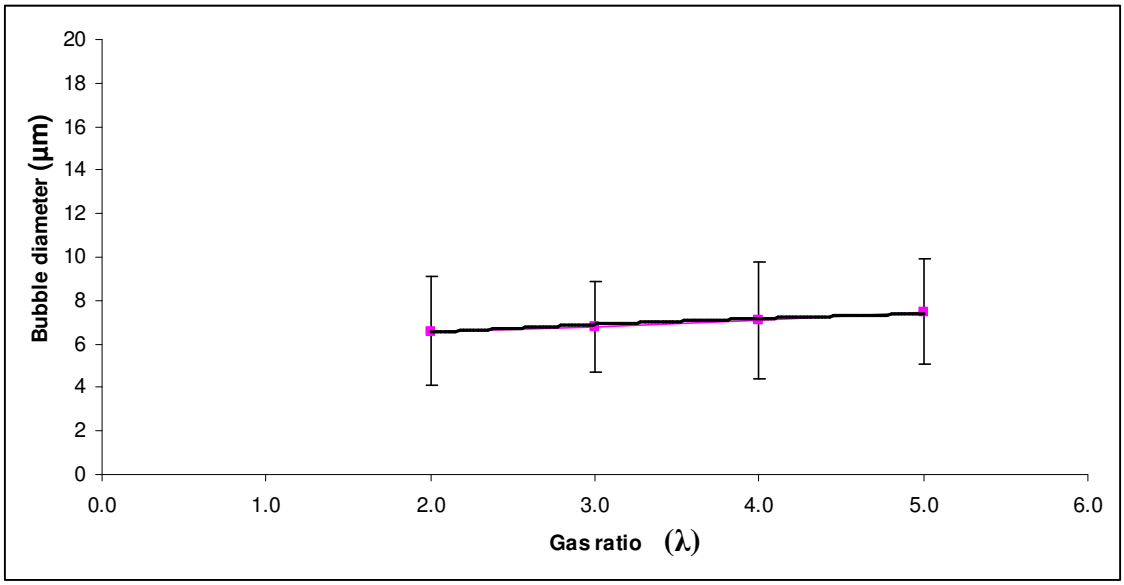

Figure 5.9. A graph of microbubble diameter versus the gas ratio (λ) for the phospholipid-air system within the continuous microbubbling zone. Bubble diameter increases with the increase of λ.

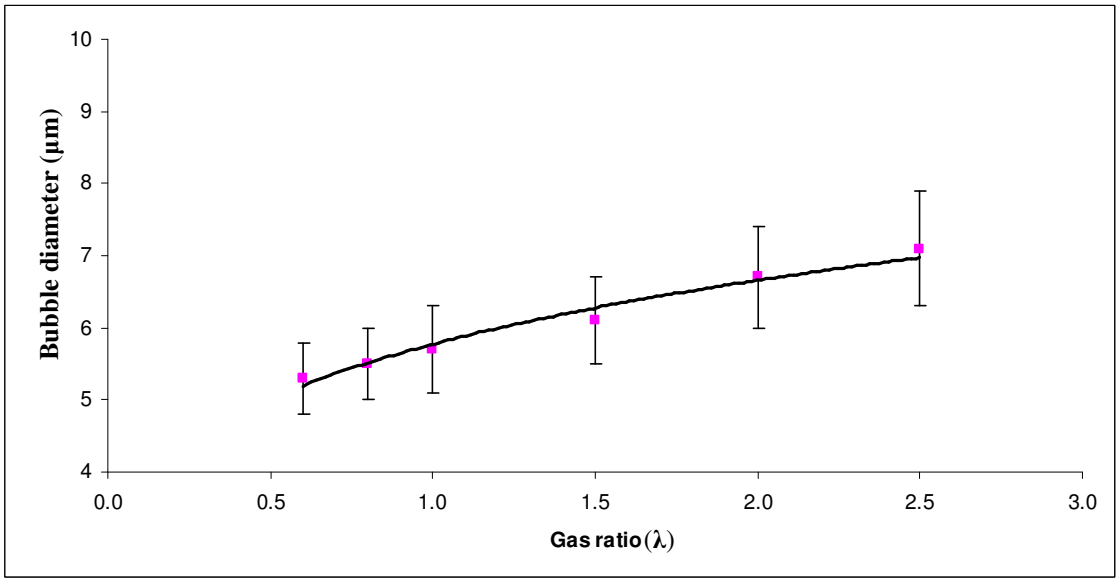

Figure 5.10. Graphs of the microbubble diameter versus the gas ratio within the continuous microbubbling zone of phospholipid suspension with Tween 80.

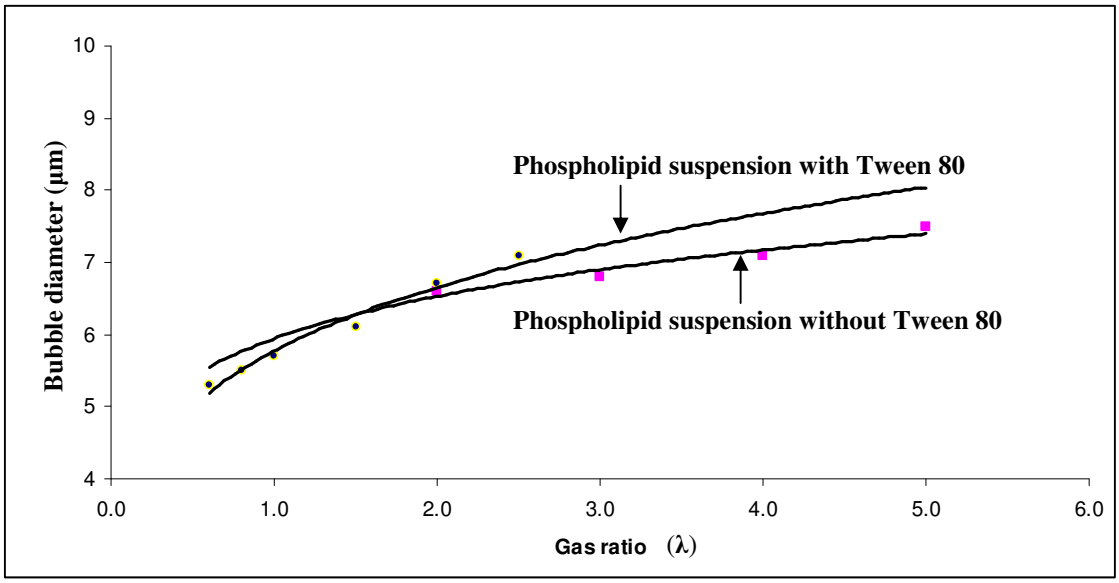

Figure 5.11. Graphs of the microbubble diameter versus the gas ratio within the continuous microbubbling zone of phospholipid suspension with and without Tween 80.

5.9.6. Stability of microbubbles prepared using phospholipid-Tween 80 system

Optical microscopy was repeated on the microbubbles prepared from the phospholipid-Tween 80 suspension at the flow rate combination 3.0 µl s^{-1} (air): 5µl s^{-1} (suspension) 18 h after preparation in order to determine any change to the mean size and polydispersivity index. The microbubble size was stable at ~ 5 µm, while the polydispersivity index was found to decrease slightly (6 %, **Table 5.8**). Although a direct comparison is not possible, overall, the microbubbles prepared in this work were more stable than those prepared in our previous work (Farook *et al.* 2009a).

Table 5.8. Size comparison 600 s and 18 h after preparation of microbubbles with flow rate combination 3 µl s^{-1} (air): 5 µl s^{-1} (phospholipid-Tween 80). For the calculation of the mean diameter and standard deviation, 100 bubbles were taken from the respective optical micrographs.

Time interval	Mean Diameter (µm)	Standard Deviation (µm)	P.I (%)
600 s	5.3	0.5	9
18 h	5.2	0.3	6

5.9.7. Ultrasound imaging using microbubbles prepared by phospholipid-Tween 80 suspension

The images obtained from the ultrasound scanner for gelatine phantoms containing distilled water without and with microbubbles (~18 h after preparation) at flow rate combination 3 µl s^{-1}(air): 5 µl s^{-1}(phospholipid-Tween 80) are shown in **Figure 5.12** and **Figure 5.13**, respectively. As may be seen, there is a significant increase in backscatter from the central cavity which confirms the presence of microbubbles and that these suspensions would be effective as ultrasound contrast agents.

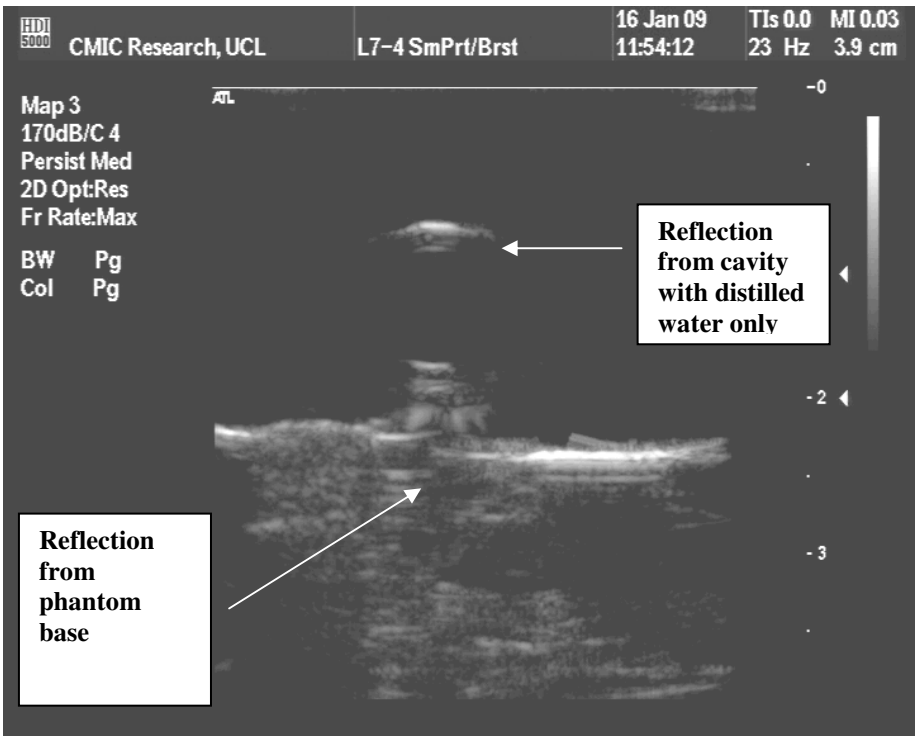

Figure 5.12. Gray-scale ultrasound image of gelatine phantom with no microbubbles.

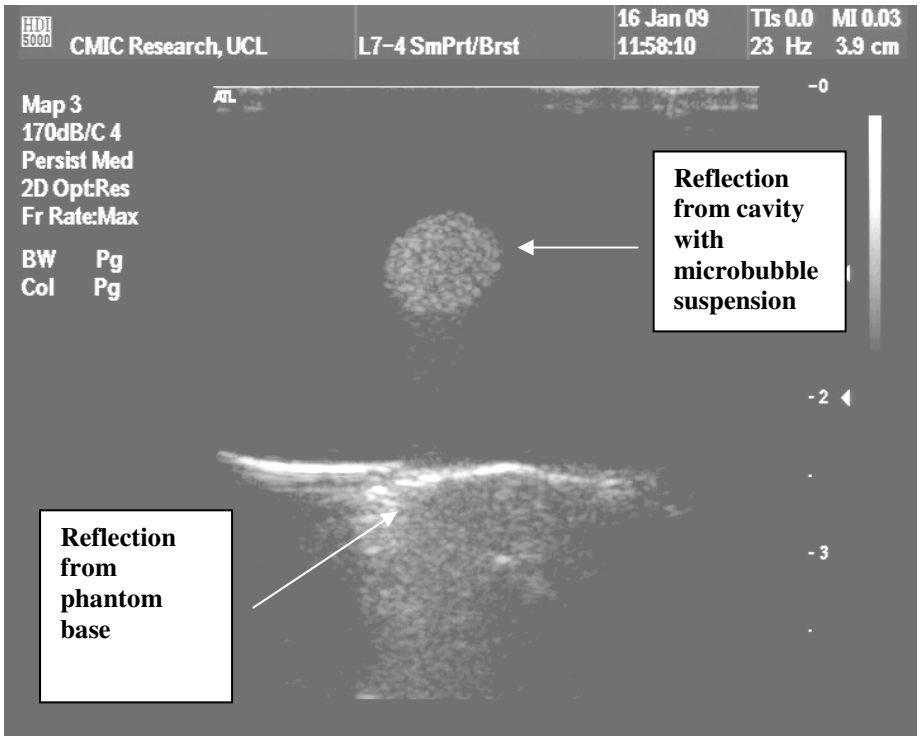

Figure 5.13. Gray-scale ultrasound image of gelatine phantom with microbubbles 20 h after preparation at flow rate combination 3 µl s^{-1}(air) : 5 µl s^{-1}(phospholipid-Tween 80).

CHAPTER 6

PREPARATION OF SUBMICROMETRE SIZE POLYMERIC SPHERES BY CO-AXIAL ELECTROHYDRODYNAMIC ATOMIZATION MICROBUBBLING

6.1. Introduction

This chapter describes an investigation of the preparation of polymeric spheres of micrometre and submicrometre size using a model polymer (polymethylsilsesquioxane) via the co-axial electrohydrodynamic microbubbling technique that has been described in **Chapter 4**. A microsphere partially filled with an entrapped therapeutic agent can transport the substance through blood vessels and release its load at a targeted site when excited by an ultrasound field. Polymeric materials can be used for encapsulating drugs in developing drug delivery systems (DDS) for sustained and controlled release. These DDS are used to provide a predetermined amount of drug at an appropriate time and at a targeted site over durations from several minutes to several years (Kawaguchi 2000, Pareta and Edirisinghe 2006, Yadav *et al*. 1997, Zhang *et al*. 2005). An ideal drug delivery system should be inert, biocompatible, mechanically strong, comfortable to the patient, capable of achieving high drug loading, safe from accidental release, simple to administer and remove, and easy to fabricate and sterilize (Brannon-Peppas 1998). A range of polymeric materials including polyurethanes, polysiloxanes, polyvinyl alcohol, polyethylene, polyethylene glycol, polylactides, polyanhydrides are employed for drug delivery because of their desirable physical properties such as elasticity, insulating ability, physical strength and transparency, toughness and lack of swelling, suspension capabilities, and the lack of leachable impurities (Langer 1998, Brannon-Peppas 1998).

Many techniques such as layer-by-layer-deposition, *in situ* polymerization on template particles, sol gel methods, and liquid phase deposition, pH-induced micellization of

grafted copolymer and core-free-template strategy have been developed to prepare spheres whose sizes range from tens of nanometres to a few micrometers. Emerging techniques for creating monodisperse microspheres utilize controlled flow fields and electrohydrodynamic forces to induce regular microsphere break-up (Sgraja *et al.* 2006). Precision particle fabrication technology and microfluidic technology have proved to be capable of producing suspensions of monodisperse microspheres, but carry limitations either with regard to the size or the stability of microspheres or the high cost of preparation technique (Berkland *et al.* 2007, Cheng *et al.* 2006, Hettiarachchi *et al.* 2007, Sgraja *et al.* 2006, Talu *et al.* 2006**,** Zoldesi *et al.* 2006).

In **Chapters 4** and **5**, it has been clearly demonstrated that co-axial electrohydrodynamic atomization can be successfully adapted to prepare suspensions of microbubbles with a mean size and size distribution suitable for medical applications. The microspheres prepared in this investigation are filled *in-situ* with the liquid in which they are collected. The polymer is dissolved in a solvent and then atomized at the outer needle of the co-axial needle arrangement, while in the inner needle air flow occurs simultaneously. The resulting sphere is formed in a way similar to that involved in solvent evaporation, where a polymer is dissolved in a solvent and dripped into a non-solvent containing a surfactant to form a stable emulsion (Kawaguchi 2000, Kim *et al*. 2003, Pekarek *et al.* 1994).

6.2. Characterisation of polymer solutions

The preparation method and the composition of polymer solutions have been described in **Section 3.3.3** of this thesis. The solutions were characterized for their density, viscosity, surface tension and electrical conductivity as described in **Chapter 3**. The

measured properties of the polymer solutions are given in **Table 6.1.** With the increase of wt. % of polymer in ethanol, the electrical conductivity of the solution decreases while viscosity increases.

Table 6.1. Properties of the polymer solutions prepared

Polymer wt.%	Ethanol wt.%	Density kg m^{-3}	Viscosity mPa s	Surface tension mN m^{-1}	Electrical Conductivity S m^{-1}/ 10^{-5}
18	82	845	2.5	23	9
24	76	865	3.8	23	8
40	60	924	9.6	23	6
60	40	1009	45	26	1

The importance of material properties such as viscosity, density, electrical conductivity, and the process parameters such as flow rates and applied voltage in determining the overall size of the microbubbles/microspheres, is described in **Chapter 4** when discussing the investigations carried out with a glycerol-air system. However, unlike glycerol, polymethylsilsesquioxane is an electrical insulator and the electrical conductivity of the ethanol/polymer solution is only due to the ethanol. At higher wt. % of polymer, microbubbling the polymer solution under CEHDA microbubbling would be extremely difficult due to its very low electrical conductivity and high viscosity.

6.3. Modes of microbubbling

The changes in viscosity and electrical conductivity with the increase in polymer wt. % influenced the ranges of applied voltage for different modes of microbubbling as shown in **Table 6.2**. In the bubble dripping mode (**Figure 6.1**a), the initial stage of bubble

formation at zero voltage, air bubbles were seen collecting in the liquid meniscus before it detached from the tip of the outer needle due to the gravitational force overtaking the surface tension force. With the gradual increase of applied voltage, the bubble dripping mode turned into the coning mode (**Figure 6.1**b) and with further increase of applied voltage, the coning changed into the microbubbling mode (**Figure 6.1**c), which can be compared with the cone-jet mode in conventional electrohydrodynamic atomization (Farook *et al.* 2007a, 2007b)

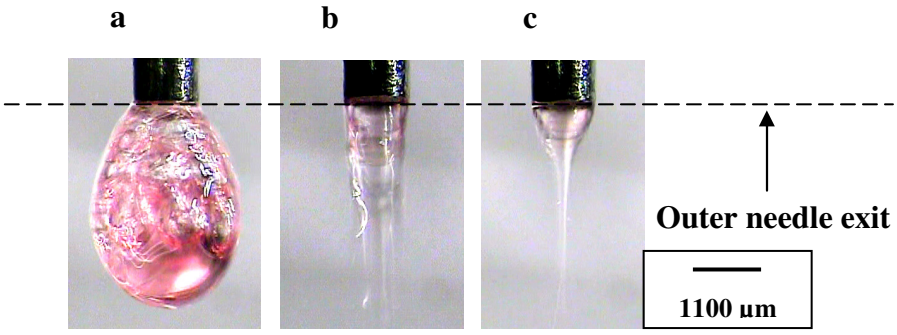

Figure 6.1. Modes of microbubbling, **(a)** bubble dripping mode **(b)** coning mode and **(c)** microbubbling mode, observed for the solution containing 18 wt.% polymer (polymethylsilsesquioxane).

Table 6.2. Applied voltage requirement for modes of microbubbling for different polymer solutions

Polymer wt.%	Bubble dripping mode kV	Coning mode kV	Microbubbling mode kV
18	0 - 2.1	2.1 - 4.9	4.9 - 5.9
24	0 - 2.1	2.1 - 4.6	4.6 - 5.2
40	0 - 2.1	2.1 - 4.4	4.4 - 4.7
60	-	-	-

At 60 wt. %, the polymer began to solidify at the tip of the outer needle almost instantaneously irrespective of voltages. At 40 wt. %, although it was possible to increase the applied voltage rapidly to 4.7 kV, polymer began to solidify at the tip of the needle very quickly between 0 and 4.7 kV. The 18 wt. % solution was found to provide the longest applied voltage range with no solidification of polymer at the needle tip during microbubbling.

6.4. Parametric plot

Using the 18 wt. % polymer solution, a parametric plot (**Figure 6.2**) was constructed between the flow rate of air and the flow rate of polymer solution. In Zone 1, below a critical minimum air flow rate of 0.6 µl s^{-1}, the polymer solution behaved as if subjected to conventional electrohydrodynamic atomization due to the low flow rates of air and as such no microbubbling occurred. Likewise, in Zone 2, there was no microbubbling due to the low flow rates of liquid. In Zone 3, the microbubbling was intermittent whilst continuous microbubbling was observed in Zone 4. Although the applied voltage was

almost always maintained at 5.7 kV during the data collection for this plot, it was also necessary to vary the applied voltage from 0 to 5.9 kV to ensure the appearance of all three modes.

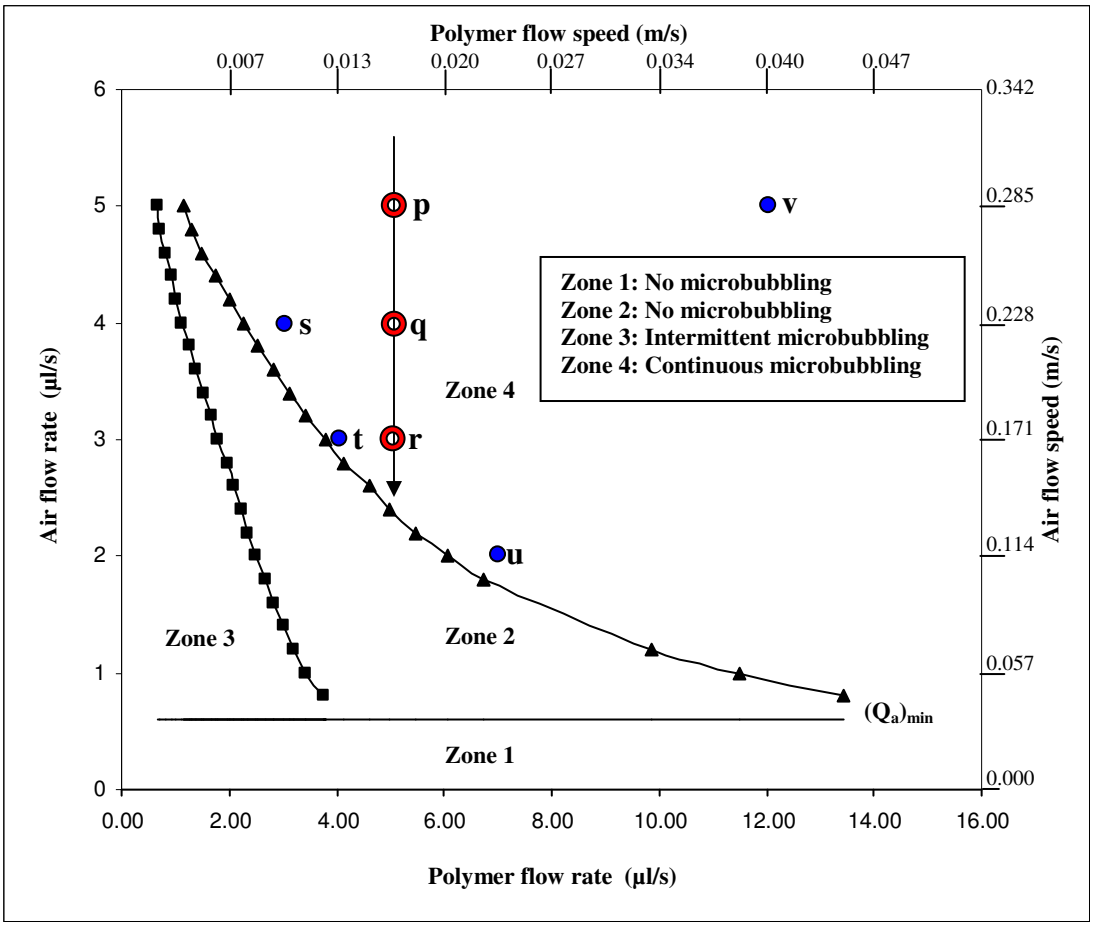

Figure 6.2. Parametric plot between the air flow rate and the polymer flow rate **Zone 1**, No microbubbling due to lower air flow rate **Zone 2**, No microbubbling due to lower liquid flow rate **Zone 3**, Intermittent microbubbling **Zone 4**, Continuous microbubbling. Points **p**, **q**, **r**, **s**, **t**, **u** and **v** denote the flow rate combinations at which microbubbling was conducted.

6.5. Characterisation of microspheres by optical microscopy

The microspheres prepared by CEHDA microbubbling were collected in a glass vial of distilled water kept just below the ring electrode. The suspensions containing polymer spheres were filtered using filter papers (particle retention down to 2.5 µm, Grade 5V, Whatman plc, Kent, UK) in order to remove any solidified lumps of polymer and transferred to a new glass vial before characterisation. Samples of 0.05 ml of the filtered suspension were taken from the glass vial using a 1 ml syringe and transferred onto glass slides for optical microscopy. Optical microscopic examination after 300 s of preparation of the suspension showed a large population of near monodisperse microspheres which appeared to be under Brownian motion during the examination (**Figure 6.3**a). This phenomenon may be attributed to the solidification of the polymer shell and the simultaneous outward diffusion of air and inward transfer of liquid across the polymer shell. The micrographs taken after 5 min and 90 min of generating the microspheres were analysed using a software written in MATLAB (The Mathsworks, Natick, USA) and showed near-monodispersivity with a mean diameter of 6 µm and a standard deviation of 2 µm (**Figure 6.3**a **& 6.3**b).

With the micrograph (**Figure 6.3**c) obtained 24 h after preparation, **Figures 6.3**(a-c) also shows that the population of microspheres in the suspensions was diminishing with the passage of time. When the suspension was left undisturbed and observed again after 48 h, it had had transformed into a supernatant with a sediment at the bottom of the glass vial. With simple agitation, the sediment dispersed once again. Microscopic examination of the agitated suspension showed that it consisted of microspheres < 5µm in diameter (**Figure 6.3**d).

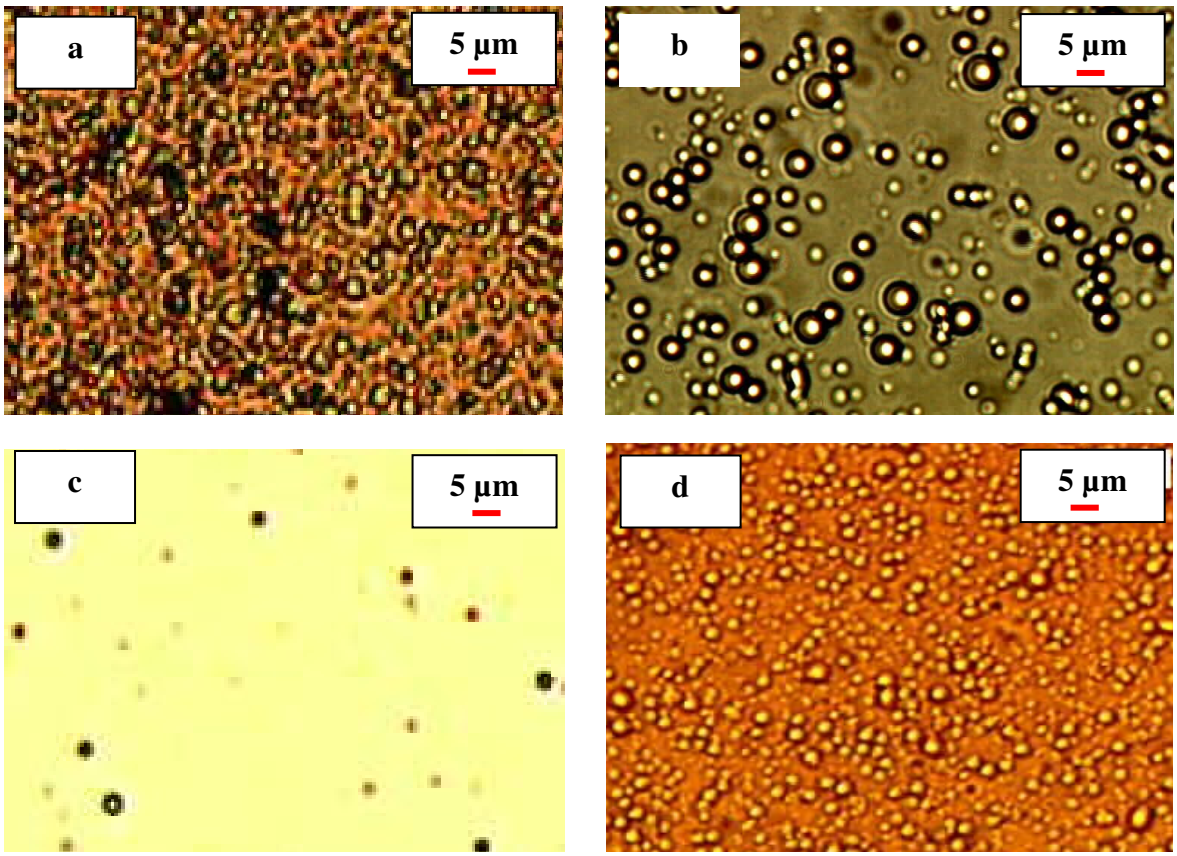

Figure 6.3 Optical micrographs of microsphere suspension after (**a**) 5 min (**b**) 90 min. (**c**) 24 h and (**d**) 48 h (after dispersing the sediment by shaking).

6.6. Characterisation of microspheres by scanning electron microscopy

A 0.05 ml sample of this agitated suspension was taken on a gold coated cover slip and allowed to dry in air at ambient temperature and pressure for 2 h before studying it using scanning electron microscopy (SEM). The SEM images (**Figure 6.4**a) show that the particles were mainly spherical but also interconnected. A sample of suspension left undisturbed for 30 days and dried on a gold coated cover slip also showed similar features (**Figure 6.4**b). However, when the sample was further dried in a desiccator for two days and observed by SEM on the 32nd day, it revealed that the microspheres had separated (**Figure 6.4**c). The difference between **Figure 6.4**b and **Figure 6.4**c shows the importance of drying the microspheres in a desiccator to produce discrete spheres. It is evident from **Figures 6.4**a and **6.4**b that drying the microspheres in air is not only inefficient but it may also have facilitated further absorption of atmospheric moisture making it difficult for the microspheres to separate. A size distribution analysis using 225 microspheres from these SEM images gives a mean diameter of 1.3 µm with a standard deviation of 0.4 µm (**Figure 6.5**).

6.7. Characterisation by ultrasound attenuation measurement

Microsphere samples were also investigated by ultrasound attenuation measurements. Details of the equipment and method used are discussed in detail in **Chapter 3** and in Pancholi *et al*. (2007). Briefly, broadband pulses with a centre frequency of 1 MHz were transmitted through the sample at a pulse repetition frequency of 0.2 kHz and captured at 50 Mega-samples per second. Measurement of attenuation was made firstly for a sample of distilled water. 1ml of the microsphere suspension was then added to the sample container and gently stirred to ensure even distribution before measuring attenuation again. The measurement was repeated for each sample. Ultrasound

attenuation measurements (**Figure 6.6**) on different microsphere suspensions show very little distinction from those in distilled water and suggest there was no air in microspheres. This supports the conclusion that the microspheres absorb liquid almost immediately after forming.

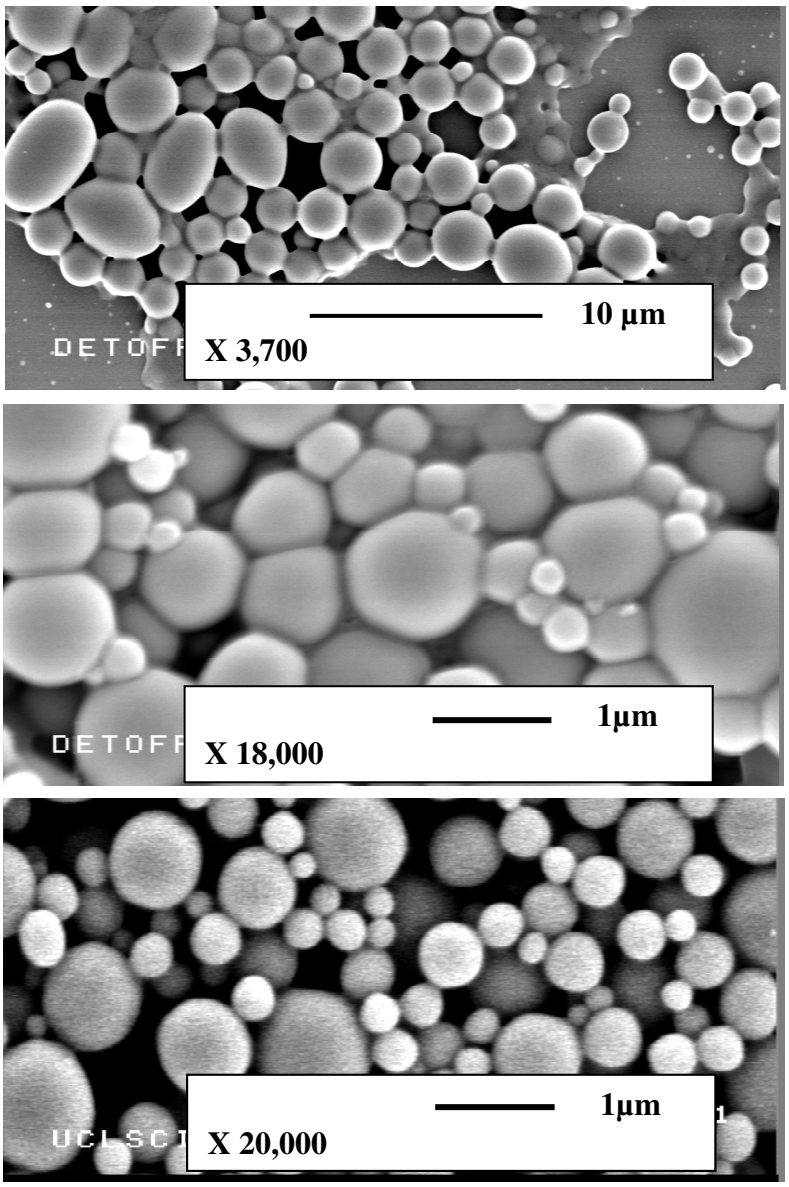

Figure 6.4. Scanning electron micrographs **(a)** after 48 h of preparation and 2 h drying under ambient conditions, **(b)** after 30 days of preparation and 2 h of drying under ambient conditions, **(c)** after 30 days of preparation and 2 days of drying in a desiccator.

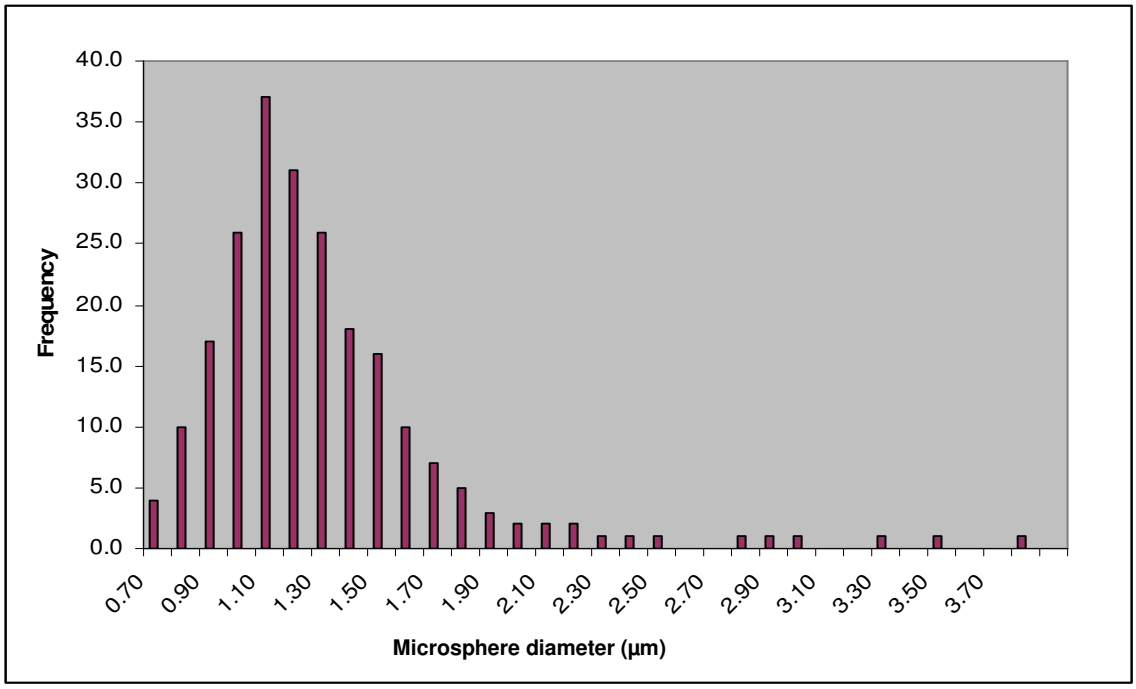

Figure 6.5. Size distribution data obtained by measuring 225 microspheres from scanning electron micrographs in **Figure 6.4**c, which also represents the point **p** in **Figure 6.2.** The mean diameter of the microspheres was 1.3 µm with a standard deviation of 0.4 µm.

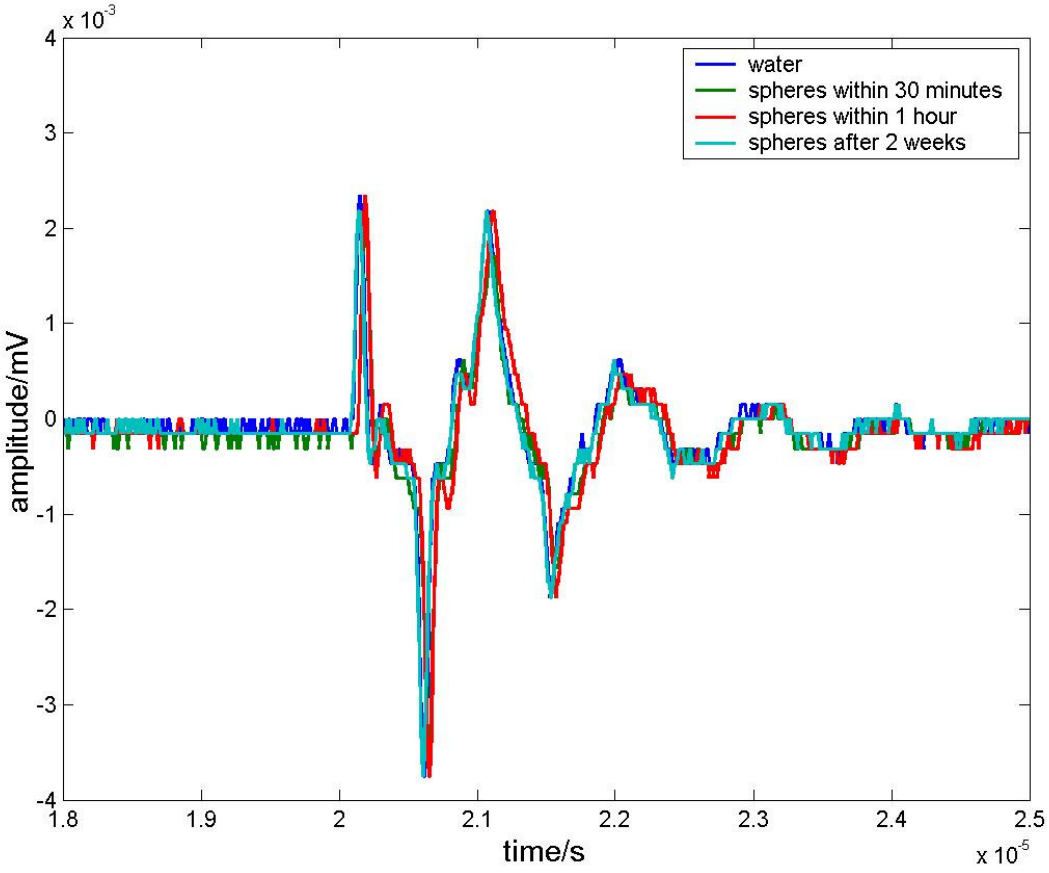

Figure 6.6. Ultrasound attenuation measurements of water, microspheres within 30 min of preparation, within 1 h of preparation, and after 2 weeks.

6.8. Atomization of polymer solution with and without air

Figure 6.7 shows the difference between the products of a polymer solution subjected to CEHDA, one with air flowing through the inner needle (**Figure 6.7**a) and without air (**Figure 6.7**b). It is clear that **Figure 6.7**a shows a bubble-like structure, while **Figure 6.7**b shows a solid structure. No investigation was conducted on the particles which were generated without the air, as it was beyond the scope of this study.

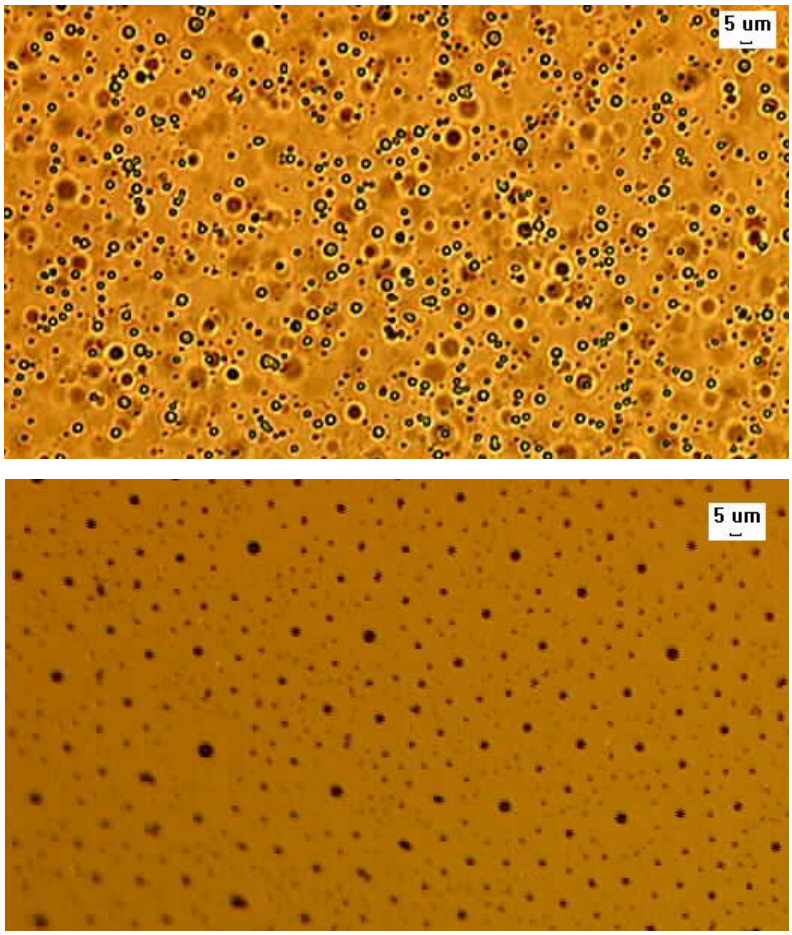

Figure 6.7. Optical micrographs of products generated from polymer suspension **(a)** with air flowing through the inner needle **(b)** without air flowing through the inner needle.

6.9. Calculation of porosity of microspheres

After 30 days, in order to calculate the weight of liquid absorbed by the spheres, a sample layer of microspheres that had been settled at the bottom of the glass vial was separated manually from the suspension and weighed after removing the surface dampness using a fine tissue. This sample was kept in a desiccator for an hour at ambient temperature and was finely crushed using a mortar and pestle and kept for further drying in the desiccator at ambient temperature for 24 h and then re-weighed.

Since the microspheres were not floating in water, it was clear that they had a higher density than the suspension medium. With the absorption of liquid and un-availability of any surfactant in suspension medium, microspheres settle at the bottom of the collecting vessel. Calculations from the weight measurements showed there was liquid absorption amounting to ~ 65 wt. % in the microspheres. The small size of the microspheres deduced by SEM analysis suggests that these microspheres can be further investigated for their effectiveness as drug delivery systems as drug release from smaller spheres is faster than from larger ones (Dinarvand *et al*. 2003). However, the growing interest in preparing spheres of submicrometre size could not be overlooked as they are preferred for their drug entrapment efficiency while greatly reducing side effects (Allemann *et al*. 1993, Nobs *et al*. 2004).

6.10. In depth investigations into the size and size distribution and the structure of microspheres

In previous **Chapters 4** & **5** and in Farook *et al.* (2007b) & Farook *et al.* (2009a), it has been clearly demonstrated that choosing gas flow rates at a suitable liquid flow rate and in a downward direction on a vertical line within the microbubbling zone of the parametric plot (e.g., line AB in **Figure 5.2**) could result in microbubbles with lower size and lower polydispersivity. The insight gained from this exercise could also be used to minimize the size and size distribution of the polymer spheres prepared in this investigation. On the other hand, although these polymer spheres have shown porosity and an ability to absorb liquid/drug, it is not yet clear whether these are spheres of reservoir system in which drug diffuses through a polymer membrane or of matrix system in which drug is evenly distributed through a polymer system (Langer 1998). Further investigations carried out in this regard are discussed in following sections.

6.10.1. Effect of flow rates on the size and size distribution of microspheres

The initial investigations described in **Section 6.6** shows that the microspheres prepared at a flow rate combination of 5 μl s^{-1}(air): 5 μl s^{-1} (polymer suspension) had a mean diameter of 1.3 μm with a standard deviation of 0.4 μm, giving a polydispersivity index of 31%. This combination of flow rates is denoted as **p** in the parametric plot shown in **Figure 6.2.** For further investigations, two more combinations of flow rates were chosen within the continuous microbubbling zone of the parametric plot and on a vertical line passing through point **p**. These two combinations of flow rates are denoted as **q** and **r**. The scanning electron micrographs of the microparticles prepared at flow rate combinations with respect to points **q** and **r** are given in **Figure 6.8**. The size distribution data measuring 300 microspheres from these micrographs with respect to

points **q** and **r** are given in **Figure 6.9** and respective flow rates, gas ratio, mean diameter, standard deviation and polydispersivity index are tabulated in **Table 6.3**.

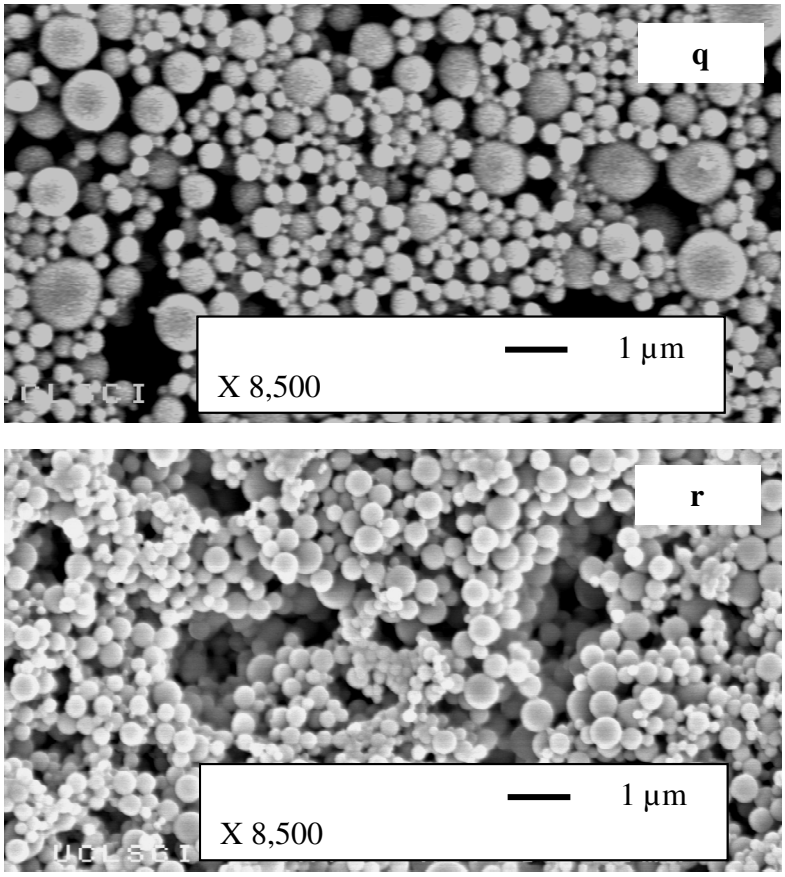

Figure 6.8. Scanning electron micrographs of microspheres prepared at flow rate combinations at **q**, 4 µl s^{-1} (air) : 5 µl s^{-1}(polymer) and at **r**, 3 µl s^{-1}(air) : 5 µl s^{-1} (polymer), respectively.

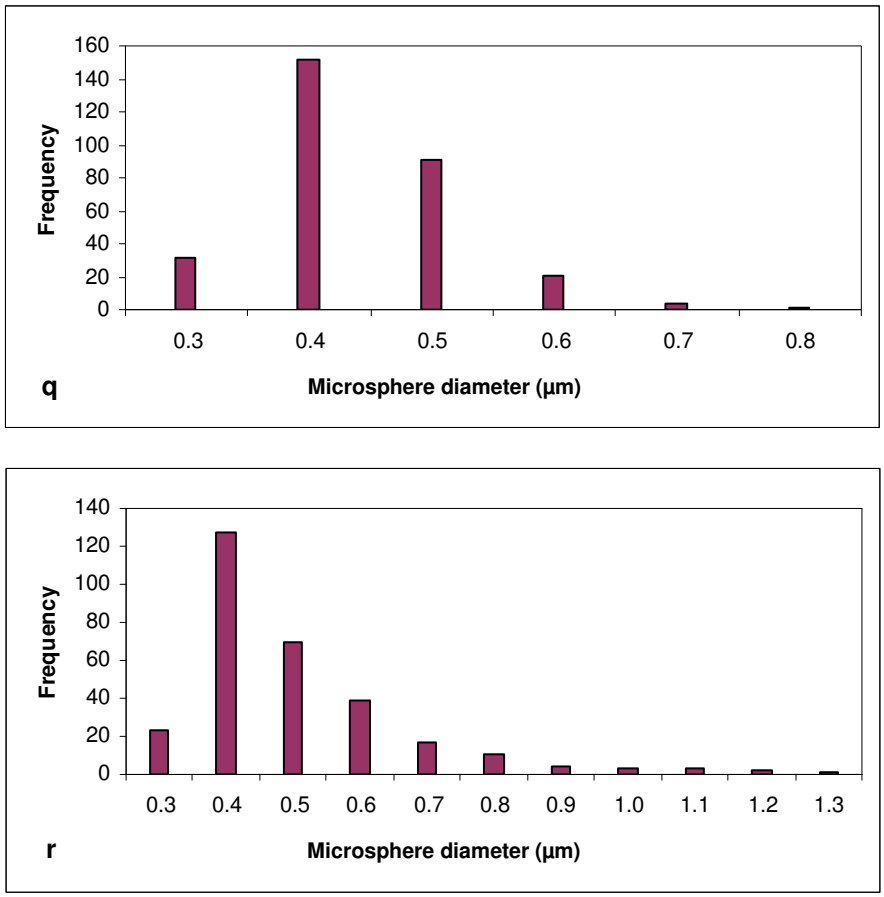

Figure 6.9. Size distribution data obtained by measuring 300 microspheres from respective scanning electron micrographs. The mean diameter and SD were at **q**, 0.5 µm and 0.08 µm; and at **r**, 0.4 µm and 0.03 µm, respectively.

Table 6.3. Microsphere sizes obtained by CEHDA microbubbling of the 18 wt. % polymer solution at ambient temperature and different combination of flow rates selected on a vertical line within the microbubbling zone of the parametric plot (**Figure 6.2**)

Position on parametric plot	Flow rate of (air) ($\mu l\ s^{-1}$)	Flow rate of (polymer) ($\mu l\ s^{-1}$)	Gas ratio (λ)	Mean dia. (μm)	Standard deviation (μm)	P.I. (%)
p	5	5	1.0	1.3	0.40	31
q	4	5	0.8	0.5	0.08	16
r	3	5	0.60	0.4	0.03	8

On a vertical line (**Figure 6.2**) passing through point **p** and at a point **r** closer to the threshold line of the continuous microbubbling zone, the size and the size distribution of the microspheres have reduced considerably, confirming the observations made in **Chapter 4** and **Chapter 5** for glycerol and the phospholipid solutions, respectively. Points **s**, **t** and **u** are chosen on both sides of the vertical line and closer to threshold line of the continuous microbubbling zone in order to compare the size and size distribution of microspheres at other possible combinations of flow rates that may result in smaller particles. The final point **v** is chosen to represent a combination of flow rates of high values. The scanning electron micrographs of the micro-particles prepared at flow rate combinations with respect to points **s**, **t**, and **u** are given in **Figure 6.10**. The size distribution data measuring 300 micro particles from these micrographs with respect to points **s**, **t** and **u** are given in **Figure 6.11**. The respective flow rate, gas ratio, standard

deviation and polydispersivity index of points **s**, **t**, **u** and **v** are tabulated in **Table 6.4.** The scanning electron micrograph with respect to point **v** is given in **Figure 6.12**.

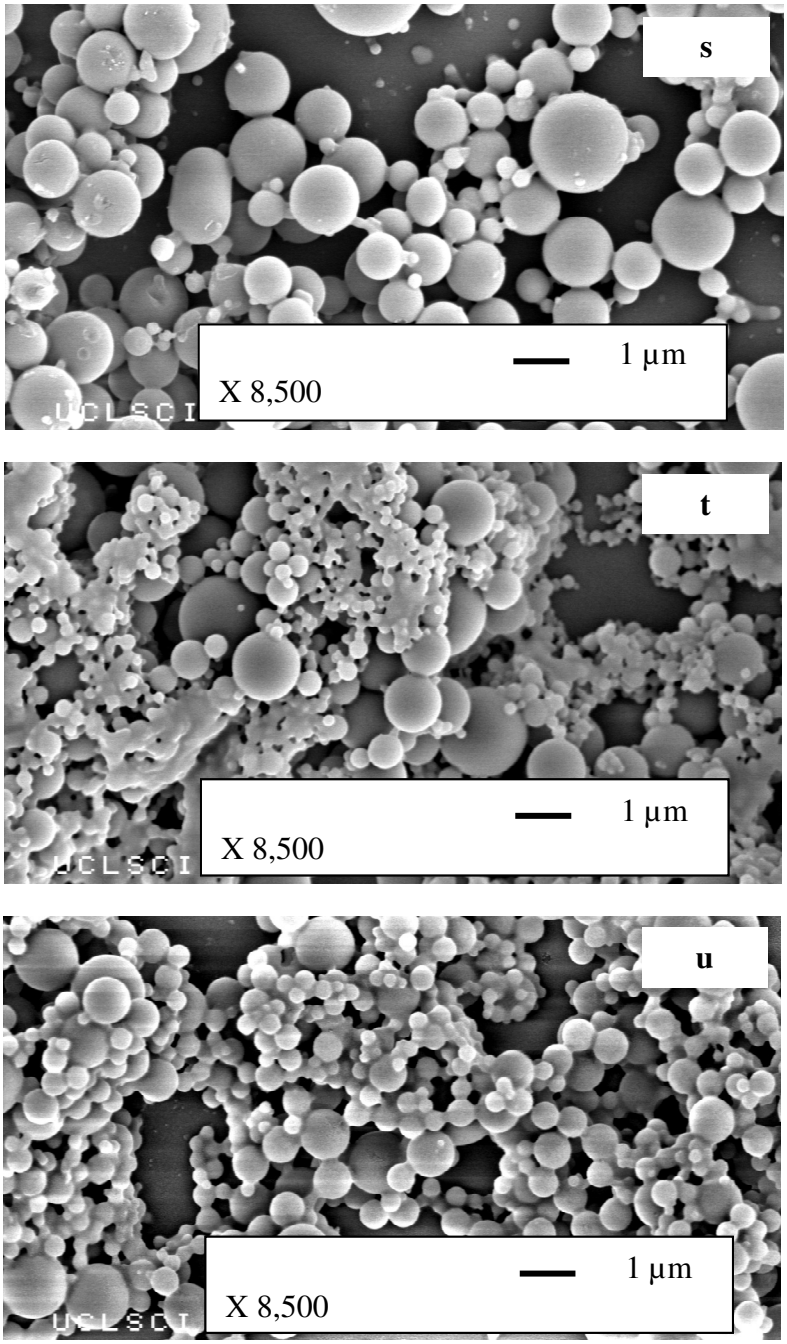

Figure 6.10. Scanning electron micrographs of microspheres prepared at flow rate combinations at **s**, 4 µl s^{-1} (air) : 3 µl s^{-1}(polymer), at **t**, 3 µl s^{-1}(air) : 4 µl s^{-1} (polymer) and at **u**, 2 µl s^{-1}(air) : 7 µl s^{-1} (polymer), respectively.

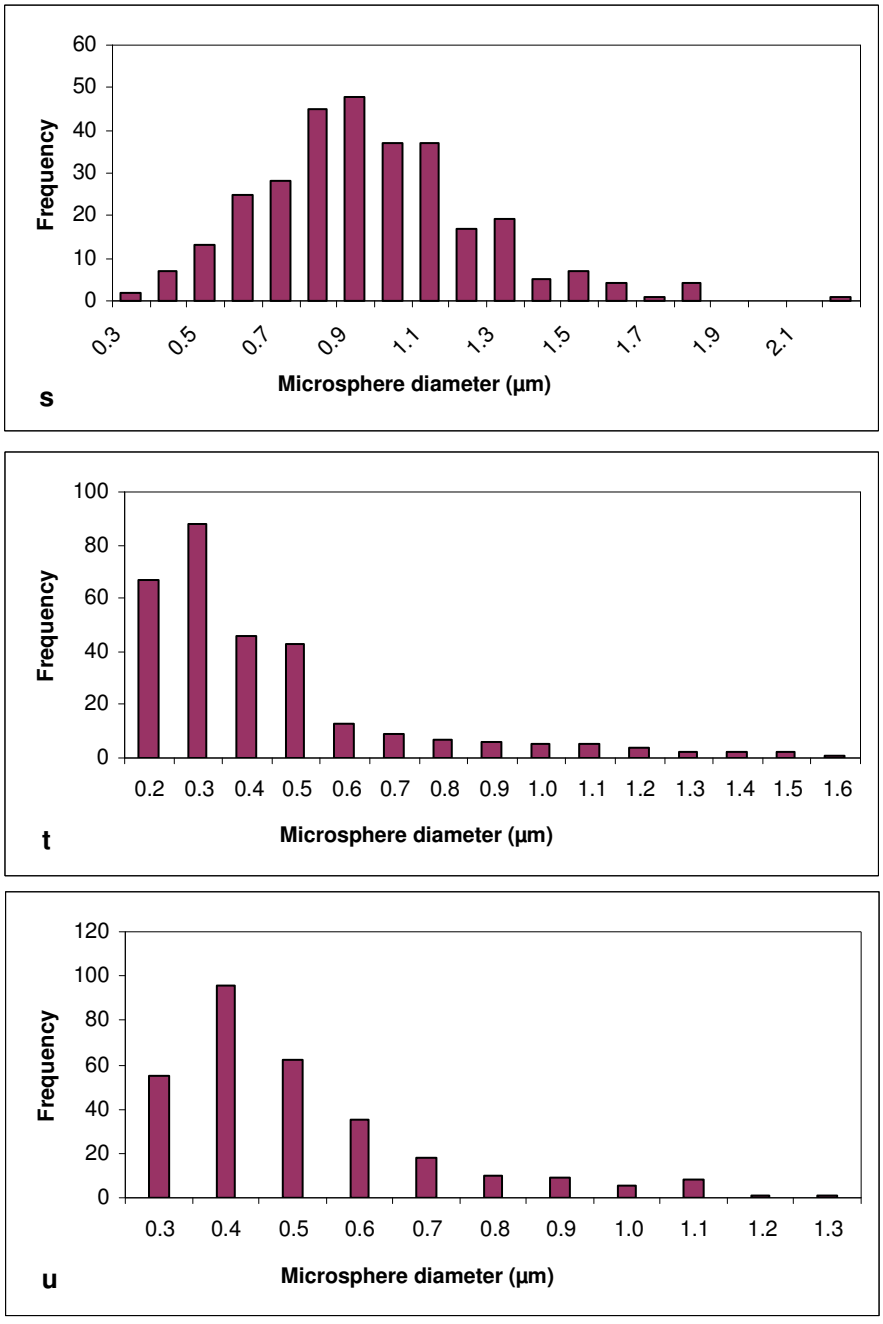

Figure 6.11. Size distribution data obtained by measuring 300 microspheres from respective scanning electron micrographs. The mean diameter and SD were at **s**, 0.9 µm and 0.2µm; at **t**, 0.4 µm and 0.14 µm and at **u**, 0.5 µm and 0.08 µm, respectively.

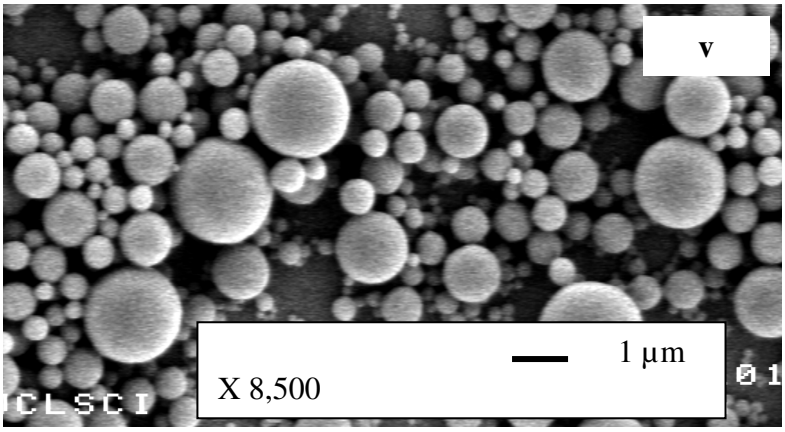

Figure 6.12. Scanning electron micrograph of microspheres prepared at flow rate combination at **v**, 5 µl s^{-1} (air) : 12 µl s^{-1} (polymer). The mean diameter of the microsphere was 1.2 µm with a SD 0.62 µm.

Table 6.4. Microsphere sizes obtained by CEHDA microbubbling of the 18 wt. % polymer solution at ambient temperature and different combination of flow rates selected at several points (except at point **v**) closer to the threshold line of the continuous microbubbling zone.

Position on parametric plot	**Flow rate of Air (µl s^{-1})**	**Flow rate of Polymer (µl s^{-1})**	**Gas ratio (λ)**	**Mean diameter (µm)**	**Standard Deviation (µm)**	**P.I (%)**
s	4	3	1.33	0.9	0.20	22
t	3	4	0.75	0.9	0.14	16
u	2	7	0.25	0.5	0.08	16
v	5	12	0.42	1.2	0.62	52

The results shown in **Table 6.3** and **Table 6.4** suggest two important points. First, a detailed investigation of a parametric plot can enable identification of flow rate

combinations that will result in small particles with very low polydispersivity indices fulfilling the main objective of preparing microspheres of submicrometre size. Second, it is not the gas ratio that always determines the size of the spheres, but also the absolute magnitude of the flow rates. For instance, although the gas ratio at point **v** is smaller (0.62) than the ratios at point **q** or **t**, the mean particle size (1.2 μm) has shown to be larger with a high polydispersivity index (52%) due to the high magnitudes of flow rates that lead to larger jet diameters at the time of microbubbling (Farook *et al*. 2007 b).

Within the continuous microbubbling zone (zone 4) and on the vertical line passing through point **p**, the mean microsphere diameter d_b, for the polymer solution-air system, scales with the gas ratio λ according to the equation (**Figure 6.13**):

$$d_b = 8.75\,(\lambda\text{-}0.67)^2 + 0.35 \qquad (6.1)$$

According to eqn (6.1), microsphere mean diameter d_b will be ~ 0.4 μm even at a gas ratio, λ, of 0.67.

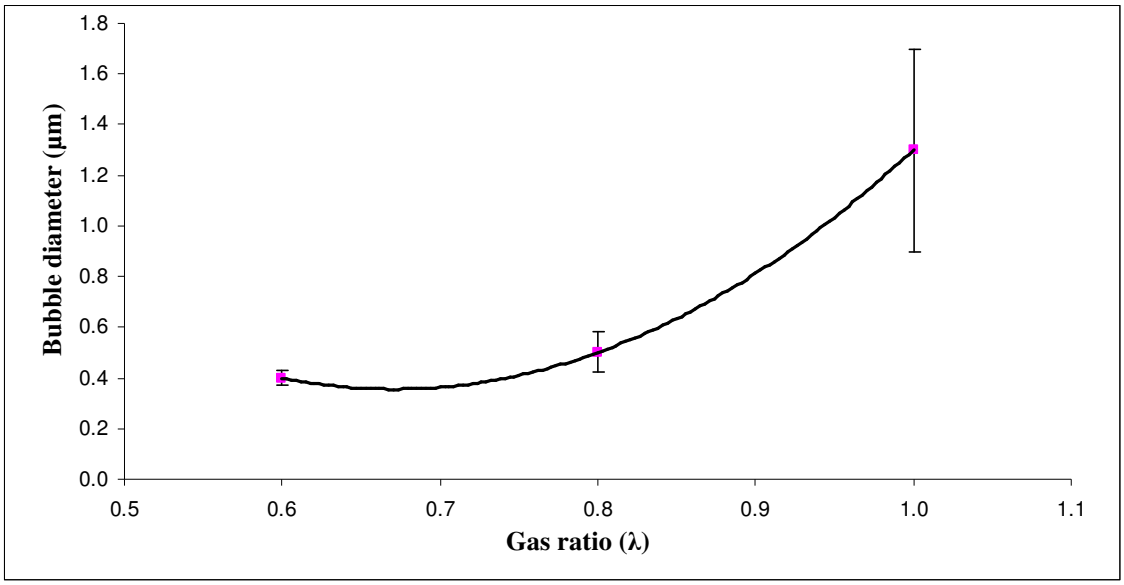

Figure 6.13. Graph of the microsphere diameter (d_b) versus the gas ratio (λ) within the continuous microbubbling zone of the parametric plot.

6.10.2. Characterisation of microspheres by transmission electron microscopy (TEM)

The TEM study indicates that the spheres are denser in the centre, giving rise to a higher contrast (**Figure 6.14**). The outer part of the spheres is markedly less dense, demonstrated by the lower contrast. Previous TEM images of microcapsules, where the centre is less dense than the outer part, show opposite features giving rise to greater contrast for outer part and lower contrast for the centre (Zhu *et al*.2008). When considering these two scenarios together, it is possible to suggest that outer part of the spheres in this investigation is composed of porous material, while the inner part is unresolved. Because of the amorphous nature of the material, the porous structure cannot be clearly imaged. As shown by the appearance of spheres within the size range of about 200 nm to 350 (**Figure 6.14**), with the decrease of sphere size, the contrast difference at the interface between the centre and the outer part decreases, showing therefore lower contrast, indicating the presence of more porous material. Smaller particles of about 150 nm diameter display more even contrast as shown in **Figure 6.15**. This observation is in agreement with the porosity study described in Section 6.9 and reported in Farook *et al*. (2008).

The higher contrast in the centre of the particles may be attributed to denser material being present in the centre of the spheres, resulting from the slower drying process before the TEM examination. As the wet suspension was directly taken to the carbon coated TEM grid and dried for a short time before examination, it may be possible that the part of the liquid absorbed by the microspheres was still trapped in the centre of the microspheres. As the evaporation of liquid from smaller particles is more efficient, the presence of trapped liquid in the centre will also be lower, giving rise to insignificant contrast difference in TEM images for smaller spheres.

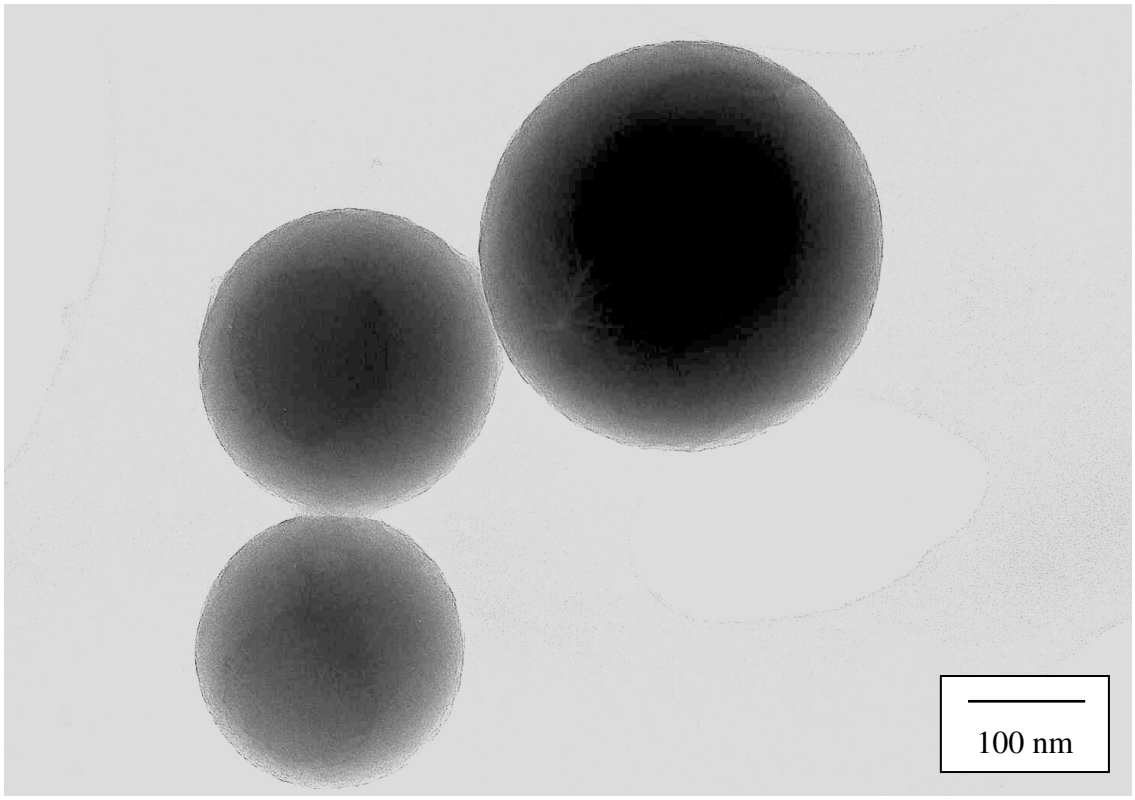

Figure 6.14. A TEM image of microspheres. Inner regions show a darker contrast and outer regions show a lighter contrast. Contrast difference is insignificant in larger spheres.

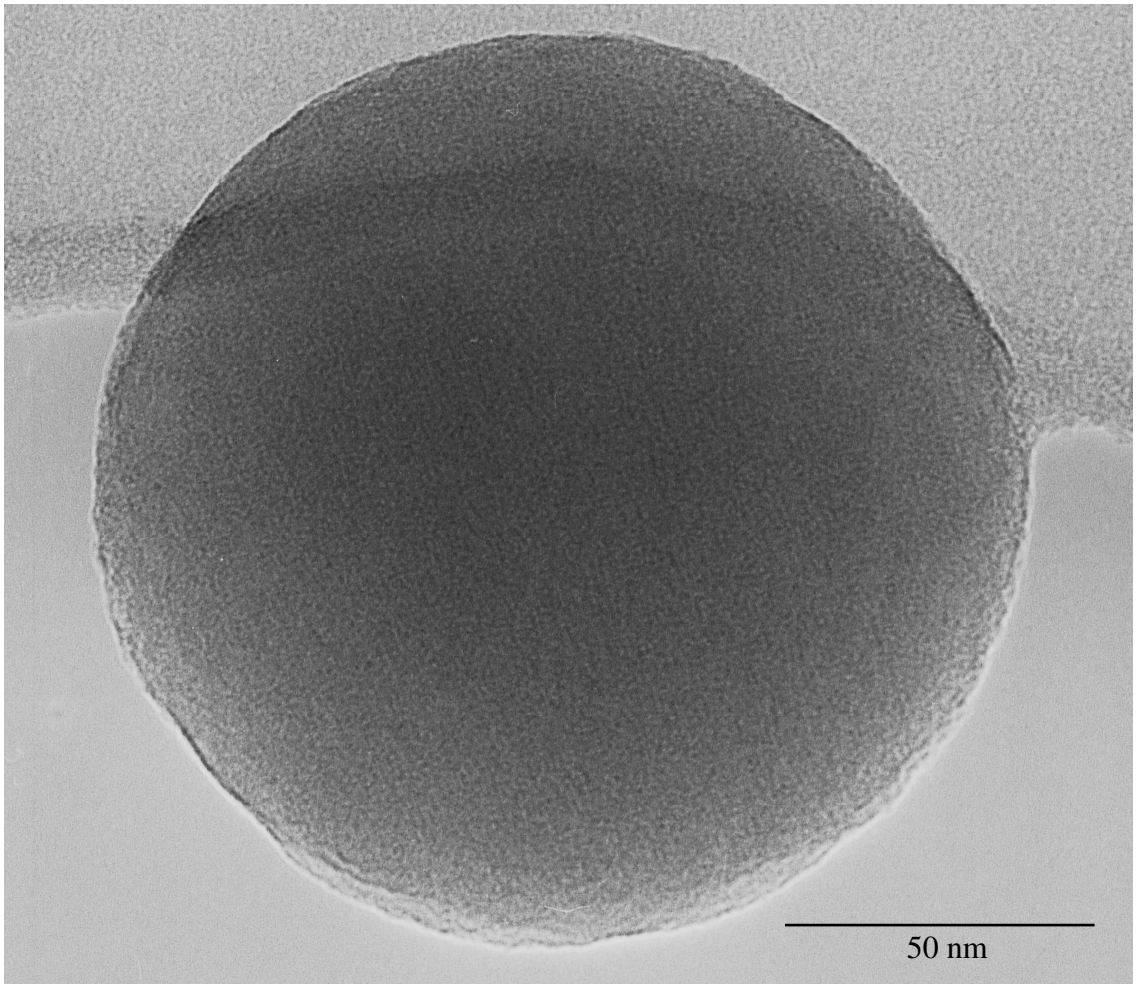

Figure 6.15. A TEM image of a microsphere (150 nm). Contrast difference is insignificant in smaller spheres.

6.10.3. Porosity study on microspheres of submicrometre size

As described in **Section 9** of this Chapter, a porosity study was also conducted on microspheres that had a mean diameter of 0.4 μm and a polydispersivity index of 8 %. Interestingly, calculations from the weight measurements showed there was liquid absorption amounting to ~ 65 wt. % in the microspheres (**Appendix**), showing an almost the same porosity value of the microspheres of the point **p** of the parametric plot.

6.11. Microspheres of submicrometre size with a matrix structure

With the characterisation, thus far carried out on the microspheres, such as ultrasound attenuation measurement, liquid absorption capacity, and more importantly, TEM examination, it is possible to conclude that with the current experimental set-up of CEHDA microbubbling technique, spheres having a matrix structure with a mean diameter as low as 400 nm with a polydispersivity index of 8% could be prepared.

Since CEHDA microbubbling is dependent on many variables such as process parameters, material parameters, needle geometry, ground electrode configuration, collection distance etc., it would always be possible to carry out further investigations by making changes in these parameters to change the characteristics of the end products. Using the same polymer that has been discussed in this Chapter but with a different liquid content (ethanol), Nangrejo *et al*. (2008) were able to reduce the size of the polymer capsules by making changes to the collection distance. Similarly, investigations are underway to reduce the size and size distribution of products by changing the needle geometry from a flat tip to an angular tip.

The use of sub micrometre size polymer particles are increasingly in demand for the delivery of drug and genes to tumour tissues. Depending on the anatomic region of the tumour, the pore size of the endothelial junction is found to be varying between 100 to 700 nm with an approximate mean of 400 nm (Amiji *et al*. 2006). As such, investigations that have been described in this Chapter could be considered as an important milestone in preparing polymeric drug and gene delivery vehicles using CEHDA microbubbling.

CHAPTER 7

CONCLUSIONS AND FUTURE WORK

7.1. Conclusions

7.1.1. CEHDA microbubbling

With a simple modification, the needle set-up conventionally used in co-axial electrohydrodynamic atomization (CEHDA) for the encapsulation of liquids and solids can be successfully adapted to encapsulate gases by liquids or suspensions or solutions, introducing a new processing technique to prepare microbubbles and microparticles that are important for various industrial applications including biomedical engineering. The new process of generating microbubbles has been introduced as co-axial electrohydrodynamic atomization microbubbling (**Chapter 4**).

7.1.2. Modes of microbubbling

Unlike the case of either conventional electrohydrodynamic atomization (EHDA) or co-axial electrohydrodynamic atomization (CEHDA), three distinct modes of microbubbling have been identified for the microbubbling process: **bubble dripping mode**, **coning mode** and **microbubbling mode**. The appearance of these three modes of microbubbling is essential for any liquid or suspension or solution to be used as an encapsulating medium to generate microbubbles. An uninterrupted appearance of the bubble dripping mode is a clear indication of a right combination of flow rates and that a continuous microbubbling can be predicted at the microbubbling mode with the increase of applied voltage. If the bubble dripping mode appears intermittently, microbubbling also would be intermittent at the microbubbling mode (**Chapter 4**).

7.1.3. Parametric plot

7.1.3.1. The role of flow speed

A parametric plot constructed between the flow rate of gas and the flow rate of liquid has proved to be an important tool throughout the investigations. With the liquid flow rate on the x-axis and the gas flow rate on the y-axis, the pattern of microbubbling exhibited in the parametric plot (e.g., **Figure 4.9**) brings out some interesting observations. At smaller values of liquid flow rates and with gradual increase of gas flow rate, microbubbling does not occur and this area has been identified as a "no microbubbling zone" due to dominance of air. Similarly, below a critical minimum value of air flow rate[$(Q_a)_{min}$] and at all values of liquid flow rate, microbubbling would not occur and this area has been identified as a " no microbubbling zone" due to dominance of liquid flow.

But, when moving from a lower liquid flow rate to a higher liquid flow rate and by increasing gas flow rate, the phenomenon moves from no microbubbling to continuous microbubbling through an intermittent microbubbling zone. At a further higher liquid flow rate than before and by increasing gas flow rate, microbubbling is reached more quickly than before. This means, with the increase of liquid flow rate, air loses its dominance to liquid flow and that microbubbling occurs even at lower flow rate of air than before.

At a lower air flow rate above $(Q_a)_{min}$, a substantial increase in liquid flow rate is necessary to reach continuous microbubbling from no microbubbling. At higher flow rates of air, moving from no microbubbling to continuous microbubbling requires only a small increase in liquid flow rate. When moving from higher liquid flow rate to lower

liquid flow rate, microbubbling is still sustainable with the increase of air flow rate. These observations indicate that the flow speed of air also plays a major role in sustaining the microbubbling process (**Chapter 4, 5 & 6**).

7.1.3.2. Material specificity of the parametric plot

The plot is material specific and as such the four different zones identified will expand or contract depending on the physical properties of the materials. It is clear from several parametric plots constructed that only above a threshold boundary, several combinations of flow rates could be chosen for continuous microbubbling. Identifying the threshold boundary between the intermittent microbubbling and continuous microbubbling is essential as only by selecting a flow rate combination in the continuous microbubbling zone can the encapsulating material be fully utilised without wastage. However, if flow rate combinations are selected in a downward direction on a vertical line that passes through continuous microbubbling zone and the intermittent microbubbling zone, the bubble size would be larger at higher values of air flow rate than the bubble size at lower values of air flow rate.

If our interest is in smaller bubbles, generating them at a smaller gas ratio within the intermittent microbubbling zone would be a waste of microbubbling liquid as part of the liquid would not be incorporated. This problem could be overcome by shifting the threshold boundary downward by using suitable additives in the microbubbling liquid, e.g., adding Tween 80 to phospholipid suspension (**Chapter 5**). If the threshold boundary could be shifted downward, a lower gas ratio could be selected to generate smaller bubbles within the continuous microbubbling zone itself. However, the additive should not alter the fundamental nature of the base liquid, e.g., the electrical

conductivity and viscosity, and that the threshold boundary line also should not move in the upward direction instead of shifting downward (**Chapters 4, 5 & 6**).

7.1.3.3. The role of the gas ratio and jet diameter

Although the reduction in gas ratio means a reduction in bubble size on a vertical line selected (at a constant liquid flow rate) within the parametric plot, it is not necessary that lower gas ratio would always lead to lower bubble size. For a flow rate combination of 5 µl s^{-1}(air) : 10 µl s^{-1} (liquid), the gas ratio is 0.5. Similarly, for a different flow rate combination with higher values of flow rates such as 10 µl s^{-1}(air) : 20 µl s^{-1}(liquid), still the gas ratio is 0.5. However, the bubble size at previous combination is smaller than that of the latter. The reason behind this is the absolute magnitudes of the flow rates, since at higher flow rates the jet diameter during microbubbling is larger. In CEHDA microbubbling, at higher flow rates, it has not been possible to reduce the jet diameter by increasing the applied voltage to reduce the bubble size. However, when reducing the gas ratio at a constant flow rate of liquid, the magnitude of the gas flow rate will anyway reduce. In order to reduce the bubble size, it is therefore fundamental to reduce the jet diameter in CEHDA microbubbling as in the case of conventional EHDA and CEHDA. Selecting a microbubbling liquid with moderate viscosity, lower surface tension and higher electrical conductivity is also therefore a strategy to reduce the jet diameter and the bubble diameter subsequently (**Chapters 4, 5 & 6**).

7.1.4. Microbubbling with insulators

In conventional CEHDA, an insulator can be pumped through the inner or outer needle if the co-flowing liquid has sufficient electrical conductivity to act as a driving liquid. However, in CEHDA microbubbling, since the inner needle carries air, if insulators are

to be used as encapsulating materials, they must be either dissolved or suspended in a suitable conductive liquid so that the solution/suspension could be used as a driving liquid in the outer needle (**Chapter 6**).

7.1.5. Microbubbles (and microspheres) with diameters < 10 µm

Generating microbubbles with diameters < 10 µm was one of the main objectives of the research. After converting conventional CEHDA into a technique that can also generate microbubbles, manipulation of the gas ratio was the initial strategy to reduce the bubble size. However, with the development of parametric plots between the flow rates of air and the flow rates of liquid, lowering the gas ratio was performed while focusing on achieving a thinner jet diameter in order to reduce the bubble diameter. As a result, at ambient temperature, suspensions of stabilized microbubbles were produced with mean diameters as low as 5 µm and a polydispersivity index 9 % (**Chapter 5**). In the case of microspheres, mean diameters as low as 400 nm with a polydispersivity index of 8 % have been achieved (**Chapter 6**). The size and size distribution thus far achieved with microbubbles and microspheres suggest that the technique of CEHDA microbubbling could be carried forward into the future to make better inroads in preparing stabilized microbubbles and microspheres for medical applications.

7.1.6. Stability of microbubbles

Improving the stability of microbubbles has been looked at from the point of view of delaying the gas diffusion from inside the bubble. The diffusion of gas could be delayed either by forming a protective layer on the bubble surface or by minimizing the gas concentration gradient. The use of a surfactant and fine solid particles has been demonstrated in extending the bubble stability by way of reducing the surface tension

and diffusivity at the gas-aqueous medium interface with an expected formation of a protective layer on the bubble surface. In order to minimize the gas concentration gradient, increasing the gas concentration of the collecting liquid has been suggested for microbubbling via CEHDA (**Chapter 4**).

The use of a phospholipid has been demonstrated in **Chapter 5** to strengthen the bubble shell by forming a monolayer which delays the gas diffusion to the immediate environment. The use of phospholipids also reduces the surface tension at the gas-aqueous medium interface. The use of a surfactant, Tween 80, along with phospholipid has helped to reduce the size and size distribution of the bubbles while retaining the stability.

7.1.7. The bubble yield

CEHDA microbubbling has the capability to generate a large number of microbubbles per unit time. The whole amount of material will be microbubbled if the combination of flow rates is selected within the microbubbling zone of the parametric plot. If a theoretical calculation is made for the smallest microbubble prepared (diameter ~ 5 μm) (**Chapter 5**), the number of microbubbles that can be generated in a minute is ~ 4 X 10^9 (**Appendix**). The number would become much higher than this, if the bubble diameter is reduced further. In terms of volume, 18 ml of liquid could be converted into microbubbles for an hour with one set of needles. The volume of microbubble suspension could be increased by increasing the number of sets of needles. In the case of microspheres, the number of microspheres prepared per minute is much higher than the number mentioned above for microbubbles as CEHDA microbubbling has been able to prepare microspheres of submicrometre size.

7.2.8. Ultrasound imaging with phospholipid-coated microbubbles

The phospholipid-coated microbubbles prepared by using a phospholipid-Tween 80 system were also examined via ultrasound imaging 18 h after preparation. This showed that CEHDA microbubbling technique is capable of preparing microbubbles suitable for ultrasound imaging (**Chapter 6**).

7.2. Future Work

Since CEHDA microbubbling has been able to generate microbubbles and spheres with the possibility of using them for ultrasound imaging and drug delivery, the future work can be divided into two different strands. The first concerns the preparation and development of microbubbles for ultrasound imaging and drug delivery. The second relates to the preparation and development of polymeric spheres for drug and gene delivery.

7.2.1. Future work in connection with microbubbles

7.2.1.1. Use of pressurised air

Although microbubbles are being prepared with variety of gases including air and PFCs, air was the only gas which was used throughout the investigations that have been described in **Chapter 4-6**. The air captured within a 10 ml plastic syringe under normal atmospheric pressure was sent through the inner needle with the help of a precision pump for the generation of microbubbles and microspheres. It always took a while for the compaction of air within the syringe before generating larger bubbles in the liquid meniscus at zero voltage to show the first mode of microbubbling. Use of pressurised

air would provide flexibility to alter the density of air that is captured by the microbubbling liquid and this may bring changes in the behaviour of microbubbles thus produced, particularly in terms of stability. The features of parametric plot that can be constructed between the flow rate of air and the flow rate of liquid also might change with the change of pressure. A detailed study on the stability and the size and size distribution of microbubbles at different values of air pressure could bring further knowledge in developing the microbubbles produced by this technique.

7.2.1.2. Use of gases with lower diffusivity

The purpose of using gases with low diffusivity is to improve the stability of microbubbles. A number of ultrasound contrast agents have been developed using perfluorochemicals, particularly perfluorocarbons (PFCs), as their core gas. Albunex®, an agent with an air core and albumin shell, was developed into Optison™ using perfluoropropane as its gas core and albumin as its shell material. Since many phospholipid-coated microbubbles have been developed with PFCs, the phospholipid-coated microbubble that was prepared through CEHDA microbubbling with an air core could be further developed to be a more stabilized microbubble with a use of a PFC or any other gas with low diffusivity.

7.2.1.3. Use of lipids with a longer hydrophobic chain length

Improving the gas permeation resistance is significant in developing phospholipid-coated microbubbles in order to control their dissolution. Shedding of lipids also has been noted in short-chain lipids in order to accommodate the shrinking volume of the gas core (Borden and Longo 2002). Increased stiffness of the shell for longer chain lengths has been attributed to the increase in attractive dispersion forces between the

hydrophobic tails of adjacent lipid molecules (Borden and Longo 2002). In order to validate this view for the microbubbles generated by CEHDA microbubbling, it may be possible to use a lipid such as 1,2-diacyl-sn-glycerol-3-phosphatidylcholine with varying chain lengths to prepare microbubbles and compare their stability with microbubbles prepared with L-α- phosphatidylcholine.

7.2.2. Future work in connection with polymeric microspheres

7.2.2.1. Encapsulating a water soluble drug

Since the microspheres prepared have shown capability to absorb liquid in which the microspheres were collected in, it provides a great opportunity to add a water soluble drug into the collecting medium (distilled water) and conduct further research such as drug release pattern, entrapment efficiency etc. Since the polymer used was not a biodegradable one (although biocompatible), it will be an added advantage if a biodegradable polymer could be used so that the research could be further extended to *in-vivo* and *in-vitro* studies with the microsphere that has encapsulated a water soluble drug.

7.2.2.2. Use of a stabilizer

A problem constantly encountered during the collection of microspheres in distilled water was the formation of coagulates in the collecting medium. These were removed using filtering tissues. However, it may be possible to identify a suitable stabilizer that could inhibit the formation of such coagulates. The traditional stabilizers such as gelatine or polyvinyl alcohol were not used as they are known to reduce the absorption capacity of the microspheres (Lu *et al.* 1999). Identifying a suitable stabilizer to suit the

polymer that is used for microencapsulation would enhance the productivity of the microspheres generated.

7.2.2.3. Preparation of nanospheres

Since microspheres of submicrometre size as low as 400 nm have been prepared with existing facilities in the current CEHDA microbubbling set-up, it may be possible to prepare nanospheres (diameter < 100 nm) using the same set-up. By modifying the parametric plot using an additive to enable the reduction of gas ratio can be a strategy for doing this. However, other options such as modifying the needle angle, varying the collection distance, narrowing the gap between the tip of the outer needle and the ring electrode also may help in reducing the size to 'nano' range. Nanospheres are very much in need for drug delivery, particularly to the central nervous system (Blasi *et al*.2007).

7.2.2.4. Use of hydrophilic polymers

The pharmaceutical industry has shown great interest in the development of controlled release systems based on hydrophilic polymers. The application of a wide variety of hydrophilic biodegradable polymers to delivery of proteins has been extensively studied (Sunggyu Lee and Lee Lee 2005). Typical polymers include hydrogels based on polyvinyl alcohol or cellulose, and natural polymers such as alginase or collagen. Since the polymer used in our investigations is a hydrophobic one, it will be a great opportunity to use hydrophilic polymers and conduct further research with CEHDA microbubbling.

7.2.2.5. Preparation of composite microspheres

Using composite microspheres to avoid a "burst" release of drugs is a very useful strategy in controlled drug delivery (Hasan *et al*. 2007). CEHDA microbubbling and conventional CEHDA could be jointly used for preparing composites. Drug loaded nano/microparticles could be prepared using CEHDA microbubbling and subsequently nano/microparticles thus prepared could be sent through the inner needle of the conventional CEHDA while sending an encapsulating polymer through the outer.

7.2.2.6. Use of microspheres for tissue engineering

Tissue engineering has emerged as a viable alternative to the problem of organ and tissue shortage. The use of microspheres, particularly of hydrophilic biodegradable polymers, as scaffold materials for the growth of cells for tissue engineering is an emerging area of application in medical engineering (Botchwey *et al.* 2004). Microspheres produced through CEHDA microbubbling had a tendency of settling down at the bottom of the collecting vessel forming a sheet of microspheres. These microspheres could be connected by raising the temperature just above their softening point so that a scaffold for cell growth could be prepared without destroying the spherical shape of the microspheres. Further research in this area could open up a new branch of application for the microspheres prepared by CEHDA microbubbling.

References

Amiji MM (2006) 'Nanotechnology for cancer therapy', Taylor & Francis, New York, NY 10016. Page 1-8.

Arshady R (1989) Microspheres and Microcapsules: A survey of manufacturing techniques. Part I: Suspension cross-linking. Polym Eng Sci 29:1746-1758.

Arshady R (1990) Microspheres and Microcapsules: A Survey of Manufacturing techniques. Part II: Coacervation. Polym Eng Sci 30: 905-914.

Balachandran W, Miao P, Xiao P (2001) Electrospray of fine droplets of ceramic suspensions for thin-film preparation. J Electrostat 50: 249-263.

Balasubramanian K, Jayasinghe SN, Edirisinghe MJ (2006) Coaxial electrohydrodynamic atomization of ceramic suspensions. Int J App Ceram Technol 3(1): 55-60.

Bamber JC (2005) Medical ultrasound: research trends that may drive sensor development. Journal of Physics Series 15: 1-6.

Bao S, Thrall BD, Miller DL (1997) Transfection of a reporter plasmid into cultured cells by sonoporation in-vitro. Ultrasound in Med & Biol 23: 953-959.

Barrero A, Ganan-Calvo AM, Davila J, Palacio A, Gomez-Gonzalez E (1998) Low and high Reynolds number flows inside Taylor cones. Phys Rev E 58: 7309-7314.

Barsoum SC, Milgram W, Mackay W, Coblentz C, Delaney KH, Kwiecien JM, Kruth SA, Chang PL (2003) Delivery of recombinant gene product to canine brain with the use of microencapsulation. J Lab Clin Med 142(6): 399-413.

Bekeredjian R, Grayburn PA, Shohet RV (2005) Use of ultrasound contrast agents for gene or drug delivery in cardiovascular medicine. Am J Cardiol 45(3): 329-335.

Berkland C, Pollauf E, Varde N, Pack D W, Kim KK (2007) Monodisperse liquid-filled biodegradable microcapsules. Pharmaceut Res 24(5): 1007-1013.

Bertling J, Blomer J, Kummel R (2004) Hollow microspheres. Chem Eng Technol 27: 829-837.

Binks B, Lumsdon S (2000) Influence of particle wettability on the type and stability of surfactant-free emulsions. Langmuir 16: 8622-8631.

Blasi P, Giovagnoli S, Schoubben A, Ricci M, Rossi C (2007) Solid lipid nanoparticles for targeted brain drug delivery. Adv Drug Delivery Rev 59: 454-477.

Bleeker H, Shung K and Barnhart J (1990) On the application of ultrasonic contrast agents for blood flowmetry and assessment of cardiac perfusion. J Ultrasound Med 9: 461-471.

Borden M, Attawia M, Khan Y, Laurencin CT (2002) Tissue engineered microsphere-based matrices for bone repair: design and evaluation. Biomaterials 23: 551-559.

Borden MA, Longo ML (2002) Dissolution behaviour of lipid monolayer-coated, air-filled microbubbles: effect of lipid hydrophobic chain length. Langmuir 18: 9225-9233.

Borden MA, Dayton P, Zhao S, Ferrara KW (2004 a) Physico-chemical properties of the microbubble lipid shell. IEEE Int Ultrasonics Ferroelectrics and frequency Control Joint 50th anniversary Conference Page 20-23.

Borden MA, Pu G, Runner GJ, Longo ML (2004 b) Surface phase behaviour and microstructure of lipid/PEG-emulsifier monolayer-coated microbubbles. Colloids Surf.B Biointerfaces 35: 209-223.

Borden MA, Kruse DE, Caskey CF, Zhao SK, Dayton P, Ferrara KW (2005) Influence of lipid shell physiochemical properties on ultrasound-induced microbubble destruction. IEEE Trans Ultrason Ferroelectr Freq Control 52: 1992-2002.

Borden MA, Caskey CF, Little E, Gillies RJ, Ferrara KW (2007) DNA and polylysine adsorption and multilayer construction onto cationic lipid-coated microbubbles. Langmuir 23: 9401-9408.

Bose GM (1745) Recherches sur la Cause et sur la veritable Theorie de Electricite. Wittenberg.

Botchwey EA, Pollack SR, Levine EM, Johnston ED, Laurencin CT (2004) Quantitative analysis of three-dimensional fluid flow in rotating bioreactors for tissue engineering. J Biomed Mater Res Part A 69A(2): 205-215.

Brannon-Peppas L (1997) Polymers in controlled drug delivery. Medical plastics Magazine, November.

Cavalieri F, Hamassi AE, Chiessi E, Paradossi G (2005) Stable polymeric microbaloons as multifunctional device for biomedical uses: synthesis and chracterisation. Langmuir 21: 8758-8764.

Chen CH, Kelder EM, Schoonman J (1998) Effects of additives in electrospraying for materials preparation. J European Ceramic Soc 18: 1439-1443.

Chen QZ, Boccaccini AR, Zhang HB, Wang DZ, Edirisinghe MJ (2006) Improved mechanical reliability of bone tissue engineering (Zirconia) scaffolds by electrospraying. J Am Ceram Soc 89: 1534-1539.

Cheng D, Xia H, Chan H S O (2006) Fabrication of polymeric hollow nanospheres, hollow nanocubes and hollow nanoplates. Nanotechnol 17: 1661-1667.

Cloupeau M, Prunet-Foch B (1990) Electrostatic spraying of liquids: main functioning modes. Journal of Electrostatics 25: 165-184.

Cui W, Bei J, Wang S, Zhi G, Zhao Y, Zhou X, Zhang H, Xu Y (2005) Preparation and evaluation of poly(L-lactide-co-glycolide) (PLGA) microbubbles as a contrast agent for myocardial contrast echocardiography. J Biomed Mater Res Part B: Appl Biomater 73B: 171-178.

Dayton PA, Ferrara KW (2002) Targeted imaging using ultrasound. J Magn Reson Imaging 16: 362-377.

De la Mora JF, Loscertales IG (1994) The current emitted by highly conducting Taylor cones. J Fluid Mech 260: 155-184.

Delie F, Blanco-Prieto MJ (2005) Polymeric particulates to improve oral bioavailability of peptide drugs, Molecules 10: 65-80.

Dinarvand R, Moghadam SH, Mohammadyari-Fard L, Atyabi F (2003) Preparation of biodegradable microspheres and matrix devices containing Naltrexone. AAPS PharmSciTech 4(3): Article 34. 1-10.

Dijkmans PA, Juffermans LJM, Musters RJP, van Wamel A, Ten Cate FJ, Van Gilst W, Visser CA, De Jong N, Kamp O (2004) Microbubbles and ultrasound: from diagnosis to therapy. Eur. J. Echocardiography 5: 245-256.

Dong W, Bodmeier R (2006) Encapsulation of lipophilic drugs within enteric microparticles by a novel coacervation method. Int J Pharm 326: 128-138.

Drozin VG (1955) The elctrical dispersion of liquids as aerosols. J Colloid Sci 10: 158-164.

Du Z, Bilbao-Montoya M, Binks B, Dickinson E, Ettelaie R, Murray B (2003) Outstanding Stability of Particle Stabilized Bubbles. Langmuir 19: 3103-3108.

Duncan PB, Needham D (2004) Test of the Epstein-Plesset Model for gas microparticle Dissolution in Aqueous Media: Effect of Surface Tension and gas undersaturation in Solution. Langmuir 20: 2567-2578.

El-Sherif DM, Wheatley MA (2003) Development of a novel method for synthesis of a polymeric ultrasound contrast agent. J Biomed Mater Res Part A 66A(2): 347- 355.

Epstein P, Plesset M (1950) On the stability of gas bubbles in liquid-gas solutions. J Chem Phys 18: 1505-1509.

Farook U, Zhang HB, Edirisinghe MJ, Stride E, Saffari N (2007a) Preparation of microbubble suspensions by co-axial electrohydrodynamic atomization. Med Eng Phys 29: 749-754.

Farook U, Stride E, Edirisinghe MJ, Moaleji R (2007b) Microbubbling by co-axial electrohydrodynamic atomization. Med Bio Eng Comput 45: 781-789.

Farook U, Edirisinghe MJ, Stride E, Colombo P (2008) Novel co-axial electrohydrodynamic in-situ preparation of liquid-filled microspheres for biomedical applications. J Microencapsul 25(4): 241-247.

Farook U, Stride E, Edirisinghe M (2009a) Preparation of suspensions of phospholipid-coated microbubbles by coaxial electrohydrodynamic atomization. J R Soc Interface 6(32): 271-277.

Farook U, Stride E, Edirisinghe M (2009b) Stability of microbubbles prepared by co-axial electrohydrodynamic atomisation. Eur Biophys J 38(5): 713-718.

Farook U, Stride E, Edirisinghe M (2009c) Controlling the size and size distribution of electrohydrodynamically prepared microbubbles. Bubble Science, Engineering & Technology 1(1-2): 53-57.

Ferrara K, Pollard R, Borden M (2007) Ultrasound microbubble contrast agents: Fundamentals and application to gene and drug delivery. Annu Rev Biomed Eng 9: 415-447.

Feshitan JA, Chen CC, Kwan JJ, Borden MA (2009) Microbubble size isolation by differential centrifugation. J Colloid Interf Sci 329: 316-324.

Folkman J, Long DM (1964) The use of silicone rubber as carrier for prolonged drug therapy. J Surg Res 4: 139-142.

Forsberg F, Ro RJ, Potoczek M, Liu JB, Merritt CRB, James KM, Dicker AP, Nazarian LN (2004) Assessment of angiogenesis: implications for ultrasound imaging. Ultrasonics 42: 325-330.

Freudenrich C, http://health.howstuffworks.com/ultrasound1.htm

Ganan-Calvo AM, Davila J, Barrero A (1997) Current and droplet size in the electrospraying of liquids. J Aerosol Sci 28: 249-275.

Ganan-Calvo AM, Gordillo JM (2001) Perfectly monodisperse microbubbling by capillary flow focusing. Phys Rev Lett 87: 2745011-2745014.

Ganan-Calvo AM (2004) Perfectly monodisperse microbubbling by capillary flow focusing: An alternate physical description and universal scaling. Phys Rev E 69: 0273011-0273013.

Gaponik N, Radtchenko IL, Sukhorukov GB, Rogach AL (2004) Luminescent polymer microcapsules addressable by a magnetic field. Langmuir 20: 1449-1452.

Garstecki P, Gitlin I, Diluzio W, Whitesides GM, Kumachewa E, Stone HA (2004) Formation of monodisperse bubbles in a microfluidic flow-focusing device. Appl Phys Lett 85: 2649-2651.

Garstecki P, Ganan-Calvo AM, Whitesides GM (2005) Formation of bubbles and droplets in microfluidic systems. Bull Pol Acad of Sci 53: 361-372.

Goldberg BB, Merton DA, Deane CR (1997 a) 'An atlas of ultrasound colour flow imaging', Taylor & Francis, Page 1-8.

Goldberg BB, Raichlen JS, Forsberg F (1997 b) 'Ultrasound contrast agents', Martin Dunitz, London, Page 3.

Gordillo JM, Cheng Z, Ganan-Calvo AM, Marquez M, Weitz DA (2004) A new device for the generation of microbubbles. Phys Fluids 16: 2828-2834.

Goulet JA, Senunas LE, DeSilva GL, Greenfield ML (1997) Autogenous iliac crest bone graft. Complications and functional assessment. Clin Orthop Relat Res 339 : 76-81.

Gramiak R, Shah PM (1968) Echocardigraphy of the aortic root. Investigat Radiol 3: 356-366.

Gramiak R, Shah PM, Kramer DH (1969) Ultrasound cardiography: contrast studies in anatomy and function. Radiology 92: 939-948.

Grayburn PA (2002) Current and future contrast agents. Echocardiography 19(3): 259-265.

Hartman RPA, Brunner DJ, Marijnissen JCM, Scarlett b (1998) Scaling laws for droplet size and current produced in the cone-jet mode. J Aeorosol Sci 29: Suppl.1, S977-S978.

Hartman RPA, Brunner DJ, Camelot DMA, Marijnissen JCM, Scarlett B (1999) Electrohydrodynamic atomization in the cone-jet mode physical modeling of the liquid cone and jet. J Aerosol Sci 30(7): 823-849.

Harvey CJ, Pilcher JM, Eckersley RJ, Blomley MJK, Cosgrove DO (2002) Advances in ultrasound. Clin Radiol 57: 157-177.

Hartman RPA, Brunner DJ, Camelot DMA, Marijnissen JCM, Scarlett B (2000) Jet break-up in electrohydrodynamic atomization in the cone-jet mode. J Aerosol Sci 31(1): 65-95.

Hasan AS, Socha M, Lamprecht A, Ghazouani FE, Sapin A, Hoffman M, Maincent P, Ubrich N (2007) Effect of the microencapsulation of nanoparticles on the reduction of burst release. Int J Pharm **344**, 53-61.

Hettiarachchi K, Talu E, Longo ML, Dayton PA, Lee AP (2007) On-chip generation of microbubbles as a practical technology for manufacturing contrast agents for ultrasonic imaging. Lab on a chip 7: 463- 468.

Hoff L (2001) 'Acoustic Characterization of Contrast Agents for Medical Ultrasound Imaging', Kluwer Academic Publishers, Page 114-138.

Holsbeke CV, Timmerman D (2005) Intravenous contrast ultrasound in gynaecology. International Congress Series 1279: 174-178.

Huang J, Jayasinghe SN, Best SM, Edirisinghe MJ, Brooks RA, Bonfield W (2004) Electrospraying of a nano-hydroxyapatite suspension. J Mater Sci 39: 1029-1032.

Huang YY, Chung TW, Tzeng TW (1997) Drug release from PLA/PEG microparticulates. Int J Pharm 156: 9-15.

Hughes MS, Lanza GM, Marsh JN, Wickline SA (2003) Targeted ultrasonic contrast agents for molecular imaging and therapy; a brief review. MEDICAMUNDI 47/1.

Iwasaki Y, Sawada S, Ishihara K, Khang G, Lee HB (2002) Reduction of surface-induced inflammatory reaction on PLGA/MPC polymer blend. Biomaterials 23(18): 3897-3903.

Jaworek A, Krupa A (1999) Classification of the modes of EHD spraying. J Aerosol Sci 30: 873-893.

Jayasinghe SN, Edirisinghe MJ (2002 a) Effect of viscosity on the size of relics produced by electrostatic atomization. J Aerosol Sci 33: 1379-1388.

Jayasinghe SN, Edirisinghe MJ (2002 b) A novel method of forming open cell ceramic foam. Journal of Porous Materials 9: 265-273.

Jayasinghe SN, Edirisinghe MJ, De Wilde T (2002) A novel ceramic printing technique based on electrostatic atomization of a suspension. Mater Res Innovations 6: 92-95.

Jayasinghe SN, Edirisinghe MJ (2003) Preparation of collagen films by electrostatic atomization. J Mater Sci Lett 22: 1617-1619.

Jayasinghe SN, Edirisinghe MJ (2004) Electrostatic atomization of a ceramic suspension. J Eur Ceramic Soc 24: 2203-2213.

Jones AR, Thong KC (1971) The production of charged monodisperse fuel droplets by electrical dispersion. J Phy Appl Phys 4: 1159-1166.

Jones JR, Boccaccini AR (2005) "Cellular Ceramics in Biomedical Applications: Tissue engineering"; pp. 550-573 in Cellular Ceramics; Structure, manufacturing, Processing and Applications, Edited by M.Scheffler and P.Colombo. Wiley-VCH Verlag GmbH & Co. KGaA, Weinheim, 2005.

Jong N, Cate FJT (1996) New ultrasound contrast agents and technological innovations. Ultrasonics 34: 587-590.

Julienne MC, Alonso MJ, Amoza JLG, Benoit JP (1992) Preparation of poly(DL-lactide/glycolide) nanoparticles of controlled particle size distribution: application of experimental designs. Drug Dev Ind Pharm 18: 1063-1077.

Kawaguchi H (2000) Functional polymer microspheres. Prog Polym Sci 25: 1171-1210.

Klibanov AL (1999) Targeted delivery of gas-filled microspheres, contrast agent for ultrasound imaging. Adv Drug Deliv Rev 37: 139-157.

Klibanov AL, Hughes MS, Wojdyla JK, Wible JH, Brandenburger GH (2002) Destruction of contrast agent microbubbles in the ultrasound field: the fate of the microbubble shell and the importance of the bubble gas content. Acad Radiol 9: S41-S45.

Krasovitski B, Kimmel E (2006) Stability of an encapsulated bubble shell. Ultrasonics 44: 216-220.

Ku BK, Kim SS (2002) Electrospray characteristics of highly viscous liquids. J Aerosol Sci 33: 1361-1378.

Langer R (1998) Drug delivery and targeting. Nature, 392: 5-10.

Langer R, Folkman J (1976) Polymers for the sustained release of proteins and other macromolecules. Nature 263: 797-800.

Linder JR (2004) Molecular imaging with contrast ultrasound and targeted microbubbles. J Nucl Cardiol 11(2): 215-221.

Liu X, Gao C, Shen J, Mohwald H (2005) Multilayer microcapsules as anti-cancer drug delivery vehicle: deposition, sustained release, and in-vitro bioactivity. Macromol Biosci 5: 1209-1219.

Loscertales IG, Barrero A, Guerrero I, Cortijo R, Marquez M, Ganan Calvo AM (2002) Micro/Nano encapsulation via electrified coaxial liquid jets. Science 295: 1695-1698.

Lopez-Harrera JM, Barrero A, Lopez A, Loscertales IG, Marquez M (2003) Coaxial jets generated from electrified Taylor cones, Scaling laws. J Aerosol Sci 34: 535-552.

Lu Z, Bei J, Wang S (1999) A method for the preparation of polymer nanocapsules without stabilizer. J Control Release 61: 107-112.

Maysinger D, Morinville A (1997) Drug delivery to the nervous system. Trends Biotechnol 15(10): 410-418.

Miao P, Balachandran W, Wang JL (2001) Electrostatic generation and theoretical modeling of ultra fine spray of ceramic suspensions for thin film preparation. J Electrostat 51-52: 43-49.

Mizushige K, Kondo I, Ohmori K, Hirao K, Matsuo H (1999) Enhancement of ultrasound-accelerated thrombolysis by echo contrast agents: dependence on microbubble structure. Ultrasound in Med & Biol 25(9): 1431-1437.

Murua A, Portero A, Orive G, Hernandez RM, Castro MD, Pedras JL (2008) Cell microencapsulation technology. J Control Release. doi:10.1016/j.jconrel.2008.08.010.

Mutoh M, Kaieda S, Kamimura K (1979) Convergence and disintegration of liquid jets induced by an electrostic field. Journal of applied Physics 50: 3174-3179.

Nagorynyi VS, Bezrukov VI (1980) Droplet emission in an electrostatic field. Magn Gidrodin USSR 16: 111.

Nanda NC, Carstensen EL (1997) 'Advances in echo imaging using contrast enhancement' Dubai, Kluwer Academic Publishers, Page 115-131.

Oeffinger BE, Wheatley MA (2004) Development and characterisation of a nano-scale contrast agent. Ultrasonics 42: 343-347.

Ogawa Y, Yamamoto M, Okada H, Yashiki T, Shimamoto T (1988) A new technique to efficiently entrap leuprolide acetate into microcapsules of polylactic acid and copoly (lactic/glycolic acid). Bull Chem Pharm 36: 1095-1103.

Pekarek KJ, Jacob JS, Mathiowitz E (1994) One-Step preparation of double-walled microspheres. Adv Mater 6(9): 684-687.

Pancholi K, Farook U, Moaleji R, Stride E, Edirisinghe M (2008a) Novel methods of preparing phospholipid coated microbubbles. Eur Biophys J 37: 515-520.

Pancholi K, Stride E, Edirisinghe M (2008b) Dynamics of Bubble Formation in Highly Viscous Liquids. Langmuir 24: 4388-4393.

Pareta R, Edirisinghe MJ (2006) A novel method for the preparation of biodegradable microspheres for protein drug delivery. J R Soc Interface 3: 573-582.

Pickering S (1907) Emulsions. J Chem Soc 91: 2001-2021.

Poliachik SL, Chandler WL, Mourad PD, Bailey MR, Bloch S, Cleveland RO, Kaczkowski P, Keilman G, Porter T, Crum LA (1999) Effect of high-intensity focused ultrasound on whole blood with and without microbubble contrast agent. Ultrasound in Med & Biol 25: 991-998.

Pomper MG, Gelovani JG (2008) 'Molecular Imaging in Oncology', Informa healthcare, New York, NY 10017. Page 332.

Postema M, Bouakaz A, Chin C, De Jong N (2003) Simulations and measurements of optical images of insonified ultrasound contrast microbubbles, IEEE. Trans. Ultrason. Ferroelectr. Freq. Control, 50: 523-535.

Rackles C, Hamaide T (2005) Synthesis and Characterisation of Water Soluble Saccharide Functionalized Polysiloxanes and their use as Polymer Surfactants for the Stabilization of Polycaprolactone Nanoparticles. Macromol Chem 206, 1757- 1768

Raisinghani A, DeMaria AN (2002) Physical principles of microbubble ultrasound contrast agents. Am J Cardiol 90: 3J-7J.

Rayleigh L (1879) On the stability or instability of certain fluid motions. Proceedings of the London mathematical Society 1-11: 57-72.

Rayleigh L (1882) On the equilibrium of liquid conducting masses charged with electricity. Philosophical Magazine 14: 184-186.

Riess JG (2003) Flourocarbon-based injectable gaseous microbubbles for diagnostic and therapy. Curr Opin Colloid In 8: 259-266.

Sato M, Kudo N, Saito M (1998) Surface tension reduction of liquid by applied electric field using vibrating jet method. IEEE Trans Ind Appl 34: 294-300.

Schmidt W, Roessling G (2006) Novel manufacturing process of hollow polymer microspheres. Chem Eng Sci 61: 4973-4981.

Schrope B, Newhouse VL, Uhlendorf V (1992) Simulated capillary blood flow measurement using a nonlinear ultrasonic contrast agent. Ultrasonic Imaging 14: 134-158.

Sgraja M, Bertling J, Kummel R, Jansens PJ (2006) Inorganic and hybrid hollow spheres by coating of microcapsules as templates. J Mater Sci 41: 5490-5494.

Shung KK (2006) 'Diagnostic ultrasound imaging and blood flow measurements', 2006, Taylor & Francis, New York, NY 10016, Page 1.

Sidhu PS (2004) Ultrasound. Clinical Radiology 59: 586-587.

Simpson DH, Chin CT, Burns PN (1999) Pulse inversion doppler: a new method for detecting nonlinear echoes from microbubble contrast agents. IEEE Trans Ultrason Ferroelectr Freq Control 46: 372-382.

Singhal S, Moser CC, Wheatley MA (1993) Surfactant-stabilized microbubbles as ultrasound contrast agents: stability study of Span 60 and Tween 80 mixtures using a Langmuir Trough. Langmuir 9: 2426-2429.

Smith DPH (1986) The electrodynamic atomization of liquids. IEEE Transaction on industry applications IA-22: 527-535.

Soetanto K, Chan M (2000) Study on the lifetime and attenuation properties of microbubbles coated with carboxylic acid salts. Ultrasonics 38: 969-977.

Stride E, Saffari N (2003) Microbubble ultrasound contrast agents: a review. J Eng Med Proc Inst Mech Eng Part H: J Eng Med 217: 429-447.

Stride E, Pancholi K, Edirisinghe MJ, Samarasinghe S (2008) Increasing the nonlinear character of microbubble oscillations at low acoustic pressures, J R Soc Interface 5: 807-811.

Stride E, Pancholi K, Edirisinghe M, Samarasinghe S (2008a) Increasing the Nonlinear Character of Microbubble Oscillations at Low Acoustic Pressures. J Roy Soc Interface 5: 807-811.

Stride E, Tang M, Eckersley R (2009) Physical Phenomena Affecting Quantitative Imaging of Ultrasound Contrast Agents. Applied Acoustics 70(10): 1352-1362.

Stride E, Edirisinghe M (2008) Novel microbubble preparation technologies. Soft Matter 4: 2350-2359.

Lee S, Lee L (2005) 'Encyclopedia of chemical processing' Taylor & Francis, New York, NY 10016, Page 1353-1355.

Talu E, Lozano MM, Powell RL, Dayton PA, Longo ML (2006) Long-term stability of lipid coating monodisperse microbubbles formed by a flow-focusing device. Langmuir 22: 9487- 9490.

Talu E, Hettiarachchi K, Powell RL, Lee AP, Dayton PA, Longo ML (2008) Maintaining monodispersity in a microbubble population formed by flow-focusing. Langmuir 24: 1745-1749.

Tang K, Gomez A (1994) On the structure of an electrostatic spray of monodisperse droplets. Phys Fluids 6(7): 2317-2332.

Tang K, Gomez A (1995) Generation of monodisperse water droplets from electrospray in a corona-assisted cone-jet mode. J Coll Inter Sci 175: 326-332.

Tang K, Gomez A (1996) Monodisperse elctrosprys of low electric conductivity liquids in the cone-jet mode. J Coll Inter Sci 184: 500-511.

Taylor G (1964) Disintegration of Water Drops in an Electric Field. Pro Royal Soc Series A Mathemat Phys Sci 280 (1382): 383-397.

Uhhlendorf V, Scholle FD, Reinhardt M (2000) Acoustic behaviour of current ultrasound agents. Ultrasonics 38: 81-86.

Unger EC, Hersh E, Vannan M, Matsunaga TO, McCreery T (2001) Local drug and gene delivery through microbubbles. Prog Cardiovasc Dis 44(1): 45-54.

Unger EC, Matsunaga TO, McCreery T, Schumann P, Sweitzer R, Quigley R (2002) Therapeutic applications of microbubbles. Euro J Radiol 42: 160- 168.

Unger EC, Porter T, Culp W, Labell R, Matsunaga T, Zutshi R (2004) Therapeutic applications of lipid-coated microbubbles. Adv Drug Deliv Rev 56: 1291-1314.

van Liew HD, Raychaudhuri S (1997) Stabilized bubbles in the body: pressure-radius relationships and the limits to stabilization. J Appl Physiol 82: 2045-2053.

van Wamel A, Bouakaz A, Bernard B, Ten Cate F, de Jong N (2004) Radionuclide tumour therapy with ultrasound contrast microbubbles. Ultrasonics 42: 903-906.

van Zomeren AA, Kelder EM, Marijnissen JCM, Schoonman J (1994) The production of thin films of $LiMn_2O_4$ by electrospray. J Aerosol Sci 25: 1229-1229.

Wang W, Moser CC, Weatley MA (1996) Langmuir trough study of surfactant mixtures used in the production of a new ultrasound contrast agent consisting of stabilized microbubbles. J Phy Chem 100: 13815-13821.

Weber C (1931) On the breakdown of a fluid jet. Journal of Mechanics and Applied Mathematics 11: 136-159.

Wells PNT (2001) Physics and engineering: milestones in medicine. Med Eng Phys 23: 147-153.

Whitesides GM (2003) The 'right' size in nanobiotechnology. Nature biotechnology 21(10): 1161-1165.

Xie J, Marijnissen JCM, Wang CH (2006) Microparticles developed by electrohydrodynamic atomization for the local delivery of anticancer drug to treat C6 glioma in-vitro. Biomaterials 27: 3321-3332.

Xu Y, Hanna M (2008) Morphological and structural properties of two phase coaxial jet electrosprayed BSA-PLA capsules. J Microencapsul 25(7): 469-477.

Yadav SK, Khilar KC, Suresh AK (1997) Release rates from semi-crytalline polymer microcapsules formed by interfacial polycondensation. J Membrane Sci 125: 213-218.

Yount DE (1979) Skins of varying permeability: A stabilization mechanism for gas cavitation nuclei. J Acoustic Soc Am 65: 1429-1439.

Zeleny J (1914) The electrical discharge from liquid points and hydrostatic method of measuring the electric intensity at their surfaces. The physical review 3: 69-91.

Zeleny J (1917). Instability of electrified liquid surfaces. Second Series 10(1): 1-7.

Zhang J, White GL, Fulton JL (1995) Spectroscopic investigation of an L-α-phosphatidylcholine gel formed in near-critical propylene. J Phys Chem 99: 5540-5547.

Zhang XZ, Lewis PJ, Chu CC (2005) Fabrication and characterisation of a smart drug delivery system: microsphere in hydrogel. Biomater 26: 3299-3309.

Zhao YZ, Liang HD, Mei XG, Halliwel M (2005) Preparation, characterization and in-vivo observation of phospholipid-based gas-filled microbubbles containing hirudin. Ultrasound in Med and Biol 31(9): 1237-1243.

Zhu Y, Fu J, Zhu L, Tang X, Huang X (2008) Preparation of novel hybrid inorganic-organic hollow microspheres via a self-template approach. Polym Int 57: 449-453.

Zoldesi CI, van Walree CA, Imhof A (2006) Deformable hollow hybrid silica/siloxane colloids by emulsion templating. Langmuir 22: 4343-4352.

Appendix

1. Calculation of liquid absorption capacity of microspheres (Section 6.9)

The mass of wet microspheres: 0.4945 g

The mass of dry microspheres: 0.2940 g

The mass of liquid absorbed: (0.4945-0.2940) g = 0.2005 g

The liquid absorption capacity of microspheres: 0.2005 x 100 / 0.2940 = 64.8 % ~ 65 %

2. Calculation of bubble yield (Section 7.1.7)

The liquid flow rate: $5\ \mu l\ s^{-1} = 5 \times 60\ \mu l\ m\text{-}1/min = 5 \times 60 \times 10^{-9} m^3/min$

Mean diameter of the bubble: $5\ \mu m = 5 \times 10^{-6}\ m$

Number of bubbles generated/min: $(5 \times 60 \times 10^{-9}) / (4/3 \times \pi \times 2.5^3\ 10^{-18}) = 4.6 \times 10^9$

$\sim 4 \times 10^9$